UNIVERSITÀ POLITECNICA DELLE MARCHE
FACOLTÀ DI INGEGNERIA

Corso di Laurea Magistrale in Biomedical Engineering

AUTOMATIC IDENTIFICATION OF TRAINING PHASES FROM HEART RATE RECORDED BY WEARABLE SENSORS

Relatore:
Prof. Laura Burattini

Tesi di Laurea di:
Alessio Scalese

Correlatore:
Dott. Agnese Sbrollini

Anno Accademico 2019 – 2020

Per mia madre

Una mamma è un mistero.
Tutto comprende,
tutto perdona.
Tutto soffre, tutto dona.
Non coglie fiori
per la sua corona.
Puoi passare da lei
come straniero.
Puoi farle male
in tutta la persona;
ti dirà: "Buon cammino,
bel cavaliero!".
Una mamma
è questo mistero.

[Francesco Pastonchi]

Per mio padre

I vostri figli non sono figli vostri.
Essi sono i figli e le figlie del desiderio
che la vita ha di sé stessa.
Essi non provengono da voi, ma attraverso di voi.
E sebbene stiano con voi, non vi appartengono.
Potete dar loro tutto il vostro amore, ma non i vostri pensieri.
Perché essi hanno i propri pensieri.
Potete offrire dimora ai loro corpi, ma non alle loro anime.
Perché le loro anime abitano la casa del domani,
che voi non potete visitare, neppure nei vostri sogni.
Potete sforzarvi di essere simili a loro,
ma non cercare di renderli simili a voi.
Perché la vita non torna indietro e non si ferma a ieri.
Voi siete gli archi da quali i vostri figli,
come frecce viventi, sono scoccati.
L'Arciere vede il bersaglio sul percorso dell'infinito,
e con la Sua forza vi piega
affinchè le sue frecce vadano veloci e lontane.
Lasciatevi piegare con gioia dalla mano dell'Arciere.
Poiché così come ama la freccia che scocca,
così Egli ama anche l'arco che sta saldo.

[Kahlil Gibran]

Per mia sorella

Non si è mai lontani abbastanza per trovarsi.

[Alessandro Baricco]

Per me stesso

Se la morte fosse un vivere quieto,
un bel lasciarsi andare,
un'acqua purissima e delicata
o deliberazione di un ventre,
io mi sarei già uccisa.
Ma poiché la morte è muraglia,
dolore, ostinazione violenta,
io magicamente resisto.
Che tu mi copra di insulti,
di pedate, di baci, di abbandoni,
che tu mi lasci e poi ritorni senza un perché
o senza variare di senso
nel largo delle mie ginocchia,
a me non importa perché tu mi fai vivere,
perché mi ripari da quel gorgo
di inaudita dolcezza,
da quel miele tumefatto e impreciso
che è la morte di ogni poeta.

[Alda Merini]

Per mia nonna

E' sola pur stando in compagnia,
Affonda su un divano,
Come una bimba
Tra le braccia di sua madre.
Gli occhi spenti,
Da me sono lontani
E guardano lontano chissà che!
La guardo, mi guarda,
La conosco:
E' la nonna delle fiabe e dei perché,
Un po' stanca e sofferente
Chissà perché!
Con uno slancio l'abbraccio
E la stringo forte a me.

[M. Assunta P.]

Per il mio amore

Ti guardo dolcemente mentre distesa
sul divano i tuoi occhi si socchiudono
pian pianoe acquista il tuo viso una
dolcezza che mi entra nel cuore e
mi fa palpitare di gioia.
Prendo quella copertina adagiata sulla
spalliera di questo sofà e la distendo sul
tuo corpo quasi dormiente. Ti guardo e
tutto ha un senso. Una ragione d'amore.
Sembra che tu abbia perso conoscenza
e ti sei addormentata. Prendo il lembo
di questa coperta di lana e avvolgo
i tuoi piedi freddi.
Hai la testa poggiata sul bracciolo di
questo nostro divano. Vorrei parlarti,
ma non voglio disturbare il tuo riposo
in questa quiete che pare vivere lontana
dai frastuoni del mondo.
Ma questo plaid si sfila dal tuo corpo e
scopre le tue spalle ormai rilassate.
Delicatamente le ricopro per non
lasciare sfuggire il tepore dentro di te.
Apri i tuoi occhi assonnati e il tuo sguardo
è dolce, e come un effluvio che si diffonde
nell'aria mi entra in questo mio immaginifico
animo che si prende cura di te, e accarezzo
questi tuoi fluenti capelli che odorano di lavandula.
Non mi può sfuggire di appoggiare le mie
labbra sulle tue. Il tuo respiro è lento e
vorrei svegliarti e baciarti dolcemente
e di passione.
Ma non posso interrompere questo tuo
dolce riposo pomeridiano, e che la tua
mente gode di sogni riposti.
Riposa, mio amore! Hai già lavorato
troppo, come ogni giorno, per rendere
questa casa sempre gradevole e splendente.
Grazie a te. Grazie, mia cara. Ti sarò
sempre grato per come dedichi le
tue forze e le tue attenzioni a questa
nostra famiglia.

[Roberto Zaoner]

Abstract

All the athletes in the world, in particular professional athletes, strive for success in practice and competition; therefore, the physiological monitoring of the training is becoming increasingly crucial because it can be used to better understand the underlying processes of performance and to subsequently increase or optimize it. Moreover, nowadays, the incidence of *sudden cardiac death* (*SCD*) in athletes ranges from 1:40.000 to 1:250.000 depending, among other things, on the sporting discipline. More than 80% of SCDs occurs during intensive training and competition. Therefore the need to have a tool able to help athletes to optimize their performances and, at the same time, to monitor their health status, is very important. Hence the idea to develop an algorithm able to perform the above-mentioned actions. In order to combat the SCD, the avanced algorithms for the monitoring of the athlete must be able to correctly and reliably identify training phases, particularly when it has to do with wearable sensors.

The most important and used wearable sensors monitoring the cardiovascular signals are listed knowing their strengths and weaknesses. Nowadays, on the market there are textile electronics, chest straps, patches, smartwatches, wristbands and some other products such as ear-rings, ear-phones or rings. Data used for the development of the algorithm have been collected by a chest strap called *Zephyr Bioharness 3.0*.

Some automatic algorithms for the identification of training phases are then analyzed, such as one based on the heart-rate variability, Dynascope and HeartScope.

The key principle of the new developed algorithm is the analysis of the angular coefficient based on both the heart-rate and tachogram signals. On the trend of this new index, all the time-instants, needed for the identification of the training phases, are determined.

The study population comprises ten middle-running athletes, all in good state of health with ages ranging from 18 and 55 years old. As regards the validation and the reliability of the algorithm, it shows a percentage of error, for both the identification of the two transition phases (from pseudo-resting to exercise, and from exercise to recovery), ranging from 0% to 1.57% in 6 subjects over 9. The remaining three subjects are characterized by a wrong identification of the exercise-recovery transition phase, despite their resting-exercise transition phase are correctly identified. The identification of the these two transition phases, if deleted from the signal for a further processing, allows the analysis of some important heart risk indeces such as QT-interval or heart-rate variability.

In conclusion, the algorithm developed in this work turns out to be a reliable tool for both the optimization of athlete's performance and the monitoring of the health status of the

athlete. Moreover, although the algorithm is specifically developed for the the analysis of data coming from middle-running athletes, it has a basic structure promising to adapt to any sport.
In short, a tool already reliable, but with still extensive room for improvement. A tool extremely attentive to the needs of any athlete.

Index

Introduction

"Smiling is the most powerful exercise to build a joyful mind and a blissful heart"
[Debasish Mridha]

The topic on which this thesis focuses, embodies what is the fundamental duty of the biomedical engineer: applying engineering principles and materials to medicine and healthcare. Indeed, this work primarily consists of two main blocks; the first one has a merely technical purpose with the development of an algorithm able to automatically identify the three training phases (pseudo-resting, exercise, and recovery), whereas the second one broadens the horizon to all the clinical implication that are of interest to the state of health of the subject under investigation.

All the athletes in the world, in particular professional athletes, strive for success in practice and competition; therefore, the physiological monitoring of the training is becoming increasingly crucial because it can be used to better understand the underlying processes of performance and to subsequently increase or optimize it. For this reason, an adequate balance between stress (training and competition load) and recovery is essential for athletes to achieve continuous high-level performance, and monitoring of the recovery-fatigue trend constitutes the first step for the performance enhancement. Regarding this aspect, the *fitness-fatigue model* describes the relationship between training load, positive (fitness) adaptations, and negative (fatigue) adaptations. The required time for recovery from exercise fatigue also depend on the organismic systems of the human body. Since the high intraindividual and interindividual variability of the recovery process makes it impossible to obtain a distinct categorization of the recovery based on specific time instants, the direct monitoring of fitness and fatigue responses is emerged as a scientific support for high-performance athletes. This also allows both training and recovery activities to be manipulated by coaches in order to produce the desired physiological outcomes. The overall aim is to enhance performance and minimize the risk of developing *non-functional overreaching* (*NFO*), *over-training syndrome* (*OTS*), illness, and injuries.

On the other hand, what is common to professional and amateur athletes – and what must be the base condition for the practice of sport - is the monitoring and health check of the athletes. Indeed, in contrast to the well-known health benefits of exercise, there are occurrences during which athletes die suddenly and unexpectedly during exercise due to congenital, inherited or acquired cardiovascular disease. In these cases, the stressors of

intense exertion may unfortunately trigger a fatal cardiac arrhythmia under circumstances of an occult structural or electrical abnormality, or silent *coronary artery disease* (*CAD*). Nowadays, the incidence of *sudden cardiac death* (*SCD*) in athletes ranges from 1:40.000 to 1:250.000 depending, among other things, on the sporting discipline. More than 80% of SCDs occurs during intensive training and competition. Data also indicate that deaths are more common in males than females, and that black athletes are more vulnerable to SCD than white athletes. Although around 50% of SCD cases are caused by inherited ion channels diseases such as *long QT syndrome*, *catecholaminergic polymorphic ventricular tachycardia* and *Brugada syndrome*, a small patient population may be due to congenital accessory electrical pathways such as in *Wolff-Parkinson-White syndrome*. In particular, long QT syndrome type 1 is usually implicated in SCD during exercise. The great news is that SCD in athletes can be diagnosed during life, and several therapies (such as implantable defibrillators) are able to potentially prevent death. Among the screening models in use, the *electrocardiogram* (*ECG*) *interpretation* has the highest sensitivity. However, it is noteworthy that a pseudo-resting ECG is not able to detect incomplete expressions of cardiomyopathy, coronary disease, or adrenergically-mediated arrhythmias in subjects with ion channel disease. In addition, exercise stress test, which is recommended for mature athletes (aged $\geq$ 35 years) not always has proved a reliable model.

This work, rather, relies on the measurement of the *heart rate* (*HR*) recorded by wearable sensors, which contain relevant informations about the identification of the training phases. The analysis, in an automated way, of these phases performed by athletes already has in itself a significant contribution to the optimization of the performance training, but it becomes in turn a starting point for the monitoring of the heart health. Indeed, the developed algorithm is able to detect the two transition intervals between pseudo-resting and exercise, and between exercise and recovery, thereby identifying the three phases (resting, exercise, and recovery) during which the HR-signal is theoretically almost linear. This apparent end point, represents instead the basis for the analysis of all the risk indeces, such as *QT* or *heart-rate-variability* (*HRV*) which requires stable cardiac conditions, even during training. The above-mentioned transition phases, if not eliminated, would contaminate the estimates of these indeces.

In conclusion, this work intends to provide a tool for the real-time monitoring of both training and state of health, with the dual aim of optimizing the athlete's performance and health protection.

Chapter 1

Cardiovascular anatomy and physiology

"There is no exercise better for the heart than reaching down and lifting people up"
[J. F. Holmes]

1.1 The heart

The *cardiovascular system* basically consists of the *heart* and the *blood vessels*. The heart can be functionally subdivided into two pumps between which find space the *pulmonary* and the *systemic circulations* (Fig. 1.1). The right pump is made up by the *right atrium* and the *right ventricle*. The left pump similarly comprises the *left atrium* and the *left ventricle*. The pulmonary circulation receives the *deoxygenated* blood from the right ventricle and pumps the *oxygenated* blood into the left atrium. It comprises the *lungs*, where oxygen and carbon dioxide are exchanged between the blood and the *alveoli*.

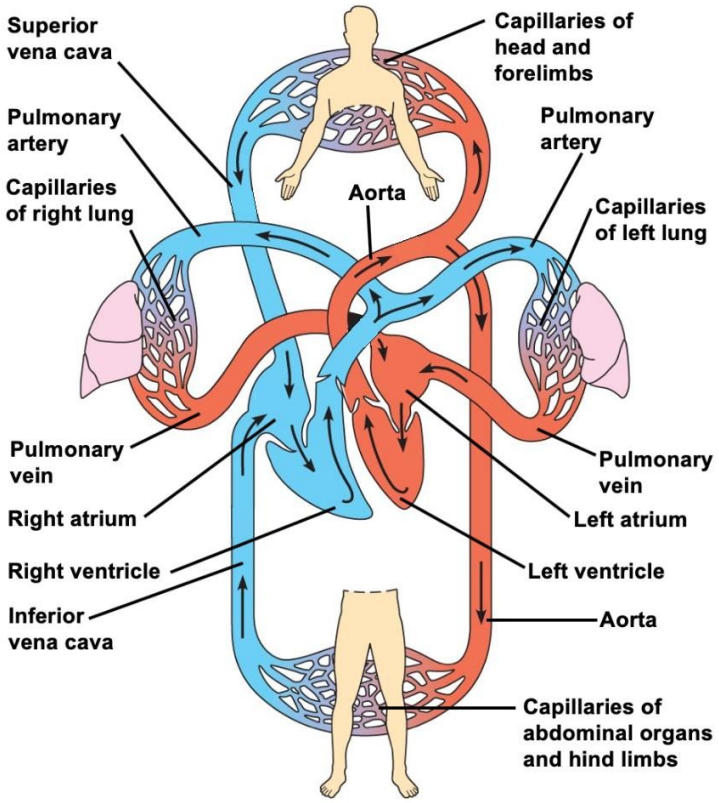

Figure 1.1 *Pulmonary veins, pulmonary arteries, aorta, superior vena cava and inferior vena cava.*

The systemic circulation picks up the oxygenated blood from the left ventricle and sends the deoxygenated blood to the right atrium. It wraps the organs with its smallest vessels, the *capillaries*, which are the primary sites of exchange of nutrients and discards of the metabolism. Going even more in detail, the oxygenated blood enters the left atrium through the *pulmonary veins*; then, it is pushed into the left ventricle which ejects it into the *aorta*. On the other hand, the deoxygenated blood enters the right atrium through the *superior* and *inferior vena cava*; then, it is sent to the right ventricle which pushes it into the *pulmonary artery*.

The heart is a muscular hollow organ which, by means of its involuntary rhythmic contractions, allows the blood to circulate within the vessels. It is embraced in the thoracic cavity by the *mediastinum*, and it rests on the *diaphragm*. It has a reverse-cone shape, whose *base* points backwards and towards the right, and whose *apex* is facing left and forwards reaching, in adults, the fifth *intercostal space*. Being a bit flattened in the antero-posterior direction, it features both an anterior face called *sternocostal surface*, and a posterior face named *diaphragmatic surface*, an *acute margin* on its right, and an *obtuse margin* on its left. The sternocostal surface (Fig. 1.2) appears divided into two different parts from a morphologic point of view: the limit is marked by the *coronary sulcus* (also called *atrio-ventricular sulcus*) which is arranged transverse to the main axis of the organ; the part located superior to the sulcus is constituted by the atria, whereas the one located inferior to the sulcus is constituted by the ventricles.

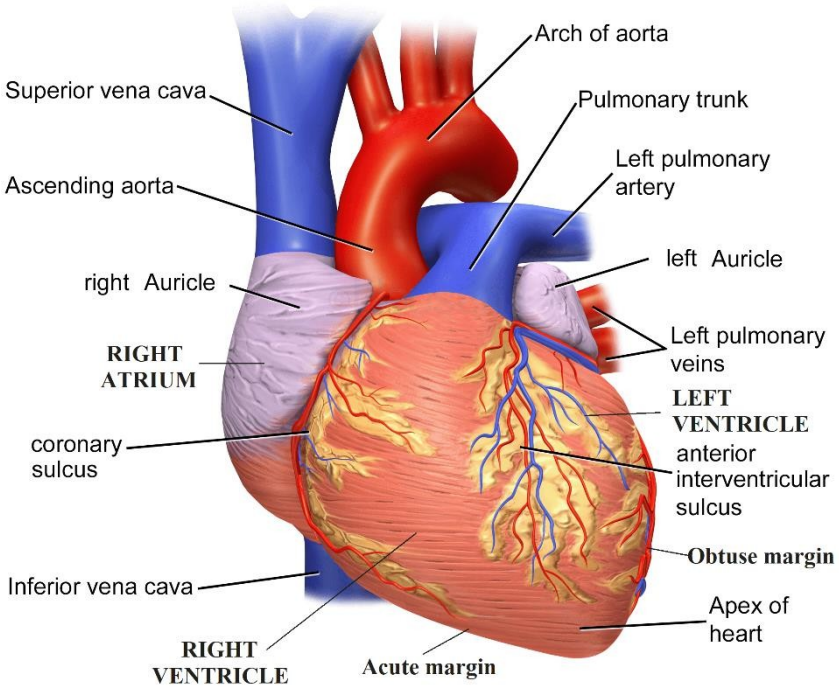

Figure 1.2 *Sternocostal surface of the heart.*

The diaphragmatic surface (Fig. 1.3) lies on the *central tendon* of the diaphragm[1] and has a triangular shape. It corresponds to the inferior surface of the ventricles and to a small portion of the atria. The coronary sulcus transversally runs the diaphragmatic part separating, also in this case, a wide ventricular portion from a small atrial portion. The *posterior longitudinal* (*interventricular*) *sulcus* runs closer to the acute margin dividing the left ventricular part (the wider one) from the right ventricular part (the smaller one). The *base* of the heart (Fig. 1.4), formed by the postero-superior face of the two atria, is at the level of the fifth-eighth thoracic vertebrae. Generally convex, its surface presents a few irregularities due to the inlet of large venous vessels in the atria. It is run by a curvilinear sulcus which, starting from the coronary sulcus, goes up to the anterior margin. This sulcus, largely covered by the terminal tract of the *right pulmonary veins* [2], marks the boundary between the atria and it is called *interatrial sulcus*. Just to the right of this sulcus, there are, superiorly, the outlet of the superior vena cava, and, inferiorly, the outlet of the inferior vena cava[3]. Below this last outlet, the base indistinctly continues with the diaphragmatic face of the atria. On the border between the posterior and the lateral parts, the right atrium features a vertical groove named *terminal sulcus*.

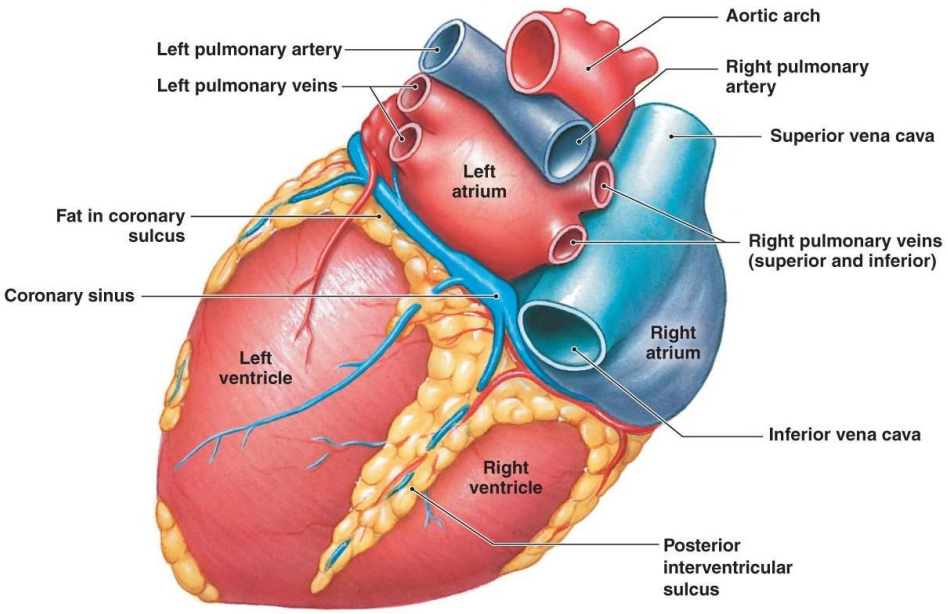

Figure 1.3 *Diaphragmatic surface of the heart.*

[1] The *central tendon* of the diaphragm is a thin but strong aponeurosis near the center of the vault formed by the muscle.
[2] The pulmonary veins are the vessels which, starting from the lungs, reach thr left atrium.
[3] The inferior vena cava drains the blood coming from the sub-diaphragmatic areas towards the right atrium.

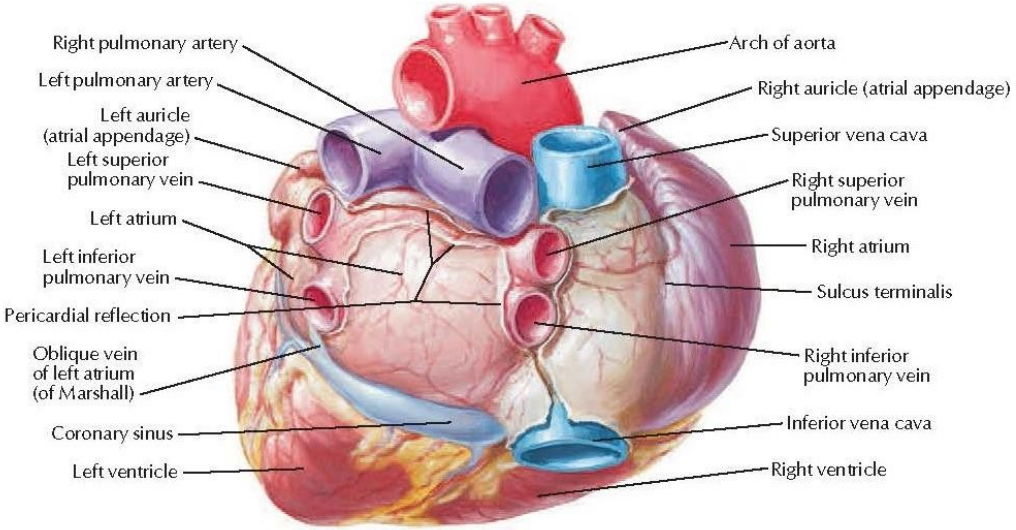

Figure 1.4 *Base of the heart: posterior view [1].*

The terminal sulcus separates, in the right atrium, two parts of different morphology: the *sinus of the venae cav*ae (the posterior one) and the *atrium proper* (the antero-lateral one). The sinus of the venae cavae appears smooth. The surface of the base situated on the left of the interatrial sulcus corresponds to the the left atrium. It has, on the right edge, the outlets of the two right pulmonary veins, and, on the left edge, the outlets of the two left pulmonary veins. The area of the atrium between the outlets of the left and right pulmonary veins is called *vestibule* of the left atrium and has the same morphologic features of the sinus of the venae cavae.

The *apex* of the heart, mainly formed by the left ventricle, points downwards, forwards and towards the left. It is covered by the left lung and by its *pleura* [4]; it is located at the level of the left fifth intercostal space, at 6-8 cm from the midline of the sternum.

The atrial and ventricular musculature are separated by the interposition of the *fibrous skeleton* of the heart, on which they attach (Fig. 1.5). The myocardium is completed by the *electrical conduction system* of the heart. The fibrous skeleton is fundamentally constituted by four fibrous rings which distinctly sorround the two atrio-ventricular orifices and the two arterial orifices.

[4] The pulmonary pleurae are the two layers of the invaginated sac surrounding each lung and attaching to the thoracic cavity.

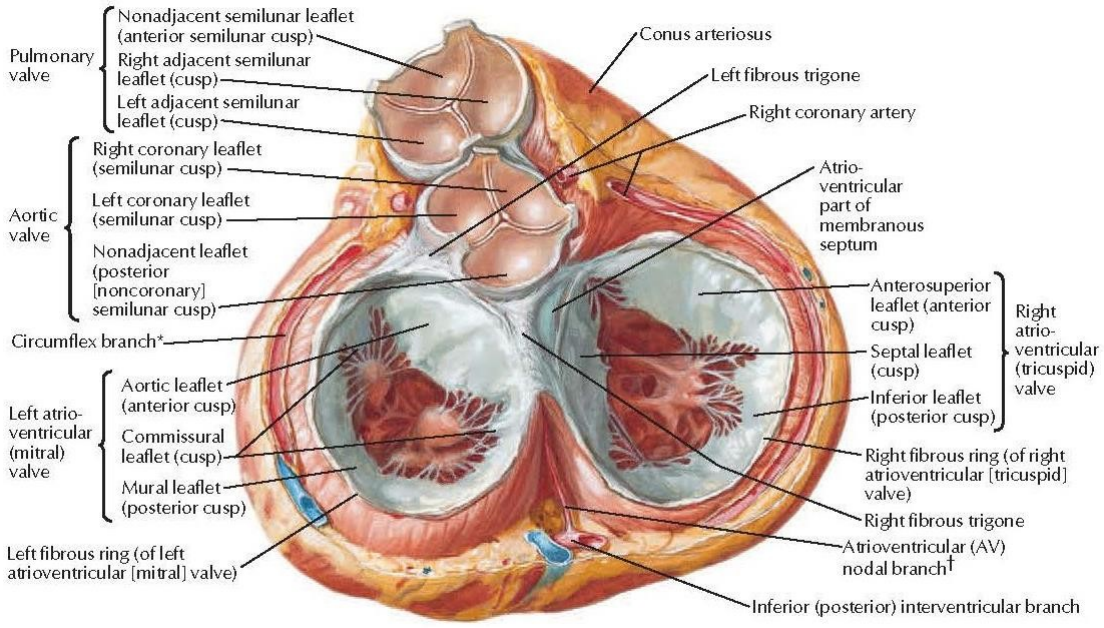

(a)

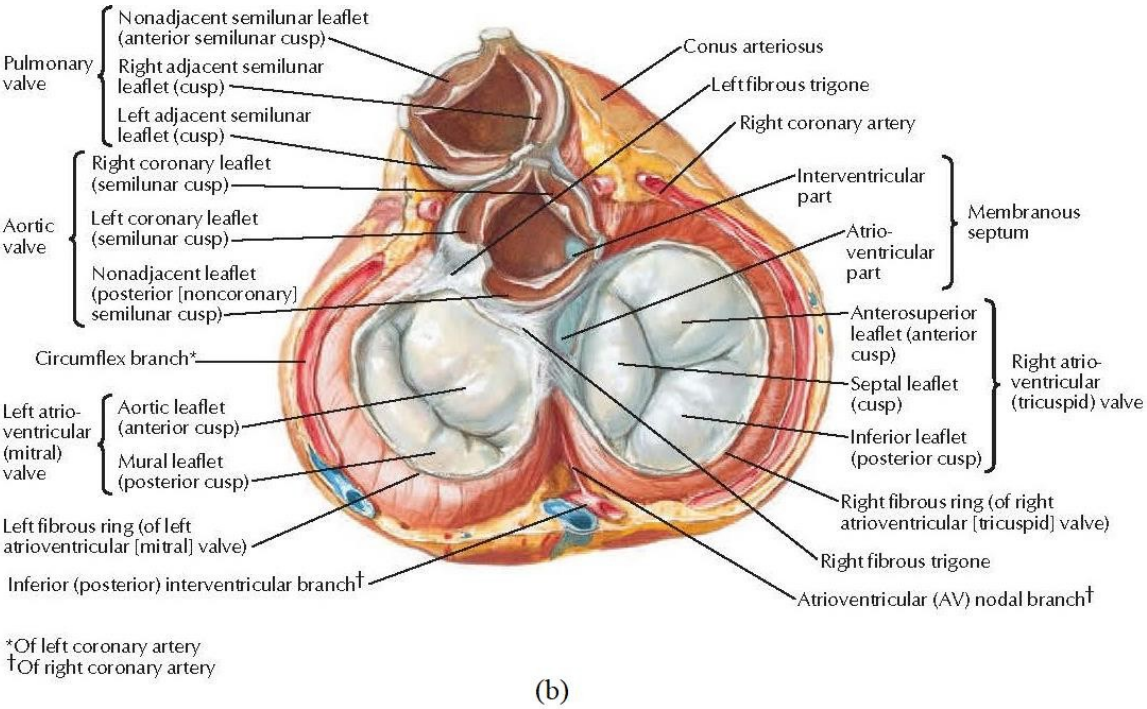

(b)

Figure 1.5 (a) *Heart in diastole: viewed from base with atria removed;* **(b)** *Heart in systole: viewed from base with atria removed* ***[1]***.

1.2 Internal configuration of the heart

The two right-half cavities indeed are separated from the two left-half cavities on the upper side by means of the *interatrial septum* (which separates the atria), and on the lower side by means of *the interventricular septum* (which seperates the ventricles). It must be remembered that the right cavities contain venous blood (rich of carbon dioxide), and the left cavities contain arterial blood (rich of oxygen).

The two atrioventricular orifices are equipped with *cuspid valves* which allow the passage of the blood from the atrial cavities to the ventricular cavities and oppose, on the contrary, the reflux from the ventricles to the atria. The base of the ventricles presents the origin of the corresponding arteries (aorta and pulmonary trunk) with which communicate through two orifices equipped with *semilunar valves*. These valves allow the passage of the blood from the ventricular cavities to the two arterial trunks, and oppose the reflux towards the ventricles. Each of the valves is costituted by three valve leaflets (Fig.1.6).

On the postero-superior surface of the right atrium (Fig. 1.7), close to the antero-posterior and postero-superior surfaces, find space the outlets of the superior and inferior venae cavae. In correspondance of the antero-inferior wall of the right atrium, there is the right atrio-ventricular orifice which is equipped with a valve formed by three cusps: the *tricuspid valve*. On the wall of the left atrium there are the outlets of some cardiac veins of minor importance.

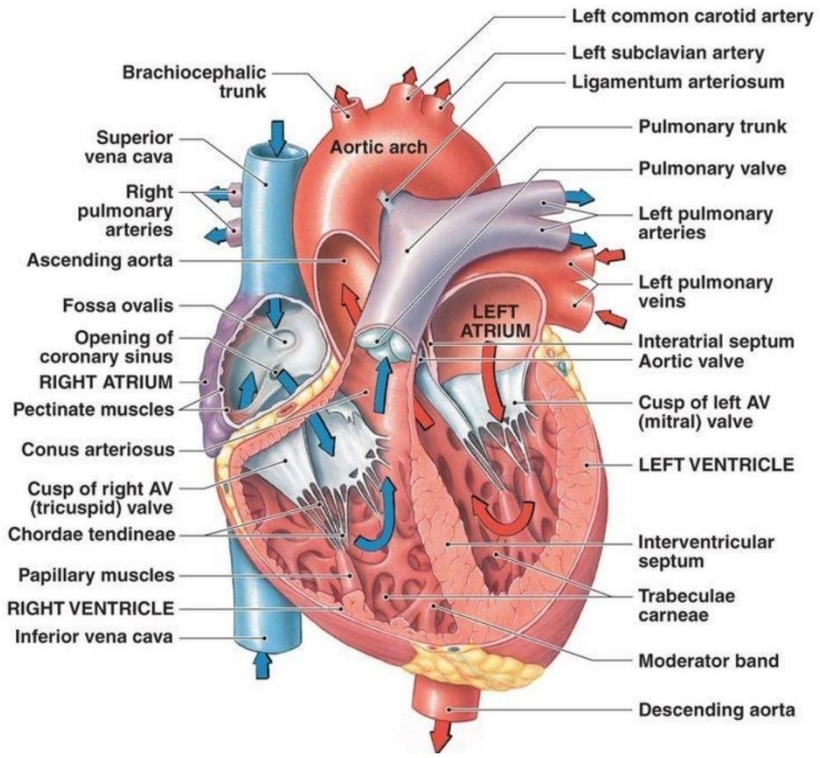

Figure 1.6 *Coronal section of the heart.*

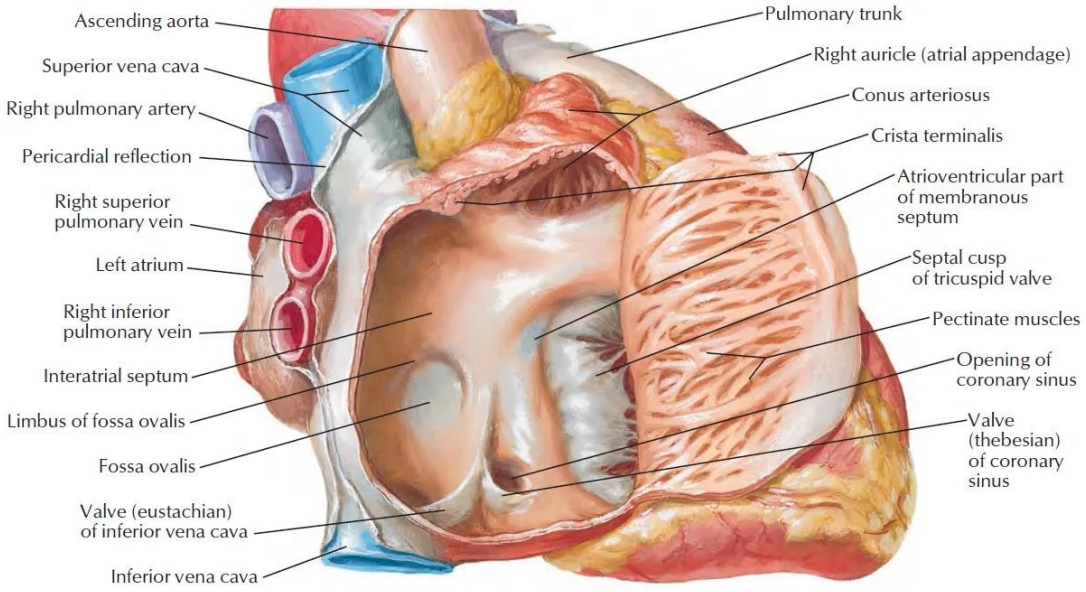

Figure 1.7 *Opened right atrium: right lateral view [1].*

Downwards and forwards, the left atrio-ventricular orifice leads into the ventricular cavity; it is equipped with a valvolar apparatus costituted by two faced cusps, that takes the name of *mitral valve* (or *bicuspid valve* or left atrio-ventricular valve).

The right ventricle (Fig. 1.8) has a triangular-pyramid shape; the base includes two orifices: the atrio-ventricular one, located backwards and towards the right, and the pulmonary one, placed forwards and towards the left.

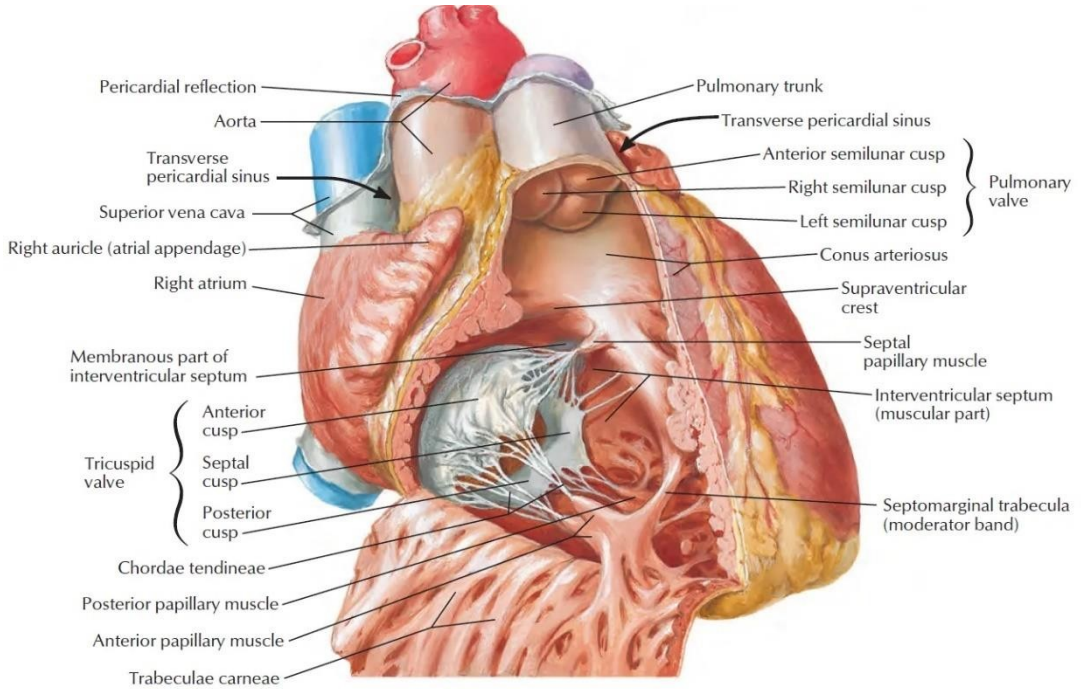

Figure 1.8 *Opened right ventricle: anterior view [1].*

Through these orifices, the ventricle communicates respectively with the corresponding overlying atrium and with the pulmonary trunk. From its medial extremity, a robust trabecola carnea brances off, the *septo-marginal trabecula* (or *Leonardo Da Vinci moderator band*) which, heading downwards and forwards, reaches the base of the *anterior papillary muscle*[5].

The venous part has irregular walls due to the presenze of muscular prominences called *trabeculae carneae*. The infundibular part has smooth walls, and terminates, upward, with the orifice of the pulmonary trunk.

The pulmonary orifice is situated close to the interventricular septum, forwards and upwards respect to the right atrio-ventricular orifice. It has a circular outline with an average circumference of 70 mm, and presents a semilunar valve costituted by three leaflets which, given their position, are distinguished in *anterior*, *left* and *right*.

The leaflets are membranous folds with a swallow's nest-shape; they present an adherent margin which attaches to a fibrous ring located on the contour of the arterial orifice, and a free margin which leans over the vessel lumen. In the right ventricle there are:

- the *anterior* (or *superoposterior*) *papillary muscle*, voluminous, from which a dozen of chordae tendineae detach;
- the *posterior* (or *inferior*) *papillary muscle*, represented by two or three small bundles, from which the chordae tendineae depart towards the medial and posterior cusps;
- the *medial* (or *septal*) *papillary muscle*, which provides chordae tendineae to the anterior and medial cusps.

The left ventricle (Fig 1.9) has the shape of a slightly flattened cone, whose apex corresponds the apex of the heart. The base has two orifices (the venous atrio-ventricular orifice and the arterial aortic orifice) through which it communicates, respectively, with the underlying atrium and with the aorta.

The left atrio-ventricular orifice has an oval outline and an average circumference of 102 mm. It is bordered by a fibrous ring which houses the mitral valve, constituted by two cusps (or valve leaflets) of different dimensions. There is the *anterior cusp*, the wider one, and the *posterior cusp*, the narrower one.

The aortic orifice (Fig. 1.10) is circular and its circumference measures on average 70 mm. It is equipped of three semilunar leaflets: the right one, the left one, and the posterior one. It presents a convex surface (which protrudes in the right ventricle) and a concave surface (which protrudes in the left ventricle).

[5] The papillary muscles are muscles located in the ventricles of the heart. They attach to the cusps of the atrioventricular valves via the chordae tendineae and contract to prevent inversion or prolapse of these valves on systole (or ventricular contraction).

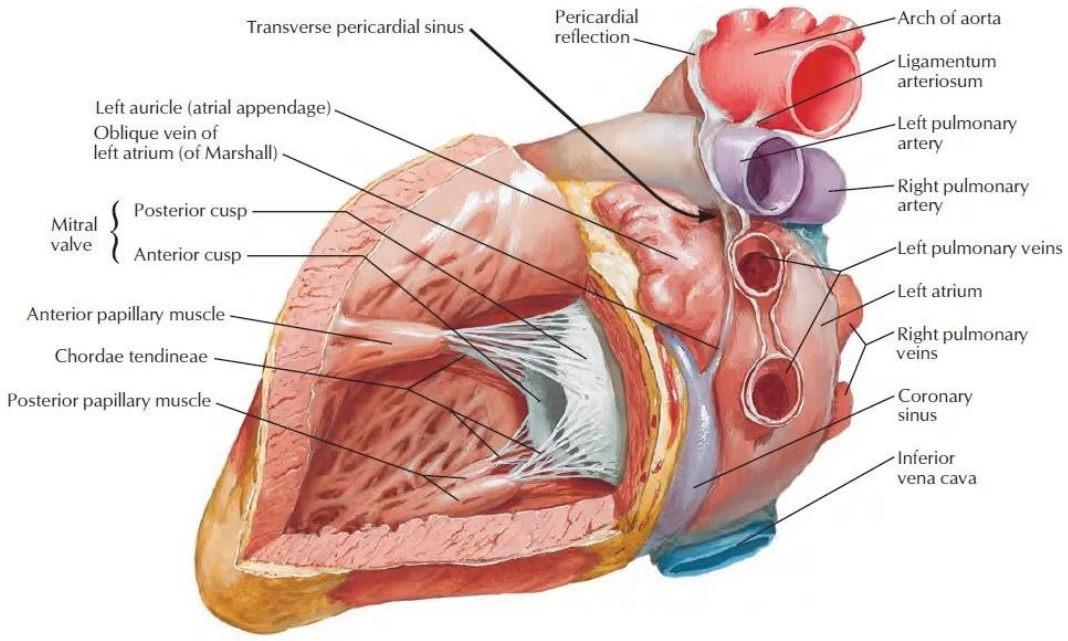

Figure 1.9 *Flap opened in the posterolateral wall of the left ventricle [1].*

Most of the septum is meaty (the thickess approximately equals that of the left ventricular walls); only a small superior portion has instead a fibrous consistency and a thickness approximately peer to 1 mm and constitutes the membraneous part of the septum.
They have structure and insertion modality similar to to the leaflets of the pulmonary trunk valve; on their free margin, they present a small swelling named body of Arantius. From their summits, the chordae tendineae detach and implant on the two leaflets of the mitral valve. The interventricular septum extends from the apex of the heart to the base of the ventricles.

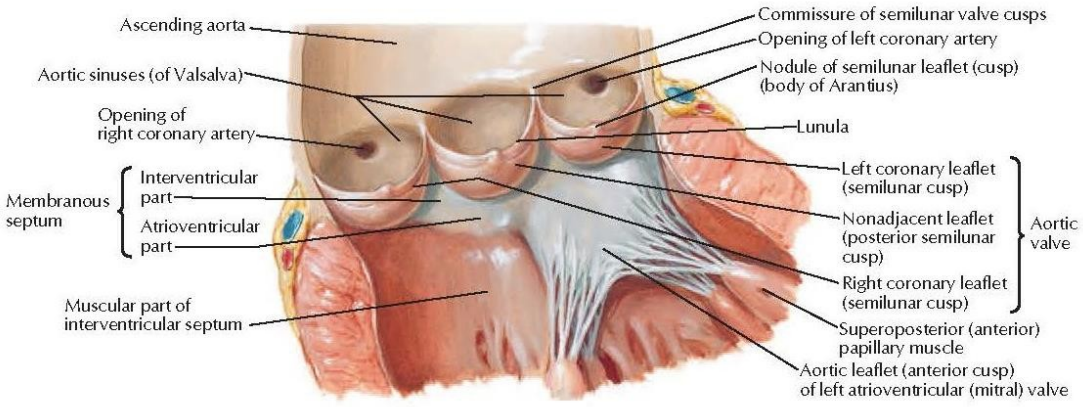

Figure 1.10 *Aortic valve [1].*

1.3 Coronary circulation

The heart ejects blood into all the body tissues, and performs this task continously, rhythmically contracting and relaxing. To “stay alive” and perform its function, cardiac muscle need the continous and uninterrupted blood supply which is received through the *coronary arteries*. The two *left and right coronary arteries* (Figures 1.11a and 1.11b) originate from the ascending aorta and reach the heart, on whose surface, they divide into branches that run below the epicardium; smaller vessels originate from these major branches and lead deep into the myocardium, vascularizing it.

The *right coronary artery* perfuses the right atrium, large part of the right ventricle, the posterior part of the left ventricle and the posterior half of the heart-septum (the posterior branch runs into the posterior interventricular sulcus. The *left coronary artery* perfuses the left atrium, large part of the left ventricle, the anterior wall of the right ventricle and the anterior half of the heart-septum (posteriorly, it presents a *circumflex artery* that runs into the coronary sulcus); anteriorly, the anterior interventricular branch runs into the anterior interventricular sulcus, reaching the apex of the heart. Regarding the venous return, the main part of deoxygenated blood coming from the myocardium, flows into the coronary sinus through the coronary veins, which run mainly in parallel to the arteries.

The *coronary sinus* is located on the diaphragmatic surface in the posterior part of the coronary sulcus, and represents the continuation of the *great cardiac vein* coming from the interventricular sulcus, the coronary sinus, flowing into the right atrium, brings the venous blood from the heart walls.

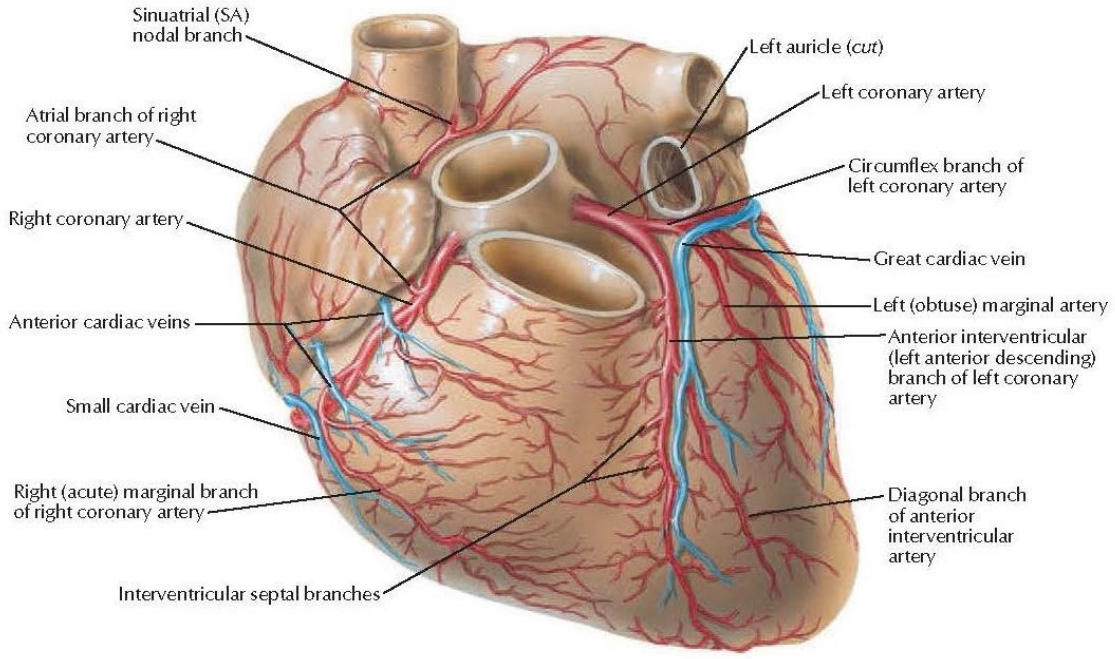

Figure 1.11a *Coronary arteries and veins: sternocostal surface [1].*

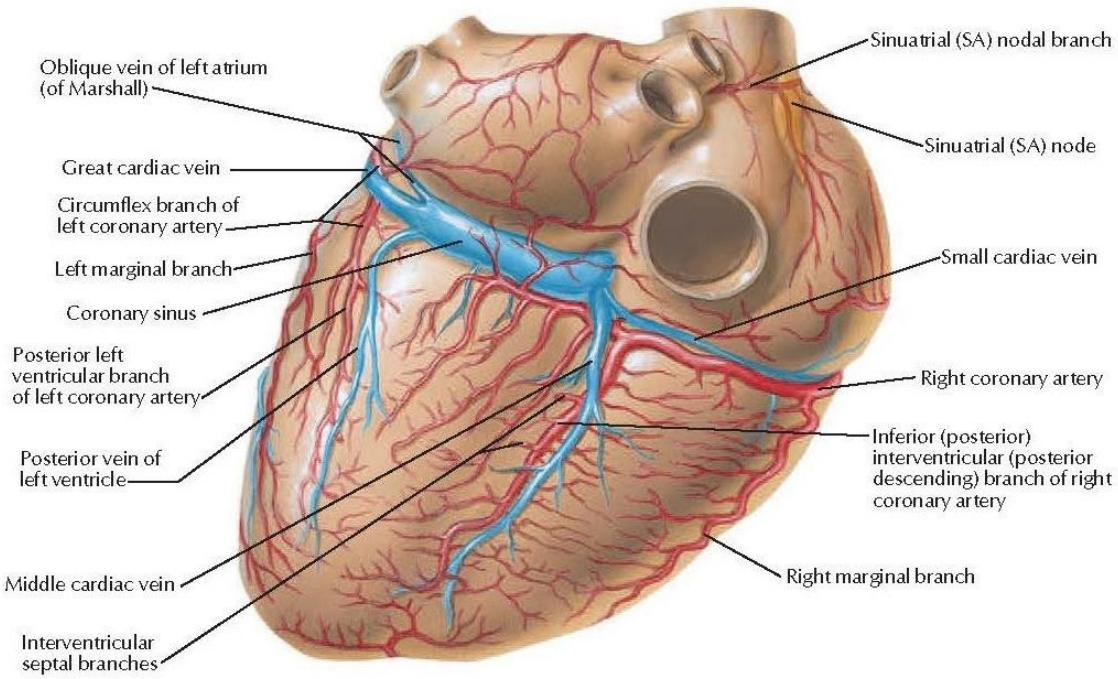

Figure 1.11b *Coronary arteries and veins: diaphragmatic surface [1].*

1.4 Electrical activity of the heart

1.4.1 Cell membrane potentials

Cardiac cells, like all living cells in the body, are characterized by an electrical potential across the cell membrane which separates the interior of the cell from the outside environment. The measurement of the electrical potential taken with a resting cardiac cell is called *resting membrane potential* (E_m), and it is mainly determined by the concentration of positively and negatively charged ions across this membrane (Table 1.1). The resting membrane potential, whose value is about -90 mV, is so called because it characterizes a state not influenced by any impulse. This condition, however, can be modified in response to specific stimuli determining ionic fluxes throught the membrane; the most famous alteration is the *action potential*, which consists in a transient reversal of the membrane potential. If the membrane is *depolarized*[6] few millivolt by a weak crossing current, the voltage-gated sodium channels activate, thus increasing the

[6] Depolarization is a change within a cell, during which the cell undergoes a shift in electric charge distribution, resulting in less negative charge inside the cell.

conductance[7] of the sodium (g_{Na}); a certain amount of sodium consequently enters the cell under the thrust of the electrochemical driving force. The entrance of these ions continues to further depolarize the membrane, thus triggering a sort of vicious circle; however, this trend is going to be interrupted, since, for small depolarization, the entering flux of the sodium is overcompensated by the exiting flux of the potassium. The result is an immediate ripolarization after the depolarizing current is depleted. It is defined *threshold potential* the critical level to which a membrane potential must be depolarized to initiate an action potential: this level is approximately -65 mV (Fig. 1.12). When the membrane potential reaches this value, a rapid *depolarization* (*phase 0*) is initiated by a transient increase in g_{Na^+} of fast sodium channels. At the same time, g_{K^+} falls: the inward sodium flux becomes stronger than the outward potassium flux, resulting in a movement of the membrane potential closer to the sodium equilibrium potential. *Phase 1* constitutes an initial *repolarization* due to the opening of the transient outward potassium channels and the inactivation of the sodium channels. This repolarization, however, is delayed due to a large increase in slow inward $g_{Ca^{2+}}$ (L-type channels open when membrane potential depolarizes to about -40 mV): the result is a *plateau phase* (*phase 2*). The actual *repolarization* (*phase 3*) occurs due to the increase of g_{K^+} and the decrease of $g_{Ca^{2+}}$. After that, the membrane returns to its resting potential (*phase 4*).
The above-mentioned phases are depicted in figure 1.13. The *effective* (or *absolute) refractory period* (ERP) is the interval in which the cell is unexcitable to the initiation of new action potentials because the h-gates are still closed; this period covers phases 0, 1, 2 and part of phase 3. The ERP of cardiac myocytes lasts almost as long as contraction. This period represents a protective mechanism in the heart because limits the frequency of the action potential that the heart can generate: therefore, the heart has an adequate time to fill and eject blood.

Table 1.1 *Intracellular and extracellular concentrations of the ions across a membrane of a cardiac cell [2].*

Ion	Intracellular concentration (mM)	Extracellular concentration (mM)
Na^+	20	145
K^+	150	4
Ca^{2+}	0.0001	2.5
Cl^-	5	120

[7] Channel conductance is defined as the ratio of ionic current through the channel to applied voltage,and it can be calculated once the current, the number of ions that traverse the channel per unit time when an external electric field is applied to the system, has been determined.

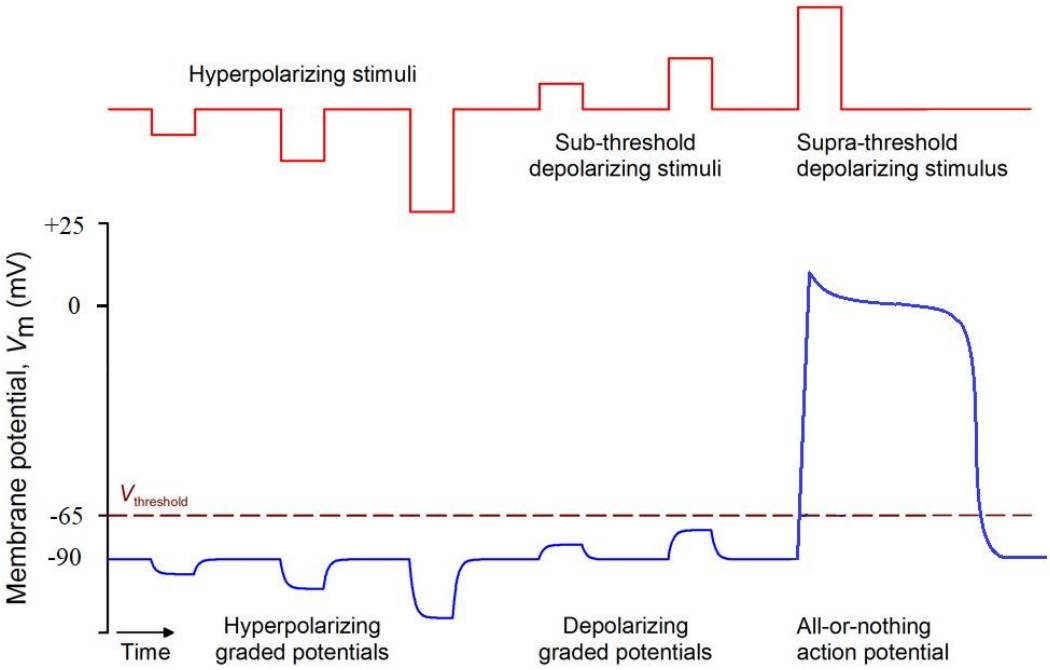

Figure 1.12 *Electrical stimulation of nonpacemaker cardiac cells.*

The *relative refractory period*, instead, occurs at the end of the ERP, and represents the period in which a suprathreshold depolarization stimuli are required to elicit action potentials. In this last case, phase 0 of the action potential has a decreased slope and lower amplitude because not all the sodium channels have recovered from their resting state.

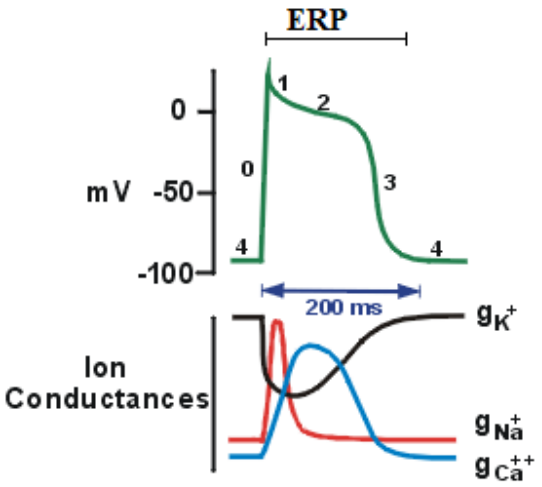

Figure 1.13 *Action Potential and corresponding conductances variations of K^+, Na^+, and Cl^- in nonpacemaker cells.*

In addition to this kind of cells, there are the so-called *pacemaker cells*, which differ from both an histological and practical point of view. In particular, the cells within the *sinoatrial node* (located within the posterior wall of the right atrium) and those of the *atrio-ventricular node* (placed below the endocardium of the medial wall of the right atrium, just above the site of the medial cusp of the tricuspid valve) play a key role in the origin of the electric impulses. The pecularity of these cells is that they have not a true resting potential, but instead generate regular, spontaneous action potentials. Indeed, the depolarizing current of the action potential is carried primarily by relatively slow inward Ca^{2+} current through L-type channels instead of by fast Na^{+} currents. The rate of depolarization is lower than that of nonpacemaker cells; the higher or lower slope of the depolarization-tract determines the instrinsic frequency of the cells and, consequently, the *heart rate*[8]. These cells are under the influence of the orthosympathetic and parasympathetic nervous system. The sino-atrial (SA) node has a higher firing rate than that of the atrio-ventricular (AV) node due to a mechanism called *overdrive suppression*: it causes the secondary pacemaker to become hyperpolarized when driven at a rate above its instrinsic rate. This process is characterized by an enhanced entry of sodium per unit time into the cells which triggers the hyperpolarization which, in turn, stimulates the activity of the electrogenic sodium/potassium pump. Therefore, in normal conditions, the sinoatrial rate is imposed to all the heart which pulses at about 70 beats per minute (bpm). In case of sinoatrial node depression or failure of connection between the sinoatrial and atrio-ventricular node, the overdrive suppression ceases, which allows a secondary site to take over as the pacemaker for the heart: if it is the atrio-ventricular node, the heart has a rate of about 40 bpm; otherwise, the new site is called *ectopic focus*. The action potential of the SA node is characterized by three phases (Fig.1.14). Phase 0 represents the depolarization due to increased $g_{Ca^{2+}}$ through L-type channels, which open when the membrane depolarizes at the threshold-value of -40 mV. After that, the membrane potential moves toward the calcium equilibrium potential, resulting in a transient decrease in $g_{K^{+}}$, which contributes to the depolarization too. Depolarization increases $g_{K^{+}}$ which, in turn, repolarizes the cell toward the equilibrium potential for potassium (phase 3). At the same time, also the slow inward calcium channels contribute to the repolarization becoming inactivated, thereby decreasing $g_{Ca^{2+}}$. Phase 3 terminates when the membrane potential is about -65 mV. Phase 4 represents the spontaneous depolarization of the potential although its responsible mechanisms are not entirely clear.

[8] Heart rate is the speed of the heartbeat measured by the number of contractions (beats) of the heart per minute (bpm).

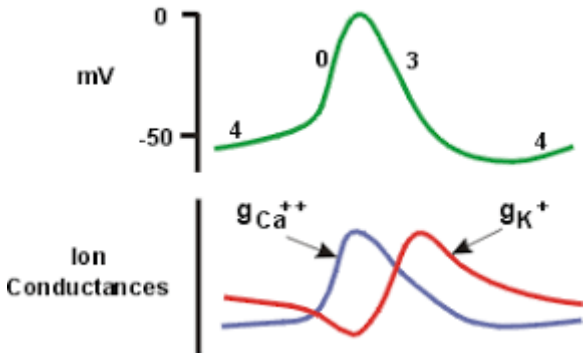

Figure 1.14 *Action Potential and conductances variations of $^{+}K$and Ca^{2+} in pacemaker cells.*

As has been said, the changes in heart rate are controlled by autonomic nerves acting on the SA node. At low resting rates, the parasympathetic (or vagal) influences are dominant over sympathetic influences. *Positive chronotropy* is defined as an increase in heart rate; on the other hand, *negative chronotropy* is defined as a reduction in heart rate. Autonomic influences modifies the pacemaker-rate by changing the slope of phase 4, by altering the threshold voltage, and by modifying the degree of hyperpolarization.

The action potential, once generated in the SA node, propagates throughout the atrial muscle with a conduction velocity of about 0.5 m/s (Fig. 1.15). This process is ensured by the *excitation-contraction coupling*, which is described in next subparagraphs.

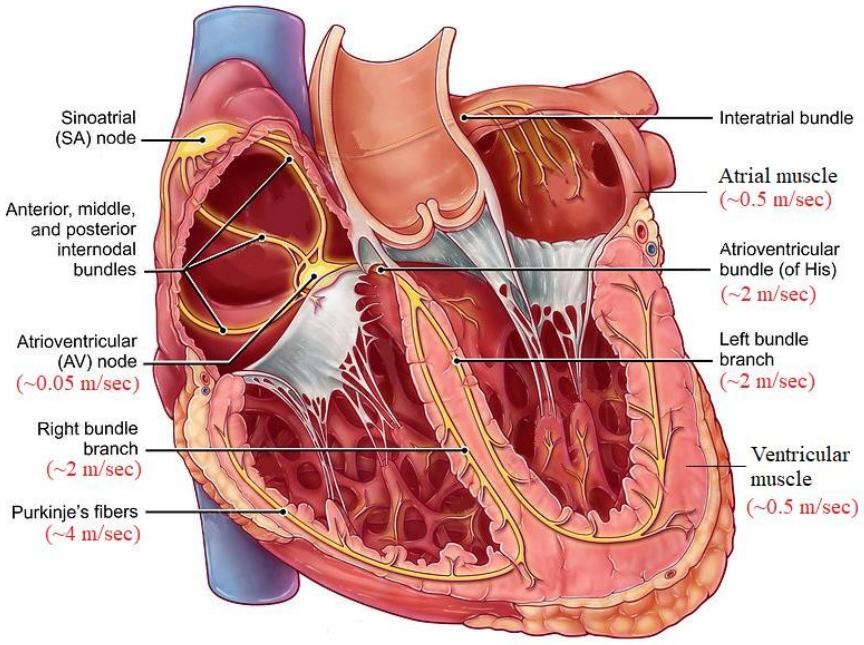

Figure 1.15 *Conduction system within the heart. Conduction velocities of different regions are noted in red in parentheses.*

1.4.2 Conduction of action potentials within the heart

The conducting pathway in the atria is facilitated by specialized myocytes called *internodal tracts* (e.g. *Bachmann bundle*). Thereafter, the action potential arrives to the AV node which slows the impulse conduction velocity to about 0.05 m/s. Afterwards, the impulse runs, first, the *bundle of His*, and then its *left and right bundle branches* along the interventricular septum. Here, the conduction velocity is about 2 m/s. Each bundle branches divide into an extensive system of *Purkinje fibers* with a velocity of 4 m/s. The action potential eventually spreads throughout the ventricular myocytes where the conduction velocity is about 0.5 m/s.

1.4.3 The electrocardiogram

Since body fluids are good conductors, the potential fluctuations representing the algebraic sums of the action potentials of the single myocardial cell, can be recorded on the torso. The recording of these fluctuations versus time is called *electrocardiogram* (*ECG*); a normal electrocardiogram presents a series of upward (positive) and downward (negative) *waves* marked with letters P, Q, R, S and T. The ECG signal, indeed, represents the continous changing of the action potentials in correlation to the cardiac cycle; the correspondance between the various sites of the conduction system and the typical elements of the ECG is shown in Figure 1.16.

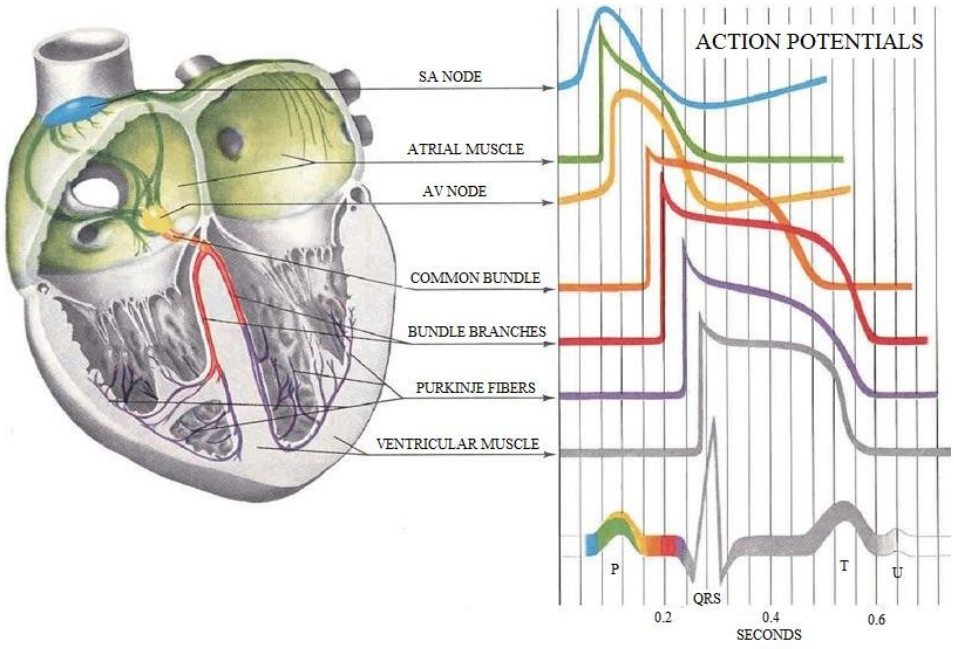

Figure 1.16 *ECG generated by the integration of the action potentials of the different sites of conduction system.*

The interval between two waves is named *tract* (or *segment*) and represents the period in which a potential difference is recorded, whereas the period which comprises both waves and tracts is called *interval* (Fig. 1.17).
The waves represent the sequence of depolarization and repolarization of the atria and ventricles. Moreover, the ECG does not measure absolute voltages, but voltages changes from a *baseline* (*isoelectric*) voltage. The *P-wave* is the first wave and represents the depolarization of the atria; indeed, the SA impulse is not recorded because its electrical activity is not enough to reach the surface of the body. The *QRS complex* is produced by the depolarization of the ventricles. It can be seen, in the ECG, that no distinctly visible wave represents atrial depolarization because it is masked by ventricular depolarization (the masked wave is simultaneous and of relatively small amplitude with respect to the QRS complex). The brief isoelectric period between the end of the P-wave and the beginning of the QRS complex corresponds to the interval in which the impulse is travelling within the AV node and is called *PR segment*. The *T-wave* identifies the ventricular repolarization and lasts longer than depolarization.

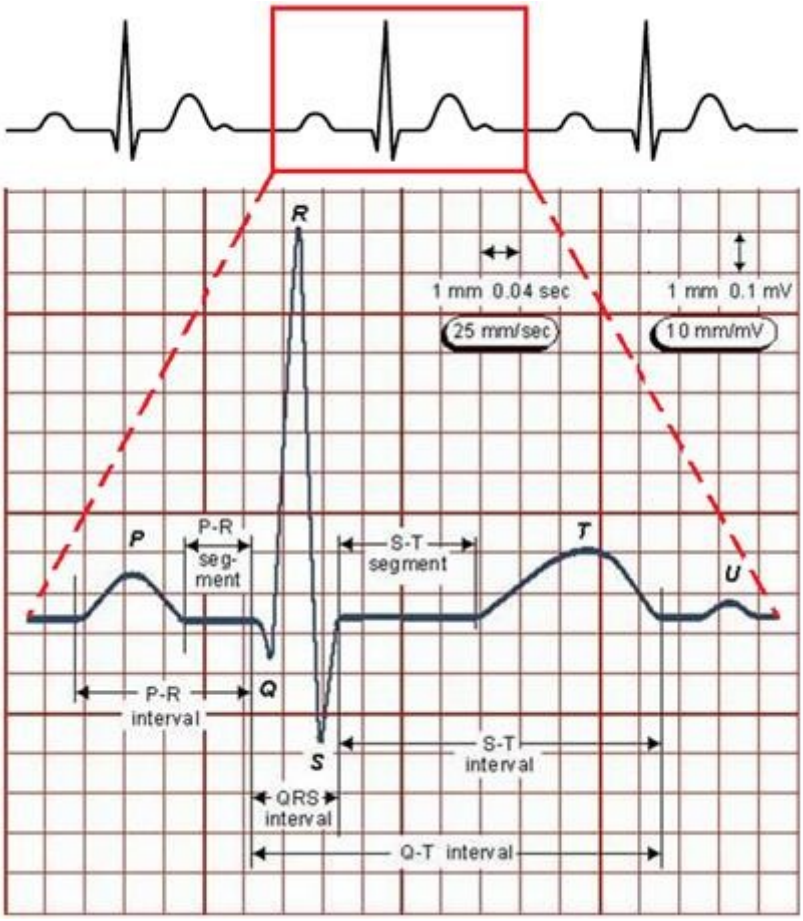

Figure 1.17 *Waves, segments and intervals of the ECG trace.*

The isoelectric period between the end of the QRS complex and the beginning of the T-wave is called *ST segment* and corresponds to the interval in which the ventricles are depolarized. The *PR interval* covers the period from the onset of the P-wave to the beginning of the QRS complex. The interval between the end of the PR segment and the beginning of the ST segment is the *QRS interval*. The *ST interval* goes from the beginning of the ST segment to the end of the T-wave. Finally, the interval between the onset of the QRS complex and the end of the T-wave is the *QT interval*. Sometimes, the T-wave is followed by another wave (called *U-wave*) representing the slow repolarization of the papillary muscles. The *RR interval* is the time elapsed between two successive R waves of the QRS signal. Table 1.2 summarizes the waves, intervals and segments of the ECG.
As has been said, the ECG records the fluctuations over time of the electrical activity within the heart. At a given instant, the recording electrodes placed on the torso detect a summation of all the regions of the heart which undergo depolarization or repolarization. To better understand this concept, figure 1.18 is taken as example: it illustrates the waves of depolarization which originate from the sinoatrial node and spread throughout the atrial muscle. When the sinoatrial node fires, several separate waves of depolarization originate from the sinoatrial node and spread throughout the atria. These independent waves are depicted, in the figure, as black arrows, and represent the individual *instantaneous electrical vectors* of depolarization. Similarly, at any given instant, many individual instantaneous electrical vectors exist; each one constitutes the conduction of the action potential in a different direction. Therefore, an *instantaneous mean electrical vector* (red arrow in the figure) can be obtained by summing the individual instantaneous vectors.
The ECG is recorded by placing an array of electrodes at specific locations on the body surface. The dutch physiologist William Einthoven was the first to describe a procedure for the placement of the electrodes. He placed them at the vertices of an equilateral triangle coincident with the *right arm* (*RA*), the *left arm* (*LA*), and the *left leg* (*LL*), as shown in figure 1.19.

Table 1.2 *Summary of ECG waves, intervals and segments [2].*

ECG component	Represents	Duration (s)	Amplitude (mV)
P wave	Atrial depolarization	0.08-0.10	0.2-0.4
QRS complex	Ventricular depolarization	0.06-0.10	1-2
T wave	Ventricular repolarization	0.18-0.20	0.4-0.5
PR interval	Atrial depolarization and AV nodal delay	0.12-0.20	-
QT interval	Ventricular depolarization and repolarization	0.20-0.40	-
RR interval	Duration of the cardiac cycle	0.80-0.90	-

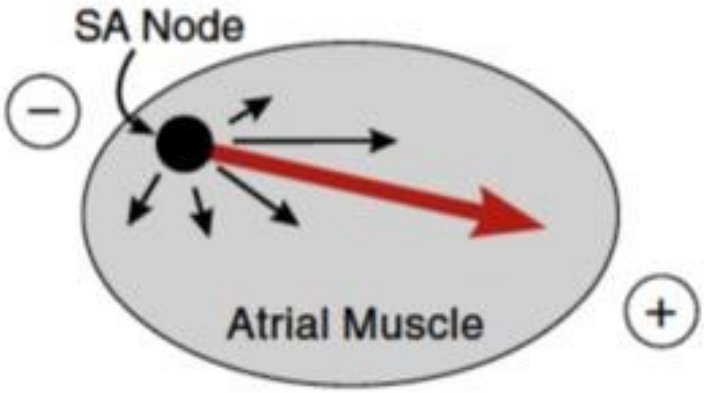

Figure 1.18 *Electrical vectors. Individual instantaneous vectors of depolarization (black arrows), and mean electrical vector (red arrow) [2].*

The potential differences measured between two electrodes are called *standard limb leads*, and referred to as *bipolar leads* because each lead uses a single pair of positive and negative electrodes.

Lead I has the positive electrode on the left arm and the negative electrode on the right arm. Lead II has the positive electrode on the left leg and the negative electrode on the right arm. Lead III has the positive electrode on the left leg and the neagtive electrode on the left arm. In these three limb leads, an additional electrode placed on the *right leg* (*RL*) is a *reference electrode* for recording purposes.

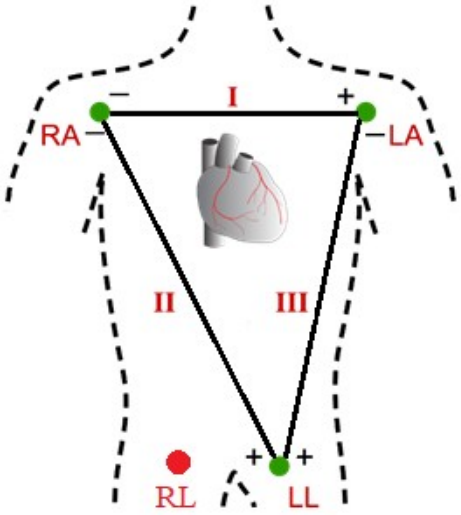

Figure 1.19 *Placement of the standard ECG limb leads (leads I, II, and III) and the location of the positive and negative recording electrodes for each of the three leads.*

Being Φ_{LA}, Φ_{RA} and Φ_{LL} the potentials detected on left arm, right arm and left leg:

$$I = \Phi_{LA} - \Phi_{RA} \tag{1.1}$$

$$II = \Phi_{LL} - \Phi_{RA} \tag{1.2}$$

$$III = \Phi_{LL} - \Phi_{LA} \tag{1.3}$$

The *Kirchoff's voltage law* (also called *Kirchoff's second law* or *Kirchoff's loop rule*) states that, at any instant, the algebraic sum of the potential differences (voltages) around any closed loop is zero; that is $I + II + III = 0$. Therefore, only two of the three standard limb leads are independent from each other.

The three *augmented limb leads* are constituted by a single positive electrode that is referenced against a combination of the other limb electrodes. The positive electrodes are located on the left arm (aV_L), the right arm (aV_R), and the left leg (aV_F). The reference potential is called *Wilson central terminal* (Φ_W), and the the augmented limb leads are said to be *unipolar*. In this case, the idea is to rely on the *Kirchoff's current law* (also called *Kirchoff's first law* or *Kirchoff's point rule*) which states that, for any node (junction) in an electrical circuit, the sum of currents flowing into that node is equal to the sum of currents flowing out of that node (or equivalently, the algebraic sum of currents in a network of conductors meeting at a point is zero). Therefore, each electrode of the triangle is connected to the Wilson central terminal by means of resistances of 5000 Ω:

$$\frac{\Phi_W - \Phi_R}{5000} + \frac{\Phi_W - \Phi_L}{5000} + \frac{\Phi_W - \Phi_F}{5000} = 0 \tag{1.4}$$

from which:

$$\Phi_W = \frac{\Phi_R + \Phi_L + \Phi_F}{3} \tag{1.5}$$

Successively, *Goldberger* calculated the Wilson potential as the average of the the other two potentials with respect to that under consideration. Therefore:

$$aV_R = \frac{-I - II}{2} \tag{1.6}$$

$$aV_L = \frac{I - III}{2} \tag{1.7}$$

$$aV_F = \frac{II + III}{2} \tag{1.8}$$

The three standard limb leads together with the three augmented leads, constitute the six limb leads of the ECG. They record the electrical activity along the *frontal plane* of the heart. If the three standard limb leads are broken apart, collapsed and superimposed over the heart (Fig. 1.20), the positive electrode for lead I is defined as being at 0° relative to the heart (along the horizontal axis). Likewise, the positive electrode for lead II is +60° relative to the heart, and the positive electrode for lead III is +120° relative to the heart. This new construction of the electrical axis is named the *axial reference system*.
The axial reference system shown in figure 1.20, also illustrates that aV_L is at -30° relative to the lead I axis; aV_R is at -150°, and aV_F is at +90°. The last six ECG leads to consider are the *precordial chest leads*, and are unipolar. Their advantage is the higher accuracy of the measure due to the close proximity of the electrodes to the heart; indeed, the electrodes are placed on the surface of the chest over the heart. They record the electrical activity in the *horizontal plane* perpendicular to the frontal plane (fig. 1.21).
The six precordial chest leads are named V_1 to V_6. Each of them is the difference between the corresponding electrode potential and the Wilson potential. V_1 is placed to the right of the sternum over the fourth intercostal space, whereas V_6 is located laterally (midaxillary line) over the fifth intercostal space. Therefore, V_1 overlies the right ventricular free wall, and V_6 overlies the left ventricular lateral wall. Figure 1.22 shows the frontal-plane leads (standard limb and augmented limb) and the horizontal-plane precordial chest leads.

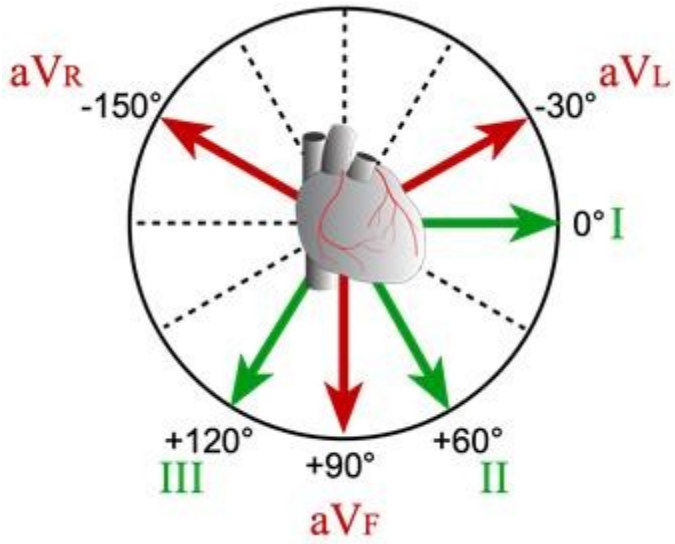

Figure 1.20 *The axial reference system showing the location within the axis of the positive electrode for each of the six limb leads.*

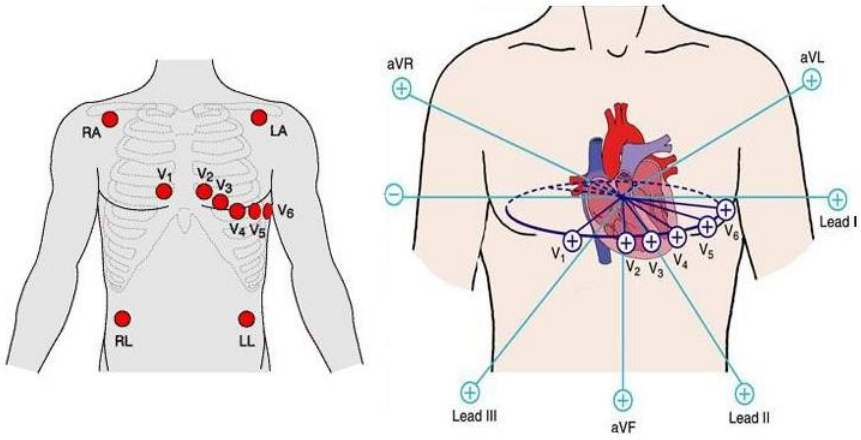

Figure 1.21 *Placement of the six precordial chest leads.*

$$V_1 = \Phi_1 - \Phi_W \tag{1.9}$$

$$V_2 = \Phi_2 - \Phi_W \tag{1.10}$$

$$V_3 = \Phi_3 - \Phi_W \tag{1.11}$$

$$V_4 = \Phi_4 - \Phi_W \tag{1.12}$$

$$V_5 = \Phi_5 - \Phi_W \tag{1.13}$$

$$V_6 = \Phi_6 - \Phi_W \tag{1.14}$$

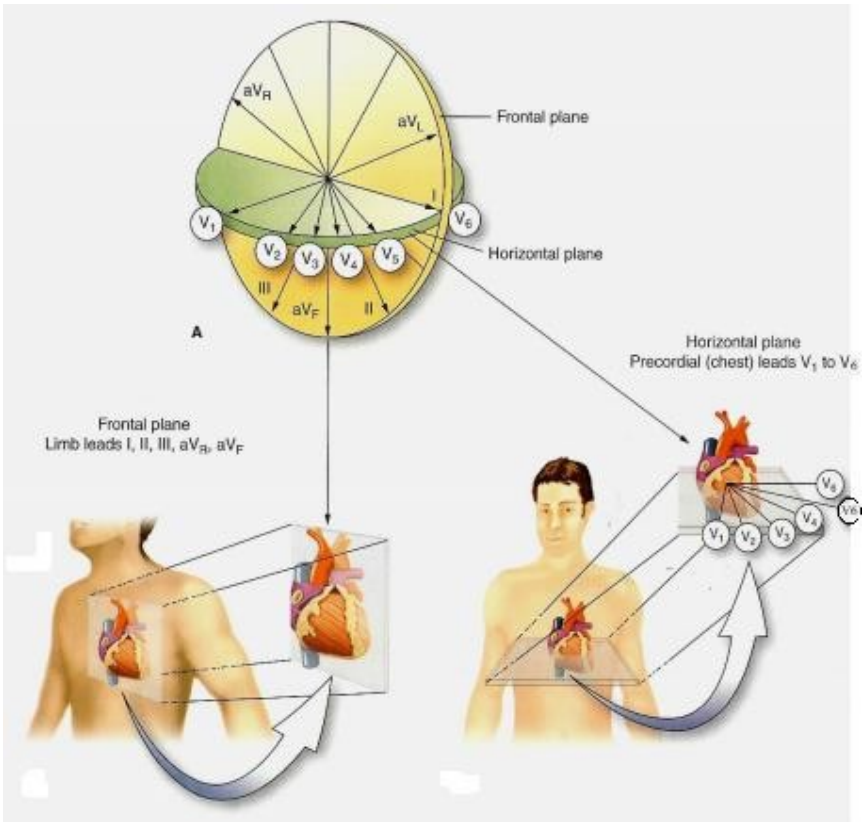

Figure 1.22 F*rontal-plane leads and horizontal-plane precordial chest leads.*

The mean electrical vector modifies, in the heart, its orientation as different regions of the heart undergo depolarization or repolarization. The direction of this vector relative to the axis between positive and negative recording electrodes determines the polarity and influences the amplitude of the recorded voltage as illustrates figure 1.23.

In general, it is possible to summurize a set of rules used in interpreting the ECG:

- a wave of depolarization traveling toward a positive electrode results in a positive deflection in the ECG trace (similarly, a wave of depolarization traveling away from a positive electrode results in a negative deflection);
- a wave of repolarization traveling toward a positive electrode results in a negative deflection (similarly, a wave of repolarization traveling away from a positive electrode results in a positive deflection);
- a wave of depolarization or repolarization oriented perpendicular to an electrode axis produces no net deflection;
- the instantaneous amplitude of the measured potentials depends upon the orientation of the positive electrode relative to the mean electrical vector;
- voltage amplitude (positive or negative) is directly related to the mass of tissue undergoing depolarization or repolarization.

Figure 1.23 illustrates the sequence of depolarization within the ventricles. The size of the red arrow is proportional to the mass of tissue that undergoes depolarization; therefore, the bigger the arrow, the greater the measured voltage by the lead.

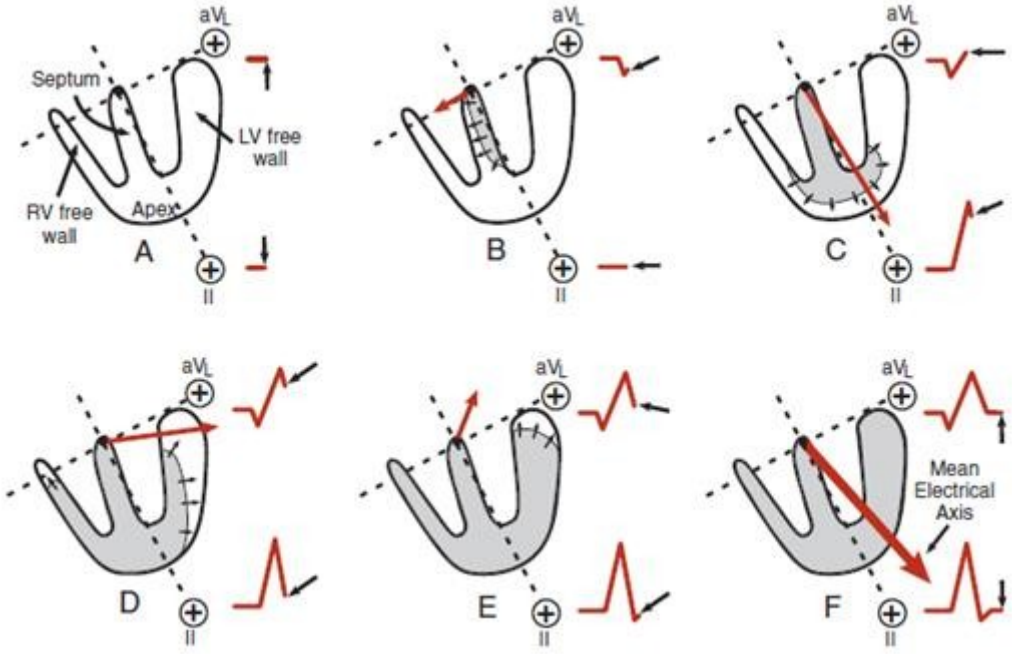

Figure 1.23 *Generation of QRS complex from two different recording electrodes [2].*

Panel F of figure 1.23 also shows the resultant vector given by the sum of the previous four mean vectors of panels B, C, D and E. This vector is called *mean electrical axis*, and represents the average of all the instantaneous mean electrical vectors occurring sequentially during ventricular depolarization. More precisely, the mean electrical axis corresponds to the axis that is perpendicular to the lead axis with the smallest net QRS amplitude. This vector is diagnostically important to identify *left and right axis deviations*, which can be caused by several pathological factors. The normal range of the mean electrical axis is between -30° and +90°. Less than -30° is considered a *left axis deviation*, whereas more than +90° is considered a *right axis deviation* (Fig. 1.24).

1.5 Cardiac function

1.5.1 The cardiac cycle

The cardiac cycle diagram illustrated in figure 1.25 (also called Wiggers diagram) is useful to understand the relationship between the sequence of mechanical events during the complete cardiac cycle and the electrical activity of the heart. In particular, it shows the trends over time of left ventricular pressure (LVP), left ventricular volume, left atrial pressure (LAP) and aortic pressure (AP). The changes in the right side of the heart are not shown because they are qualitatively similar to those in the left part, except for the pressures. Indeed, for example, the pressure in the right ventricle ranges between a minimum of 0-4 mm Hg (during filling), to a maximum of 25-30 mm Hg (during contraction).

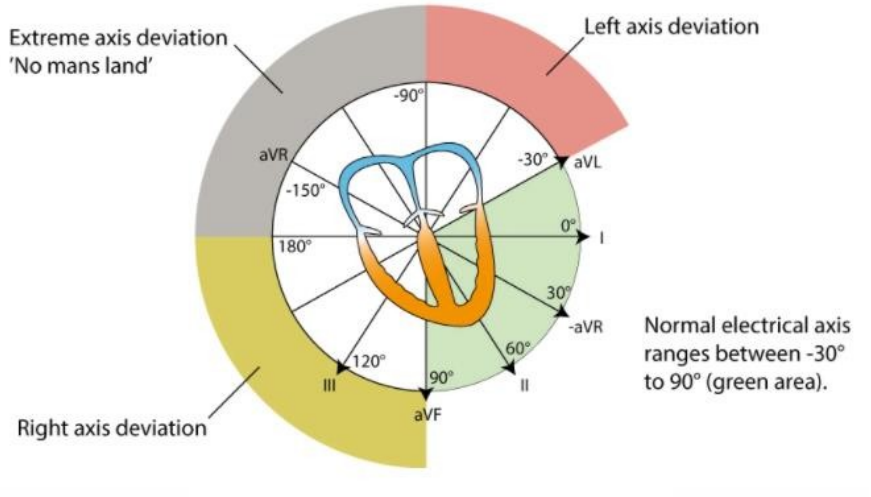

Figure 1.24 *Mean electrical axis and its possible deviations.*

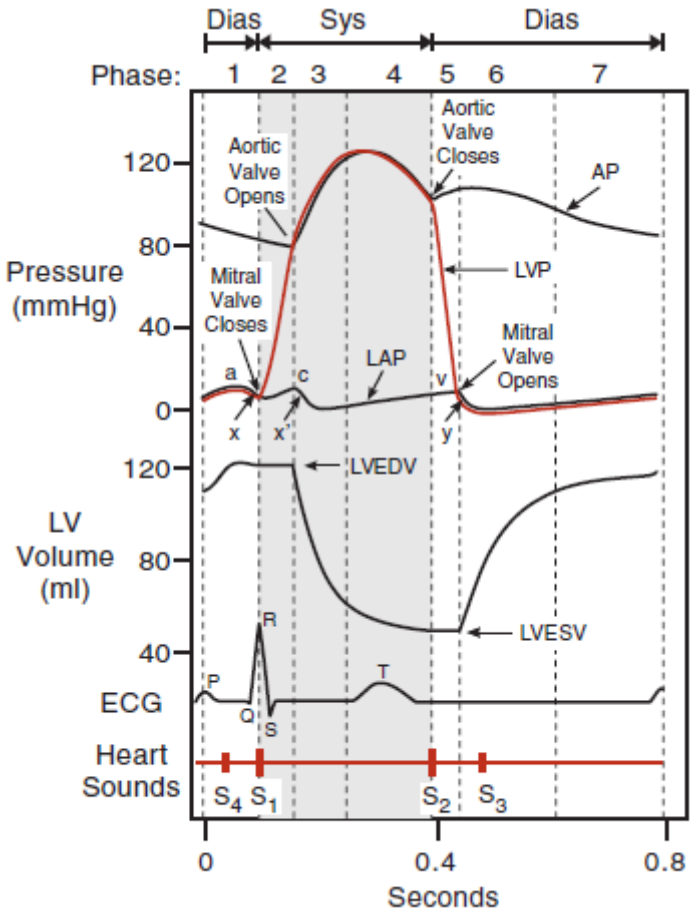

Figure 1.25 *Cardiac cycle (Wiggers diagram) with its seven phases [2].*

The first important partition of the cardiac cycle is between *systole* and *diastole*. Systole is defined as the period in which the ventricles contract and, thus, eject blood; diastole is defined as the period in which the ventricles relax and fill with blood.

Then, the cardiac cycle is further divided into seven phases, starting from the P-wave:

- atrial systole;
- isovolumetric contraction;
- rapid ejection;
- reduced ejection;
- isovolumetric relaxation;
- rapid filling and reduced filling.

During the atrial systole, the AV valves are open and the semilunar valves are closed. The P-wave triggers the contraction of the atria, whose pressures increase. These pressures causes the blood to flow from the atria to the ventricles. The atrial contraction produces a small transient increase in both atrial pressures called "*a wave*". Under resting

condition (low HR), the atrial contraction accounts for only the 10% of the left ventricular filling: indeed, most of the filling is passive and occurs before the atrial contraction. On the other hand, during exercise (high HR), the contribution of the atrial contraction to the ventricular filling rises up to the 40%. Moreover, the atrial contribution is enhanced by an increase in the force of atrial contraction, which is under the influence of the sympathetic nerve activation.

After the completion of the atrial contraction, the pressure begins to decrease resulting in the *x-descent*. The *end-diastolic volume* (*EDV*) is defined as the amount of blood in a ventricle immediately before the contraction, at the end of diastole; in the left ventricle (LVEDV) is typically about 120 mL. The isovolumetric contraction is considered the beginning of the systole, and it is triggered by the QRS complex.

The depolarization of the ventricles increases the intraventricular pressure which, in turn, causes the closure of the AV valves (intraventricular pressure exceeds atrial pressure). During this phase, the *first heart sound* (S_1) is heard due to the closure of the AV valves; more precisely, this sound is split (about 0.04 seconds) because mitral valve closure precedes tricuspid valve closure, even if these events are heard as a single sound. This phase is called "isovolumetric" because the the abrupt rise in ventricular pressure is not accompanied by a change in the ventricualar volume: indeed, there is no ejection of blood by the ventricles into their corresponding arteries. Atrial pressures increase resulting in a "*c wave*".

The semilunar valves open only when the interventricular pressures exceeds the pressures in the aorta and pulmonary artery. This permits the ejection of the blood out of the ventricles. Therefore, ventricular pressures continue to increase until they exceed the respective outflow tract pressure by only few mm Hg; typical maximal values are about 120 mm Hg in the aorta and 25 mm Hg in the pulmonary artery. At the same time, atria continue to fill with blood but, even if atrial volumes increases, atrial pressures initially decrease due to the downward traction of the heart base, resulting in the *x'-descent*. The opening of the semilunar valves are silent. The phase described above is the rapid ejection.

The reduced ejection is triggered by the T-wave. This latter causes the relaxation of the ventricles with the subsequent reduction of the rate of ejection. Ventricular pressure slightly decreases below the outflow tract pressure; however, the ventricular volume continues to fall due to the kinetic (or inertial) energy of the blood into the outflow tracts. Atrial pressures increase due to the respective venous return. This phase concludes systole.

The beginning of the diastole si accompanied by the second heart sound (S_2), which is split due to the closure of the aortic valve before that of the pulmonary valve. This fifth

phase is called isovolumetric relaxation because, even if the pressure of the ventricles decrease, their volumes remain constant: indeed, all valves are closed. The *end-systolic volume* (*ESV*) is defined as the residual volume of blood that remains in a ventricle after ejection. Its typical value for the left ventricle (LVESV) is approximately 50 mL. The *stroke volume* (*SV*) is defined as the difference between EDV and ESV:

$$SV = EDV - ESV = 120 - 50 = \sim 70\ mL \tag{1.15}$$

Normally, about the 60% of the EDV is ejected. The *ejection fraction* (*EF*) is defined as the ratio between the SV and the EDV:

$$EF = \frac{SV}{EDV} \tag{1.16}$$

Normally, EF is higher than 0.55 (55% of the EDV). During this period, atrial pressures and volumes continue to increase due to the venous return.

The sixth phase is the rapid filling. The ventricular pressures fall below the atrial pressures; therefore, the AV valves open and the ventricles begin to fill. However, in the early phase, the ventricles are still relaxing, resulting in a further decrease in intraventricular pressures despite the ongoing passive filling. Once the relaxation is completed, the pressures begin to increase as the ventricles fill. The *v-wave* is defined as the peak of the atrial pressure,and occurs just before the valve opening. This wave is immeditaley followed by the *y-descent* representing thr blood that leaves the atria. normally, no sounds are heard in this phase; if a *third heart sound* (S_3) is present, it corresponds to the tensing of the chordeae tendineae and the AV ring. Despite this sound is normal in children, it is considered pathologic in adults.

The last phase is the reduced filling (also called *ventricular diastasis*) during which the ventricles continue to fill. This causes an increase in the ventricular pressures. Since the intraventricular pressure reduces the pressure gradient across the AV valve, the rate of filling decreases despite a further increase in atrial pressures. Pulmonary artery and aortic pressures continue to decrease.

It is necessary to specify that the cardiac cycle represented in figure 1.24 is relative to an HR of about 75 bpm. Higher heart rates (for example, during exercise) reduce the overall cycle length (reduction of the duration of both systole and diastole). More precisely, the duration of the diastole decreases much more than that of the systole; therefore, compensatory mechanism (see chapter 2) are needed in order to maintain adequate ventricular filling.

Figure 1.26 shows the normal values of the intracardiac pressures as well as those within the veins and arteries entering and leaving the heart.

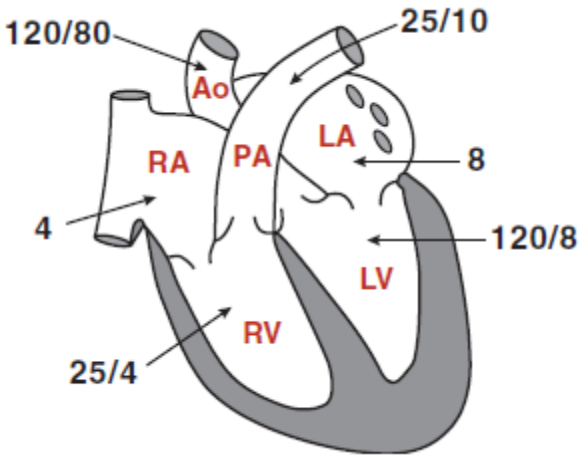

Figure 1.26 *Normal pressures within the cardiac chambers and great vessels expressed in mm Hg. Ao, aorta; RA, right atrium; RV, right ventricle; LV, left ventricle; LA, left atrium; PA, pulmonary artery. Higher values in Ao, PA, RV, and LV represent systolic pressure; lower values represent end-diastolic pressures. Pressures in RA and LA represent average values during the cardiac cycle.*

An evident difference between the right side and the left side can be immediately noted; moreover, the pressure values in the pulmonary circulation are lower than those in the systemic circulation.

The cardiac cycle can also be analyzed by the so-called *pressure-volume loops* (figure 1.27) generated by plotting the left ventricular pressure against the left ventricular volume.

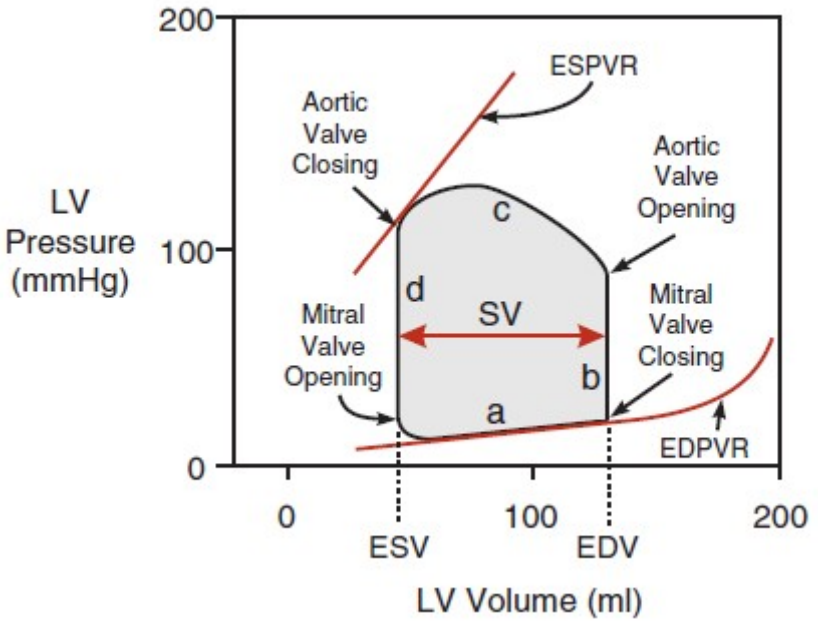

Figure 1.27 *Ventricular pressure-volume loops. a, ventricular filling; b, isovolumetric contraction; c, ventricular ejection; d, isovolumetric relaxation [2].*

The *ventricular stroke* (SV) work is defined as the area within the pressure-volume loop. The graph shows how the filling phase moves along the *end-diastolic pressure-volume relationship* (*EDPVR*). The slope of this curve is the reciprocal of ventricular *compliance*[9]. On the other hand, the *end-systolic pressure-volume relationship* (*ESPVR*) describes the maximal pressure that can be developed by the ventricle at any given ventricular volume.

1.5.2 Cardiac output

The *cardiac output* (*CO*) is the product of the SV by the HR (Eq. 1.17), and represents the volume of blood being pumped by the left ventricle per unit time.

$$CO = SV \cdot HR \tag{1.17}$$

Therefore, a change in SV or HR influences the CO. The measure unit for CO is either millileters/minute (mL/min) or liters/minute (L/min). Co, for an adult in resting condition, is about 5-6 L/min.
CO is also expresses as a *cardiac index* defined as the ratio between CO and the estimated body surface area (BSA) in square meters (m^2). BSA can be estimated using different formulas, among which the *Mosteller formula* (Eq. 1.18).

$$BSA = \sqrt{cm \cdot \frac{Kg}{3600}} \tag{1.18}$$

where cm is the height and Kg is the weight of the individual.

The advantage of the cardiac index is that it normilizes the CO to individuals of different size. A normal range for the cardiac index ranges from 2.6 to 4.2 L/min/m^2.
Usually, CO is measured using indirect methods such as the *thermodilution technique* [10], the *Doppler echocardiography*[11], and the *Fick method*. The Fick principle (Eq. 1.19) calculates the time-averaged CO from measurements of *arterial blood oxygen content* (CaO_2; mL O_2 /mL blood), *venous blood oxygen content* (CvO_2; mL O_2 /mL blood), and the *whole body oxygen consumption* ($\dot{V}O_2$; mL O_2 /min):

$$CO = \frac{\dot{V}O2}{(CaO2 - CvO2)} \tag{1.19}$$

[9] Ventricular compliance refers to the distensibility of the relaxed ventricle.
[10] Thermodilution method uses a special multilumen, thermistor-tipped catheter (Swan-Ganz) inserted into the pulmonary artery from a peripheral vein.
[11] Doppler echocardiography permits to estimate the real-time changes in flow within the heart (SV); this value, multiplied by the HR, allows to determine the CO.

Changes in HR have an higher weight in the determination of CO with respect to the SV. Indeed, HR may have an increase from 100% to 200% (for example during exercise), whereas SV may increase by less than 50%. On the other hand, a change in HR does not necessarily have a proportional response in CO. Indeed, an increase of HR from 70 bpm to 140 bpm due to a pacemaker stimulation, does not double the CO because HR also lowers SV (the decreased diastole period decreases the ventricular filling). However, during exercise, a doubling of HR causes a more than doubling of CO because also SV actually increases. Thus, it is important to understand the mechanisms that regulate SV.

1.5.3 Preload, afterload, inotropy and stroke volume

Preload is defined as the initial stretching of the cardiac myocytes prior to contraction, hence it concerns the length of the sarcomeres at the end of the diastole. Since it is impossible to determine the sarcomere length in real time, other measures are used in order to analyze the effects of changes in preload on SV, such as the EDV and the end-diastolic pressure (EDP).

The *compliance* of the ventricle is defined as the ratio between a change in volume and a change in pressure, and it is determined by the physical properties of the myocardial tissue. The lower the compliance, the ventricle becomes stiffer. This means that compliance and stiffness are reciprocally related. Decreased compliance increases the EDP at a given EDV, whereas increased compliance decreases EDP at a given EDV. Ventricular hypertrophy is characterized by an increased muscle thickness which decreases compliance. In summary, it can be said that preload (represented by the sarcomere length) depends on EDV which, in turn, depends on EDP and compliance, even if this interpretation is not so correct.

The *Frank-Starling mechanism* (Fig. 1.28) states that increasing venous return and ventricular preload leads to an increase in SV. Indeed, an increase in venous return causes an increase in ventricular filling which, in turn, increases the preload. The increased stretching of the myocytes (increased preload) increases the generated force, resulting in an increase of the blood ejected by the heart: this causes an increases in SV.

The most important factors influencing ventricular preload are: venous pressure, ventricular compliance, heart rate, atrial contraction, inflow resistance, outflow resistance and ventricular inotropy.

Afterload is defined as the “load” against which the heart must contract to eject blood. Therefore, an important component for the left ventricle is represented by the aortic pressure, which has to be overcome by the ventricular pressure.

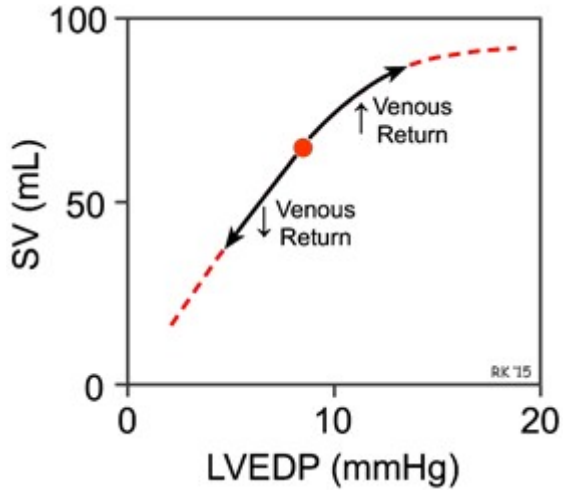

Figure 1.28 *Frank-Starling mechanism [2].*

Afterload can be estimated by examining the ventricular wall stress (σ), which depends on intraventricular pressure (P), ventricular radius (r) and wall thickness (h):

$$\sigma \alpha \frac{P \cdot r}{h} \tag{1.20}$$

Increased afterload decreases the velocity of fiber shortening. Moreover, an increase in afterload decreases SV. This is translated, in the Frank-Starling curve, in a displacement towards the right and downwards (Fig. 1.29). An increase in afterload at a constant preload (EDV), increases the ESV resulting in a decrease in SV. Indeed, the ventricle generates an increase in pressure in order to overcome the increased aortic pressure. Ventricular SV is influenced not only by changes in preload and afterload, but also by changes in inotropy.

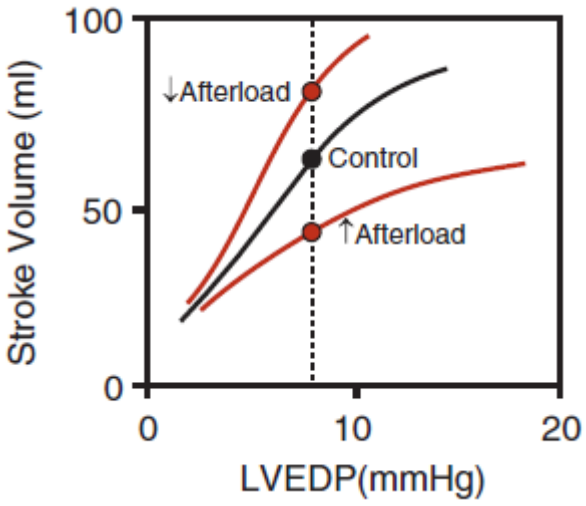

Figure 1.29 *Effects of aterload on Frank-Starling curves [2].*

An increase in inotropy increases the force of myocyte contraction independently of changes in either preload or afterload. Furthermore, increased inotropy augments the velocity of contraction. An increase in inotropy at a given preload, increases SV, and shifts the Frank-Starling curve upwards (Fig. 1.30). The increased rate of ventricular pressure development (dP/dt) caused by the increase in velocity of fiber shortening, increases EF and SV and reduces ESV. Therefore, EF is often used as a clinical index in the evaluation of inotropic state of the heart.

It is also important to analyze the interdependence of preload, afterload and inotropy (Fig. 1.31). The increased SV caused by an increase in preload, increases CO which, in turn, leads to an increase in SVR. The increased arterial pressure increases afterload. Moreover, the increased EDV increases ventricular wall stress, which represents an increase in afterload. Instead, if an increase in afterload is accompanied by an increase in preload, the result is a small increase in ESV, which attenuates the increase in SV (Panel A of figure 1.31). Increased afterload causes a decrease in SV and an increase in ESV. However, the increased ESV also increases EDV because, inside the ventricle, the ESV is summed to the venous return. This results, after several beats, in a decrease in the difference between EDV and ESV (represented by the width of the pressure-volume loop in panel B of figure 1.31). Moreover, this increase in preload following the increase in afterload, activates the Frank-Starling mechanism which attenuates the reduction in SV. Increased SV caused by an increase in inotropy, increases CO and arterial pressure which, in turn, increases afterload. Increased afterload increases ESV, which compensates the effects of increased inotropy on ESV. Moreover, decreased ESV causes a reduction of EDV because less blood remains in the ventricle that is, then, added to the venous return. Therefore, the net effect of these alterations, is an increase in SV, a reduction in ESV, and a decrease in EDV (Panel C of figure 1.31).

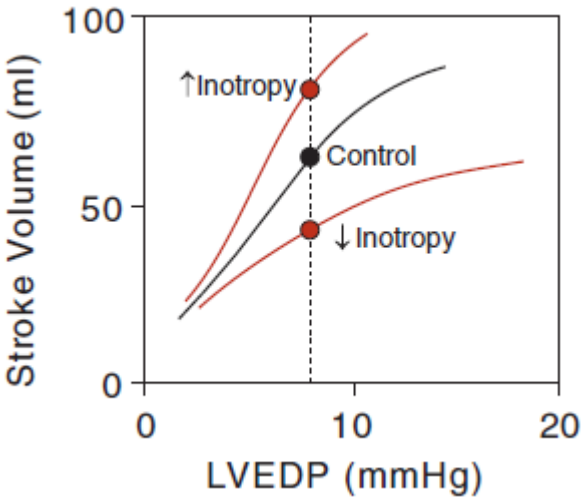

Figure 1.30 *Effects of inotropy on Frank-Starling curves [2].*

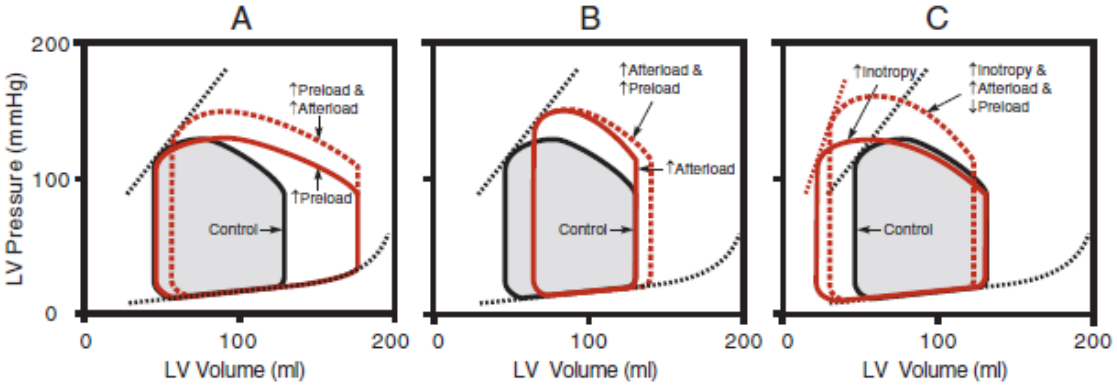

Figure 1.31 *Interdependent effects of changes in preload, afterload and inotropy on left ventricular pressure-volume loops. Panel A: continous red line, effects of increasing preload (EDV); dashed red line, effects of increasing preload (EDV) with secondary increase in afterload (aortic pressure). Panel B: continous red line, effect of increasing afterload; dashed red line, effects of increasing afterload with secondary increase in preload. Panel C: continous red line, effects of increasing inotropy; dashed red line, effects of increasing inotropy with secondary changes in preload and afterload [2].*

1.5.4 Myocardial oxygen consumption

It has been seen how changes in preload, afterload and inotropy alter the SV. However, it must be said that changes in SV, together with changes in heart rate, influence the oxygen consumption of the heart. Indeed, the heart needs to regenerate a huge amount of ATP during both contraction and relaxation at the expense of this consumption of oxygen. Moreover, also noncontracting cells require oxygen for the synthesis of ATP.
Oxygen consumption is defined as the volume of oxygen consumed per minute, and it is usually expressed per 100 g of tissue weight (mL O_2/min per 100 g). In particular, the myocardial oxygen consumption ($M\dot{V}O_2$) is calculated based on the Fick principle:

$$M\dot{V}O_2 = CBF \cdot (CaO_2 - CvO_2) \tag{1.21}$$

where CBF is the coronary blood flow, CaO_2 is the arterial oxygen content, and CvO_2 is the venous oxygen content.
Typical values for a heart contracting at a resting heart rate are 80 mL O_2/min per 100 g for CBF, 0.2 mL O_2/mL blood for CaO_2, and 0.1 mL O_2/mL blood for CvO_2, resulting in a $M\dot{V}O_2$ of about 8 mL O_2/min per 100 g. During exercise, however, myocardial oxygen consumption can increase up to 70 mL O_2/min per 100 g. Since direct measures of CBF and venous oxygen content are not feasible except in experimental studies, indirect indices are used such as the *pressure-rate product* (also called the double product). This

index can be non-invasively calculated multiplying the heart rate by the systolic arterial pressure (also mean arterial pressure sometimes is used).
Several factors affect myocardial oxygen consumption, among which frequency of contraction, inotropic state, afterload and preload. Doubling heart rate approximately doubles oxygen consumption due to double myocytes generation with respect to number of tension cycles per minute. Also increased inotropy causes an increase in myocardial oxygen consumption because both rate of tension development and magnitude of tension are increased. Increased afterload, likewise, increases oxygen consumption due to the tension that myocytes must develop. Similarly, increased preload increases oxygen consumption, even if it has less impact than that of afterload.

1.6 Vascular function

1.6.1 Anatomy and function

The vascular network, which distributes the blood throughout the body, is divided into the arterial part and the venous part. The arterial network extends from the aorta to the capillaries (the smallest vascular vessels); the venous network extends from capillaries to the inferior and superior vena cava (Fig. 1.32). The different blood vessels comprised in the vascular network, can be also classified from a functional point of view: distribution/resistance function, exchange function, and capacitance function.
The *aorta*, the biggest vessel of the vascular network, dampens the pulsatile pressure caused by the ejection of blood from the left ventricle. The dampening function depends on the compliance of the aortic vessel. *Large arteries*, which branch off the aorta, direct the blood flow to specific organs. Being elastic (they are made up by elastin and collagen), they accommodate SV and smooth the blood flow by means the *windkessel effect*[12]. *Small arteries*, which branch off the large arteries, distribute the blood within the organs. If these small arteries have a diameter lower than 200 μm, they are called *arterioles*. Small arteries, together with arterioles, constitute the resistance vessels. They are highly innervated by autonomic nerves; that is, they constrict or dilate in response to changes in nerve activity. They are rich of hormones-receptors which also influences vessel diameter. If arteries have a diameter lower than 10 μm, they lose their smooth muscle, and are called *capillaries.* They have the greatest surface are for exchange.
Capillaries converge into small, postcapillary *venules*. They also are devoid of smooth muscle, and have exchange function of fluid and macromolecules. Postcapillary venules, in turn, converge into larger *venules*, which are constituted instead also by smooth muscle.

[12] Windkessel effect refers to the compliance of the aorta with the arterial pressure wave, produced by the ejection volume from the left ventricle.

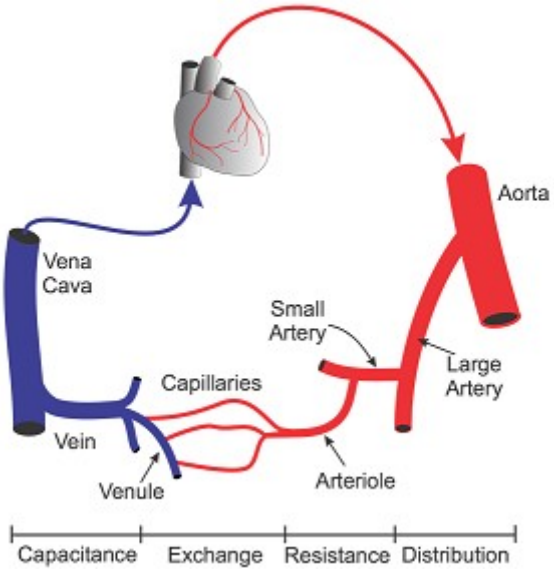

Figure 1.32 *Major types of blood vessels found within the circulation.*

They, similarly to arteries and arterioles, dilate and constrict. Venules converge into larger *veins*. Veins, together with venules, are the capacitance vessels. The final venous vessels are the inferior and superior vena cavae, which transport the blood into the right atrium. The highest mean blood pressure in found in the aorta (about 95 mm Hg); this value progressively decreases as the blood flows away from the heart. This drop in pressure is due to the loss of energy as heat of the circulating blood. Indeed, according to equation 1.24, the pressure drop (ΔP) is related to blood flow (F) and resistance to the flow (R):

$$\Delta P = F \cdot R \qquad (1.22)$$

The biggest drop in pressure occurs in the small arteries and arterioles because these vessels have a high resistance relative to their blood flow. Indeed, approximately 50% to 70% of the pressure drop occurs within the resistance vessels.
The greatest volume (60% to 80%) of blood within the systemic circulation resides within the venous vessels (venules, veins, superior vena cava and inferior vena cava). This is the reason why these vessels are called capacitance vessels.

1.6.2 Arterial blood pressure

Figure 1.33 shows the waveform of the aortic pressure pulse due to the ejection of blood into the aorta. The aortic *pulse pressure* is defines as the difference between the systolic pressure and the diastolic pressure.

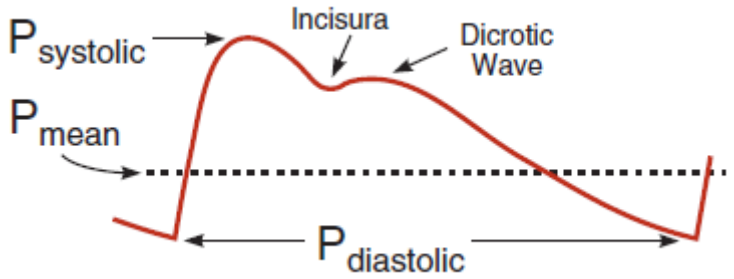

Figure 1.33 *Pressure pulse within the aorta [2].*

The *systolic pressure* corresponds to the peak pressure of the aortic pressure; the *diastolic pressure* is the minimal value of the aortic pressure. The peak of the systolic pressure, in particular, is followed by a small increase in pressure called *dicrotic wave*. Therefore, the same factors that influence both systolic and diastolic pressure (measured by means of a *sphygmomanometer*[13]), also alter the pulse pressure. The pressure that drives blood into organs is called *mean arterial pressure* (*MAP*), and is the average pressure of the pulse pressure over time. At normal resting heart rates, MAP can be estimated using equation 1.25:

$$MAP = P_{dias} + \frac{1}{3}(P_{sys} - P_{dias}) \tag{1.23}$$

Equation 1.23 explains that MAP is calculated based on a geometric mean and not on an arithmetic mean. However, at higher heart rates, MAP is approximated by an arithmetic average; indeed, the period of diastole shortens more than does systole. There is no a typical standard value for MAP; in children, it is only 70 mm Hg, whereas in adults, it may be 100 mm Hg. Also increasing age influences the value: systolic pressures increases more than diastolic pressure, resulting in an increase in pulse pressure. The most important factors affecting MAP are CO, *systemic vascular resistance* [14](*SVR*) and *central venous pressure* [15](*CVP*):

$$MAP = (CO \cdot SVR) + CVP \tag{1.24}$$

[13] A sphygmomanometer is composed of an inflatable cuff to collapse and then release the artery under the cuff in a controlled manner, and a mercury or aneroid manometer to measure the pressure. Manual sphygmomanometers are used with a stethoscope when using the auscultatory technique.
[14] Systemic vascular resistance is the resistance to blood flow offered by the systemic circulation.
[15] Central venous pressure describes the pressure in the thoracic vena cava near the right atrium.

CO, SVR and CVP are constantly changing, and they are interdependent. For example, an increase in SVR increases the afterload which, in turn, decreases CO and affects CVP. Moreover, these variables are also influenced by extrinsic control mechanisms (such as standing).
The change in the shape of the pressure pulse depends on several factors including decreased compliance of distal arteries and reflective waves which travel down the aorta and arteries. Furthermore, MAP decreases as the pressure pulse goes through distributing arteries. This means that the values measured for arterial pressure depends on the site of the measurement. *Compliance* (C) is defined as the ratio between the change in volume (ΔV) and the change in pressure (ΔP) at a given pressure:

$$C = \frac{\Delta V}{\Delta P} \tag{1.25}$$

In summary, an increase in aortic pulse pressure is due to both an increase in stroke volume or a decrease in aortic compliance. Decreased aortic compliance is due to factors such as age, arteriosclerosis and hypertension. Stroke volume is increased by an increase in preload, increased inotropy, a decrease in afterload and a decrease in heart rate.

1.6.3 Hemodynamics

Hemodynamics describes the physical factors governing blood flow within the circulatory system. Equation 1.24 explains how blood flow through an organ is determined by the pressure gradient driving the flow and by the resistance to flow. Blood flow is mainly determined by changes in resistance. Three factors affect the resistance (R): the vessel length (L), the blood viscosity (η) and the radius of the vessel (r):

$$R\alpha\frac{\eta \cdot L}{r^4} \tag{1.26}$$

1.6.4 Systemic vascular resistance

Systemic vascular resistance (*SVR*) is the resistance to blood flow offered by all of the systemic vasculature. It depends on CO, MAP and CVP:

$$SVR = \frac{(MAP - CVP)}{CO} \tag{1.27}$$

1.6.5 Venous blood pressure

Central venous pressure (*CVP*) describes the blood pressure in the thoracic vena cava near the right atrium. Several factors affect CVP, including CO, respiratory activity, contraction of skeletal muscles (in particular leg and abdominal muscles), sympathetic vasoconstrictor tone, and gravitational forces. All of these factors alter CVP (ΔP_v) by changing either venous blood volume (ΔV_v) or venous compliance (C_v):

$$\Delta P_v \alpha \frac{\Delta V_v}{C_v} \tag{1.30}$$

During exercise, the rhytmic muscular contraction (in particular, contraction of the limbs) compresses the veins and facilitates the venous return into the thoracic compartment, resulting in an increase in CVP. Indeed, veins contain one-way valves which allows blood flow toward the heart preventing retrograde flow (Fig. 1.34).

1.6.6 Venous return and cardiac output

Venous return is the flow of blood back to the heart. The return to the right atrium is determined by the pressure gradient between the abdominal vena cava and the right atrium, divided by the resistance of the vena cava.
Figure 1.35 shows the effects of cardiac output on mean aortic pressure and right atrial pressure. P_{mc} is the *mean circulatory filling pressure*, and represents the pressure throughout the vascular system when there is no blood flow. Its value depends on both the vascular compliance and blood volume.

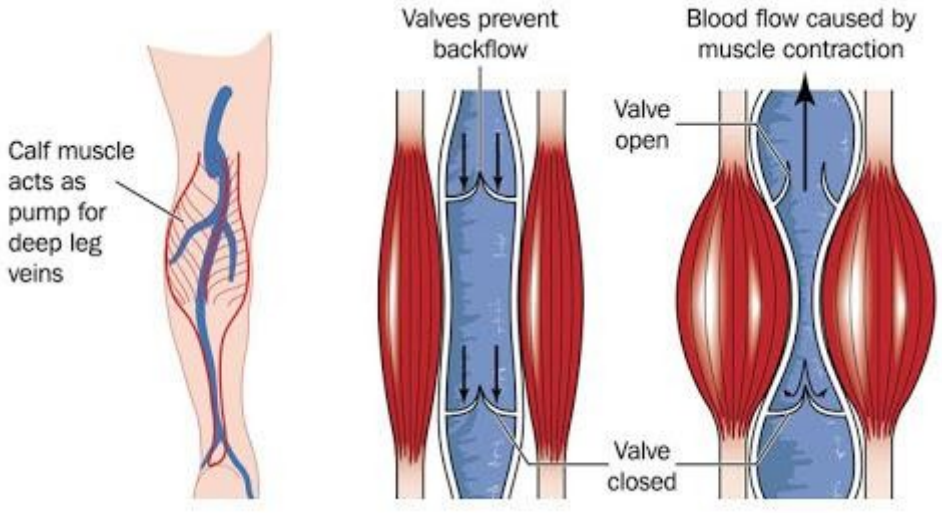

Figure 1.34 *Skeletal muscle contraction compresses veins propelling blood toward the heart.*

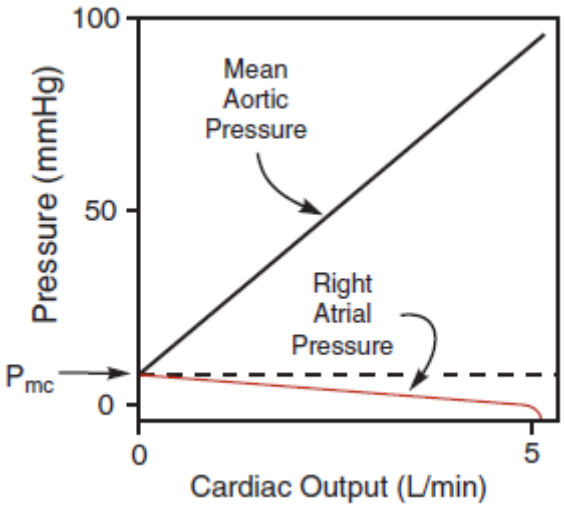

Figure 1.35 *Effects of cardiac output on mean aortic pressure and right atrial pressure [2].*

When CO is null, mean aortic pressure and right atrial pressure equilibrate at P_{mc}. Decreased CO results in an increase in right atrial pressure and in a decrease in mean aortic pressure.

Figure 1.36 illustrates the *systemic vascular function curves* obtained plotting cardiac output versus the right atrial pressure. These curves result from influences of either cardiac output on right atrial pressure or right atrial pressure on venous return. Panel A shows how increased blood volume (Vol) or decreased venous compliance (Cv) causes a shift of the systemic vascular function curve towards the right.

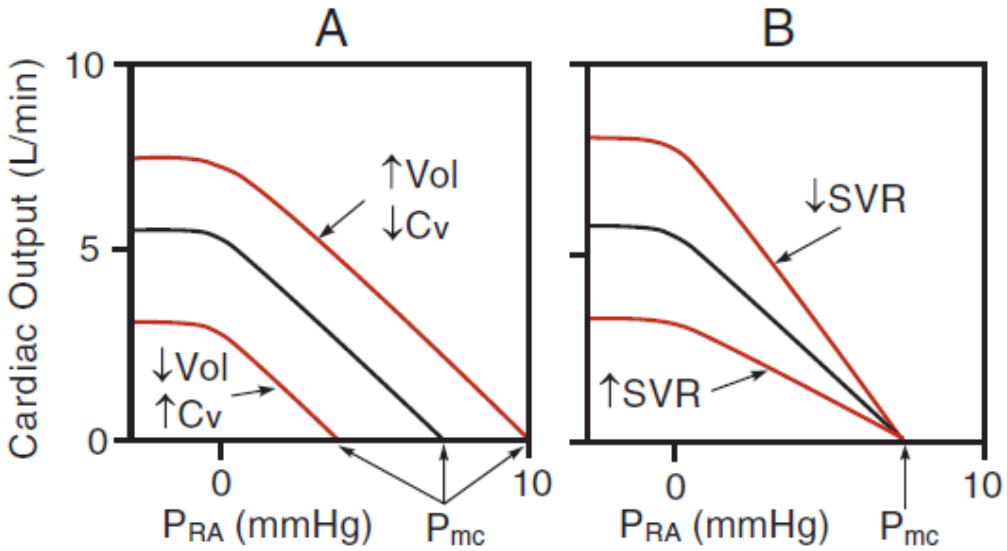

Figure 1.36 *Systemic function curves. Panel A: effects of changes in cardiac output on right atrial pressure and mean circulatory filling pressure. Panel B: alteration of the slope of the systemic function curves due to changes in systemic vascular [2].*

This causes an increase in the mean circulatory filling pressure (P_{mc}). Viceversa, decreased blood volume or increased venous compliance causes a shift of the curve towards the left and a decrease in P_{mc}. Panel B shows how decreased SVR increases the slope without changes in P_{mc}. Increased SVR decreases the slope while keeping the same P_{mc}. Therefore, at a given CO, a decrease in SVR decreases right atrial pressure. Therefore, at a given cardiac output, increased blood volume (or decreased venous compliance) causes an increase in right atrial pressure.

Figure 1.37 illustrates the cardiac function curves plotted versus the right atrial pressure; according to the Frank-Starling relationship, increased right atrial pressure increases cardiac output. Also changes in heart rate influences the cardiac function curve. With a normal function curve, the cardiac output is about 5 L/min at a right atrial pressure of about 0 mm Hg. An increase in heart rate or in inotropy or a decrease in afterload, shifts the cardiac function curve upward and towards the left.

On the other hand, a decrease in heart rate or in inotropy or an increase in afterload, decreases the cardiac output at any given right atrial pressure. It must be taken into consideration that the entity of the cardiac output changes is largely determined by the state of systemic vascular function.

Figures 1.36 and 1.37 plotted together explain how cardiac and vascular functions are coupled. Point A of figure 1.38 represents the equilibrium point which defines the relationship between cardiac and vascular function. Indeed, the heart works at this equilibrium until one or both curves change. For example, point B represents an increase in cardiac output and a decrease in right atrial pressure caused by a stimulated heart rate or inotropy. Point C represents a further decrease in venous compliance, resulting in an increase in cardiac output. Point D represents a further decrease in systemic vascular resistance, resulting in an increase of cardiac output.

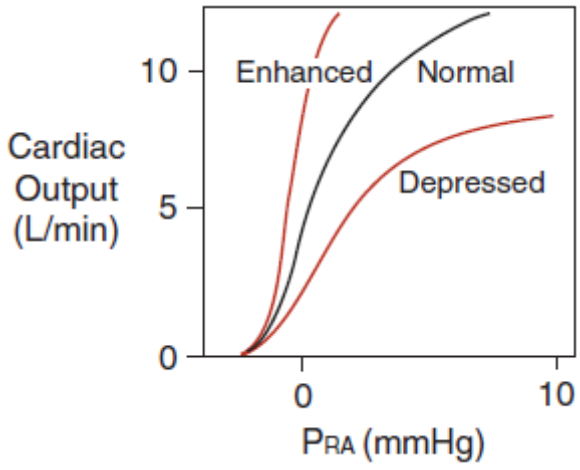

Figure 1.37 *Cardiac function curves [2].*

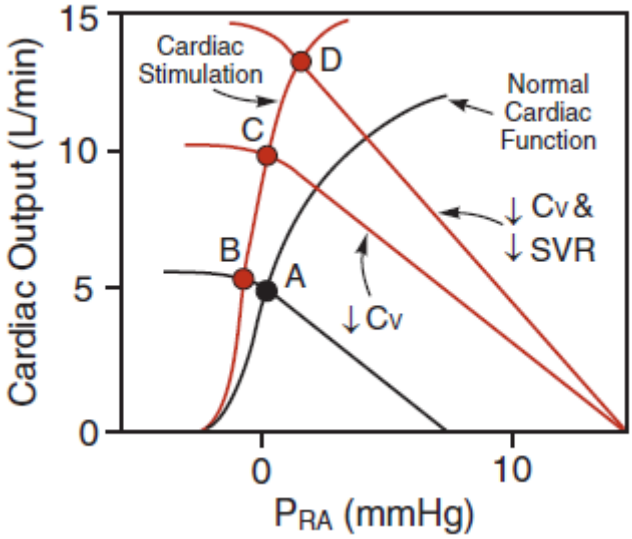

Figure 1.38 *Combined cardiac and systemic function curves: effects of exercise [2].*

Changes in venous compliance and systemic vascular resistance, which occur during exercise, result in an increase in cardiac output. In summary, in the normal heart, cardiac output is limited by factors that determine vascular function.

Chapter 2

Cardiovascular monitoring of the athlete

"Exercise should be regarded as tribute to the heart"
[Gene Tunney]

2.1 Cardiovascular responses to exercise

2.1.1 Introduction

Previous chapter deepened physicological concepts concerning both cardiac and vascular function in normal resting states. The aim of this chapter is to integrate these concepts and to analyze the response of the cardiovascular system under conditions of increased organ demand for blood flow such as during exercise. The most important characteristic of this response is an increase in cardiac output, up to 4 or 5 times its resting value; this is mainly due to an increase in heart rate (~3 times control) rather than to an increase in stroke volume (~1.5 times control).

2.1.2 Mechanisms involved in cardiovascular response to exercise

The cardiovascular response to physical activity has both early and late components; it originates from higher centers in the *central nervous system* (early), from mechanical and chemical changes triggered by contracting skeletal muscles (delayed), and from various reflexes (delayed). Regarding the early component, when exercise is anticipated or already under way, a central command influences the activation of both the *motor cortex*[16] and the *cardiovascular centers* (which are regions located in the *medulla oblongata* regulating heart rate through nervous and endocrine systems). The central command, in turn, controls the medial prefrontal cortex (involved in the thinking and planning exercise) and cortical parts of the *limbic system* [17]. Indeed, the central command centers project to the lateral hypothalamus, rostral ventrolateral medulla and nucleus tractus solitarius (NTS) in order to coordinate autonomic outflow to the cardiovascular system (Fig. 2.1).

[16] The motor cortex is the region of the cerebral cortex involved in the planning, control, and execution of voluntary movements.
[17] The limbic system is the part of the brain involved in our behavioural and emotional responses. The two main structures are the hippocampus and the amygdala, but it involves the thalamus, the hypothalamus and basal ganglia.

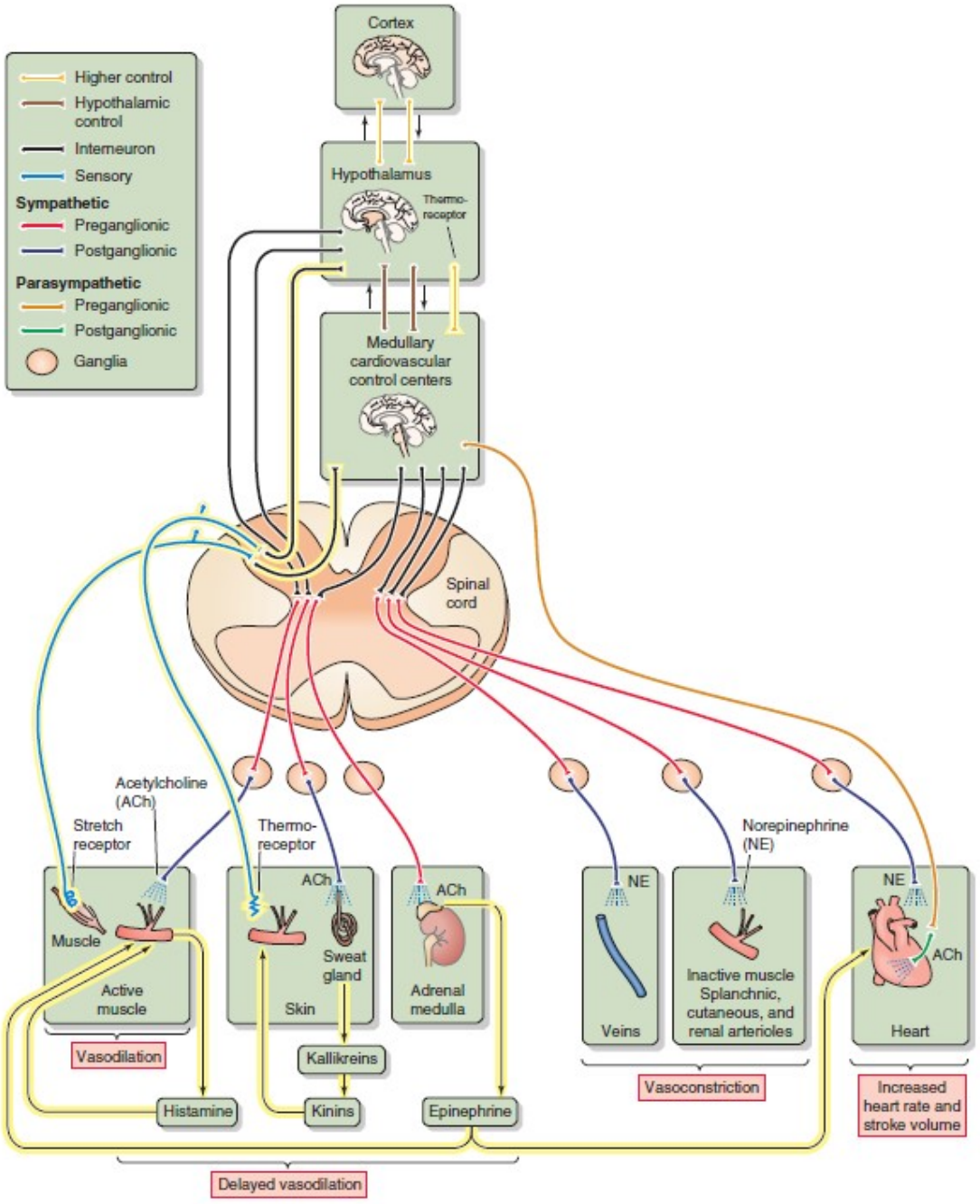

Figure 2.1 *Integrated cardiovascular response to exercise [3].*

The cardiovascular responses generated by the control of the command center are:

- Increased cardiac output: it is caused by an increase in contractility which, in turn, is due to an increase in the sympathetic output to the heart;
- Vasoconstriction in inactive muscles and renal, splanchnic, cutaneous circulations: it too is caused by an increase in the sympathetic output from the medulla.

In particular, the net effect of the second response is to collect more blood from the inactive regions for the redirection towards the contracting muscles. Indeed, these regions undergo a decrease in the fractional blood flow (local blood flow normalized to cardiac output), including the skin blood flow. However, this latter eventually rises due to the attempt of the temperature regulatory system to prevent that body temperature rises too much. These anticipatory cardiovascular adjustments prepare the body for the increased metabolism of the exercising skeletal muscle.

Indeed, regarding the delayed component (when physical activity is underway), the muscle receptors respond to changes in muscle mechanical activity and tissue chemical environment, relaying these information to the central nervous system (CNS) via afferent fibers. These integrated cardiovascular responses are:

- Exercise pressor reflex: it is a neural pathway that originates within the contracting muscle. The contraction activates both the stretch receptors, which sense the muscle tension, and the chemoreceptors, which sense metabolites. These informations are sent to the spinal cord, and then to the medullary cardiovascular control centers, which reinforces the sympathetic output to the heart;
- Arterial baroreflexes: arterial baroreceptors are stretch receptors that are stimulated by distortion of the arterial wall when pressure changes; the *baroreflex* (or *baroreceptor reflex*) is one of the body's homeostatic mechanisms that helps to maintain blood pressure at nearly constant levels. Normally, increased MAP would slow the heart rate; however, during exercise, central command resets the sensitivity of the arterial baroreflex, resulting in a decrease in heart arte only at much higher arterial pressures;
- Vasodilation in skeletal muscles: it is due to the local release of metabolites which decrease the resistance of the vessel and recruit capillaries that had received no blood flow at rest. This results in a huge increase in blood flow to active skeletal muscles;
- Increased venous return: muscle pump (limb movement) enhances venous return, which causes an increase in stroke volume based on the Frank-Starling mechanism, resulting in an increase in cardiac output;
- Histamine release: histamine is a vasodilator released by cells near the arterioles when the sympathetic output (releasing norepinephrine) wanes. This causes a relaxation of the arterioles, with a subsequent increase in pressure in the muscle capillaries, leading to increased extravasation of fluid and enchanced lymph flow;
- Epinephrine (Epi) release: during severe exercise, preganglionic sympathetic fibers to adrenal medulla stimulates Epi release, resulting in an increase of both cardiac output and vasodilation in skeletal muscle;

- Regulation of body temperature: increased metabolism causes the rise of body core temperature, activating temperature-sensitive cells in the hypothalamus. The hypothalamus both dictates the medulla to inhibit the vasoconstrictor effect increasing cutaneous blood flow, and activates sympathetic cholinergic fibers to sweat glands causing an increase in sweat production as well as an indirect cutaneous vasodilation.

2.1.3 Cardiovascular steady-state changes during exercise

Responses of the cardiovascular function also depend upon the level of the physical exertion. Figure 2.2 shows the systemic hemodynamic responses at different levels of exercise intensity (low, moderate and heavy). As workload increases, HR, CO and MAP increase; on the other hand, SVR decreased due to vasodilation in the active muscles. In particular, SV increases at low-to-moderate workload and then declines at high workloads. This is caused by an increase in HR which, in turn, shortens the period of the ventricular filling (decreased preload) activating the Frank-Starling mechanism.
Figure 2.3 illustrates, instead, the blood flow to the major organs depending upon the same levels of physical activity. Whole-body exercise (e.g., running) can increase the blood flow to working muscles more than 20-times. This blood flow, which is about 20% of the CO at rest, can reach the 90% of the CO during strenous exercise. On the contrary, splanchnic circulation (gastrointestinal, splenic and hepatic circulations) and non active muscles undergo a decrease in blood flow during exercise. Also renal blood decreases at very strenous exercise. Lastly, skin blood flow increases with increasing workloads; however, it can decrease at heavy exercise due to the control of the hypothalamic thermoregulatory centers.

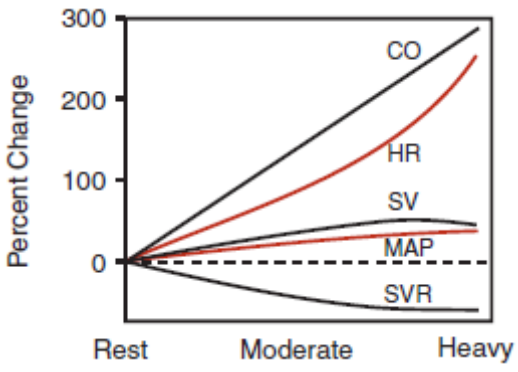

Figure 2.2 *Systemic hemodynamic responses at different levels of exercise intensity [2].*

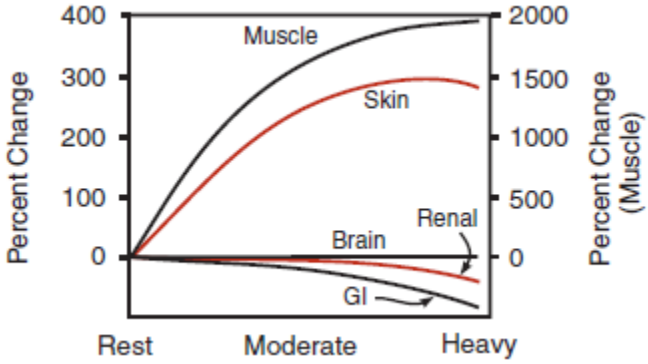

Figure 2.3 *Organ blood flow responses at different levels of exercise intensity. GI, gastrointestinal circulation [2].*

2.1.4 Factors influencing cardiovascular response to exercise

In addition to the level of exercise intensity, several other factors influence the cardiovascular response at a given workload.

The type of exercise affects the response because it makes an important distinction between dynamic exercise and static exercise. The above-described dynamic exercise (such as running, walking, bicycling or swimming) involves the joint movements as muscles rhythmically contract. On the contrary, static exercise (or isometric contraction) produces a different response. This activity (such as lift a weight at maximal effort like during bench or leg press) does not involve rhythmic contraction of muscles. This does not result in an increase in venous return and, therefore, CO increases relatively little. In addition, the abdominothoracic pump contribution is absent, especially if the breath is held. Moreover, unlike dynamic exercise, SVR increases, especially if the muscles contract at maximal effort.

Also body posture influences the cardiovascular response due to the effect of the gravity on venous return and CVP; indeed, CVP is higher in the supine position (e.g., swimming) than in the upright position (e.g., running). At rest, ventricular SV is higher in the supine position than in the upright position, whereas the heart rate is lower in the supine position than in the upright position. On the other hand, during exercise, SV increases more in the upright position than in the supine position. On the whole, the change in CO, during exercise, does not differ much between the supine and the upright position.

Physical conditioning can increase CO, whole-body oxygen consumption and workload with respect to a sedentary people. In addition, the ejection fraction (EF) of a conditioned person can exceed the 90% during physical activity, whereas a sedentary individual cannot have an EF higher than 75%. Moreover, a conditioned person at rest has an higher

SV and a lower HR with respect to a sedentary individual, resulting in a not necessarily different CO. Another difference between conditioned and sedentary people is that, for a given workload, the conditioned person has a lower HR. Lastly, the conditioned individual can sustain higher workloads for a longer duration, and recovers from the exercise much earlier than sedentary person.
Another factor is the environmental conditions. High altitudes causes a decrease in both maximal stroke volume and cardiac output due to reduced oxygen content at decreased atmospheric pressure. Indeed, reduced oxygen supply to tissues results in the achievement of the anaerobic threshold (production of lactic acid) at a lower workload. Increased temperature and humidity, instead, diverts a greater fraction of CO to the skin to strenghten the heat removal from the body, resulting in a lower availability of blood for muscles. Furthermore, maximal CO and oxygen consumption are reached at lower workloads. Lastly, dehydration reduces blood volume and CVP resulting in an attenuation of the normal increase in cardiac output during activity. The subsequent fall in arterial pressure can lead to *heat exhaustion*[18].
Increased age causes the reduction of about 40% of oxygen consumption. In addition, it decreases both the maximal HR and the maximal SV. In particular, the latter is caused by impaired ventricular filling due to decreased ventricular compliance. Also the inotropic responsiveness to sympathetic stimulation is reduced. Overall, the CO is decreased, as well as the maximal muscle blood flow due to the decreased muscle mass.
Regarding the gender, generally, males reach and sustain higher workloads and maximal oxygen consumption than females. Moreover, maximal CO is about 25% less in females, even if the maximal HR is similar. A reason is that males have increased mass of both skeletal muscle and cardiac muscle.
Finally, cardiac disease can significantly limit exercise capacity due to a decrease in CO (like in case of heart failure or arrhythmias).

2.1.5 Cardiovascular responses to aerobic exercise

Aerobic exercise is characterized by the need of more energy (thus, more oxygen) than either static or dynamic resistance exercise. The amount of oxygen needed depends on both the intensity and the duration of the activity. This paragraph makes a distinction between short-term light-to-moderate submaximal exercise, long-term moderate-to-heavy submaximal exercise and incremental exercise to maximum. Short-term exercise lasts about 5-10 minutes, whereas long-term exercise last more than 30 minutes. Light

[18] Heat exhaustion is a condition whose symptoms may include heavy sweating and a rapid pulse, a result of body overheating.

exercise, moderate exercise and heavy exercise are characterized by 30-49%, 50-74% and 60-85% of maximal oxygen consumption ($V\dot{O}_2$max), respectively. The *total peripheral resistance* (*TPR*) decreases as vasodilation occurs in the active muscles; it is defined as the ratio between the mean arterial pressure (MAP) and the CO (indicated, in this paragraph, with $\dot{Q}$ and no longer with CO):

$$TPR = \frac{MAP}{\dot{Q}} \tag{2.1}$$

Moreover, the *rate pressure product* (*RPP*), an index used in cardiology and exercise physiology to determine the myocardial workload, is defined as the product of heart rate (HR) and systolic blood pressure (SBP):

$$RPP = HR \cdot SBP \tag{2.2}$$

2.1.5.1 Short-term, light to moderate submaximal aerobic exercise

During this kind of exercise, CO, SV, HR, SBP and rate pressure product increase rapidly at the onset of exercise and then reach a steady state within 2 minutes. On the other hand, diastolic blood pressure (DBP) remains quite constant, whereas TPR decreases rapidly and then plateaus at about 2 minutes (Fig. 2.4).

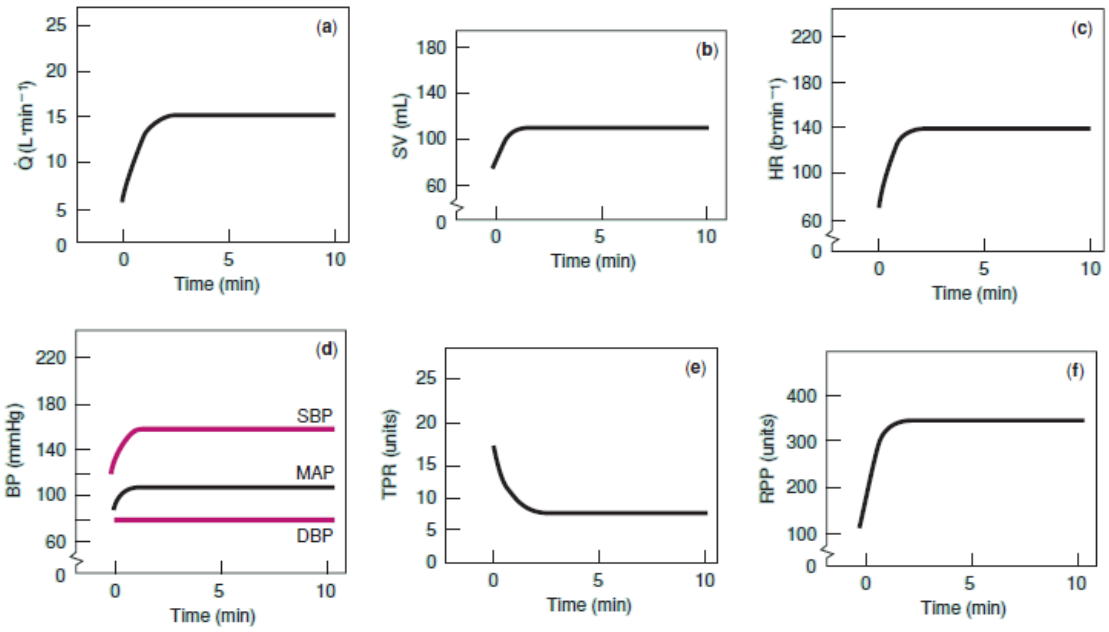

Figure 2.4 *Cardiovascular responses to short-term, light to moderate aerobic exercise [4].*

2.1.5.2 Long-term, moderate to heavy submaximal aerobic exercise

During this kind of exercise, CO, SV, HR, SBP and rate pressure product increase rapidly at the onset of exercise. *Cardiovascular drift* is defined as che changes in cardiovascular variables during prolonged, heavy submaximal exercise without a change in workload. After the achievement of the staedy state, cardiac output remains quite constant; indeed, on one hand, the stroke volume has a downward drift, on the other, the heart rate has an upward drift. In addition, both SBP and TPR have a downward drift in case of prolonged heavy exercise; this is due to the increase in body temperature (Fig. 2.5). These drift are influenced by *fluid ingestion*. Indeed, when ingested water is enough to replace that lost through sweat, $\dot{Q}$ remains constant during the first hour, and then increases. The reason is that SV does not drift downward. In addition, HR is lower in case of fluid replacement.

2.1.5.3 Incremental exercise to maximum

This kind of exercise consists of a series of progressively increasing work intensities that continue until the person can do no more. The duration of each work intensity ranges between 1 and 3 minutes in order to achieve a steady state (at least at the lower workloads). $\dot{Q}$, HR, SBP and RPP increase linearly as workload increases. SV initially increases and then plateaus at a workload of approximately 40-50% of $\dot{V}O_2$max. DBP remains quite constant for the entire duration of the exercise. TPR initially decreases reaching its minimum at the maximal work (Fig. 2.6).

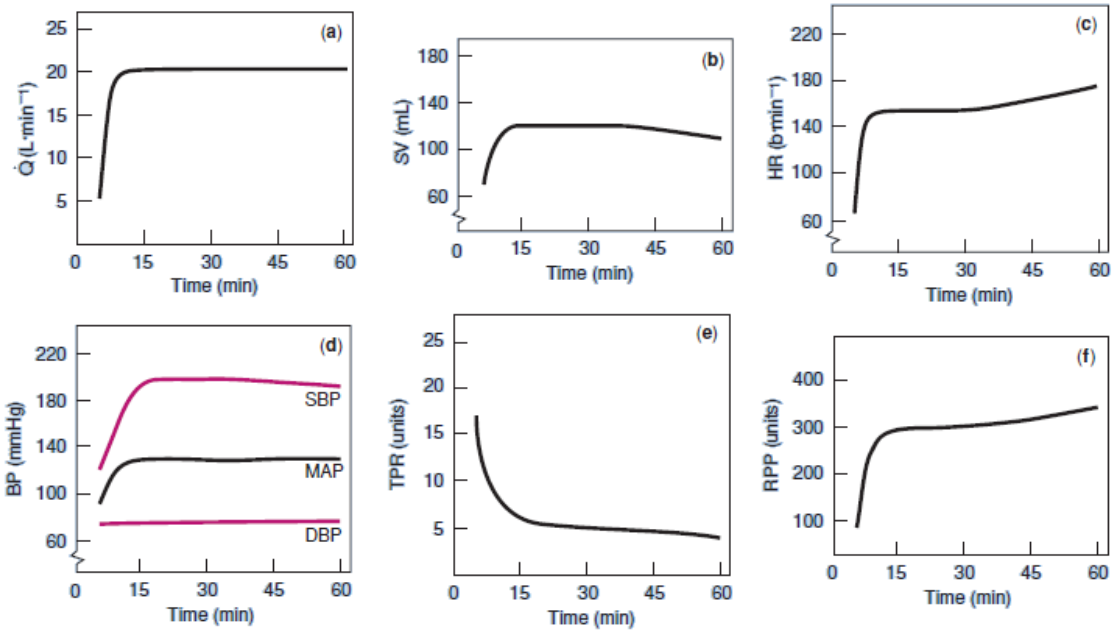

Figure 2.5 *Cardiovascular responses to long-term, moderate to heavy aerobic exercise [4].*

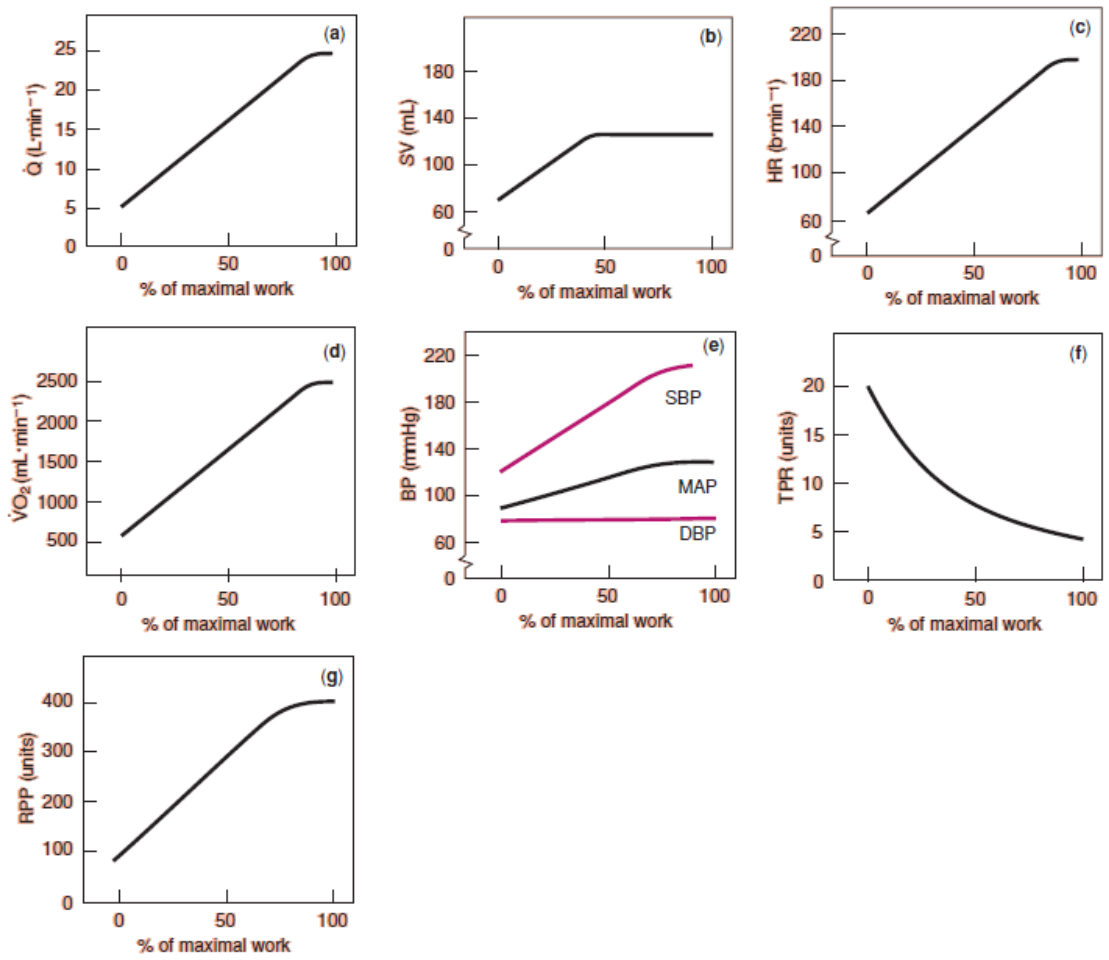

Figure 2.6 *Cardiovascular responses to incremental maximal exercise [4].*

The decrease in TPR has a double consequence: first of all, it permits a greater blood flow towards the working muscles; then, it prevents an excess of the blood pressure which, otherwise, would increase too much in response to increased CO. Regarding the increase in SV, instead, it is caused by a simultaneous increase in left ventricular end-diastolic volume (due to venous return to the heart by means of active muscles pump) and a decrease in left ventricular end-systolic volume (due to an increased contractility of the heart which ejects more blood leaving less in the ventricle).

2.1.5.4 Upper-body versus lower-body aerobic exercise

This distinction is likewise based on the incremental exercise to maximum. From figure 2.7, it is immediately clear that lower-body exercise reaches an higher peak $\dot{V}O_2$. However, at a given level of $\dot{V}O_2$, cardiac output is similar for upper-body and lower-body exercise, although the mechanisms are different.

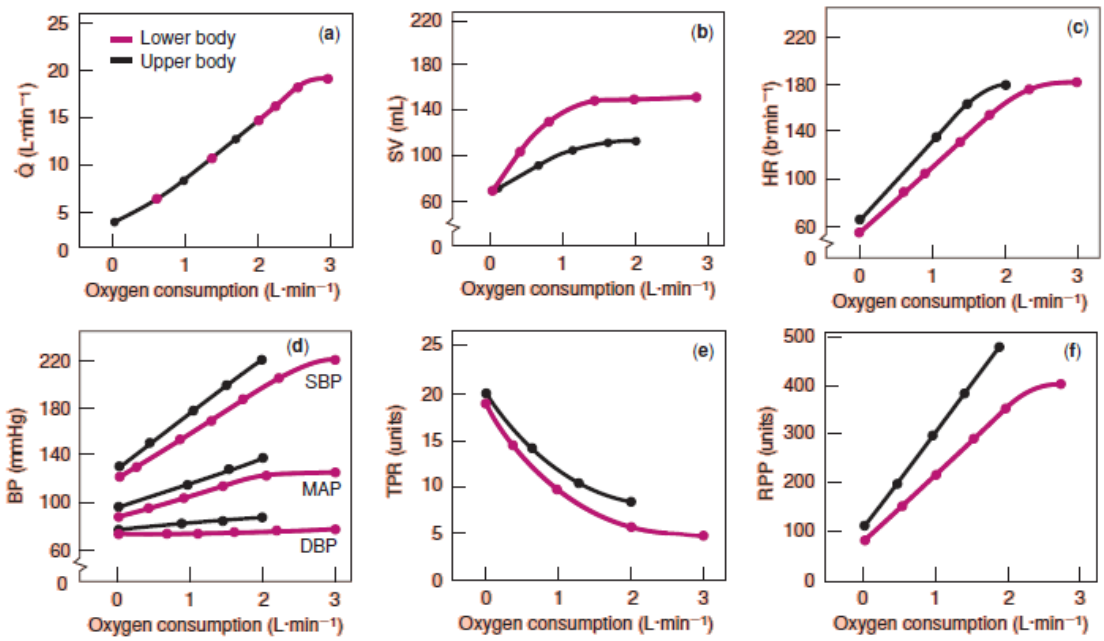

Figure 2.7 *Cardiovascular responses to incremental maximal upper-body and lower-body exercise [4].*

Indeed, upper-body exercise is characterized by a lower SV and an higher HR with respect to lower-body exercise. SBP, DBP, MAP, TPR and RPP are higher in upper-body exercise at a given $\dot{V}O_2$. The likely reasons are manifold: the higher HR results from a greater sympathetic stimulation during upper-body exercise; the decrease in SV during upper-body exercise is thought to be a consequence of the absence of the venous return from legs. In addition, blood pressure increases during upper-body exercise because it involves a static component (such as during the use of arm-cranking ergometer) which is known to produce this response (see next paragraphs). $\dot{V}O_2$max values at maximal upper-body exercise are approximately 30% lower than those of maximal lower-body exercise. Maximal HR values at maximal upper-body exercise are 90-95% of those of maximal lower-body exercise. SV at maximal upper-body exercise is 30-40% less than that of maximal lower-body exercise. Maximal SBP and RPP are usually similar for both types of exercise, although DBP is about 10-15% higher during upper-body exercise.

2.1.5.5 Sex differences during aerobic exercise

At the same absolute workload, females have a higher CO than males during submaximal exercise, resulting in a greater stress of the cardiovascular system. Because of this relative disadvantage, due to a smaller heart, less muscle mass and lower $\dot{V}O_2$max, it is better to discuss the response in terms of *relative workload*, that is a comparison made at the same

percentage of $V\dot{O}_2$max. Table 2.1 summarized the difference between the sexes in cardiovascular variables at various exercise levels.

2.1.5.6 Aerobic training

Aerobic training must meet four conditions:

- The intensity of the activity must overcome a critical threshold;
- Each period of activity must be of sufficient duration;
- The activity must be repeated over time on a regular basis;
- The activity must be followed by sufficient rest, because *adaptation* (training effect) occurs during the recovery period.

Aerobic training increases both $V\dot{O}_2$max and the body's ability to remove excess heat. In particular, $V\dot{O}_2$max increases by either optimizing O_2 delivery to active muscles or optimizing O_2 extraction by these same active muscles:

$$V\dot{O}_{2max} = HR_{opt} \cdot SV_{opt} \cdot (Ca_{O_2} - Cv_{O_2})_{max} \quad (2.3)$$

where HR_{opt} is the optimal heart rate, SV_{opt} is the optimal stroke volume, and $(Ca_{O_2} - Cv_{O_2})_{max}$ is the maximal arterial-venous difference of O_2 content. The product of HR_{opt} and SV_{opt} determines the maximal cardiac output.

Since aerobic training does not increase the maximal heart rate and has a small influence on the O_2 extraction, almost all the increase in $V\dot{O}_{2max}$ is due to an increase in maximal cardiac output. This increase in cardiac output is reached by the athlete by an increase in the maximal cardaic stroke volume. The increment of the maximal cardiac output during aerobic training is between the 40 and 50%, depending on the increased extraction based on $(Ca_{O_2} - Cv_{O_2})_{max}$. The increse in cardiac output is caused by an increase in preload which, in turn, is due to the expansion of the plasma compartment. Increased preload, is accompanied by an hypertrophy of the heart.

Table 2.1 *Cardiovascular variables for women when compared to men. -, study non conducted; ?, discordant results [4].*

	Exercise Condition			
Variable	**Rest**	**Absolute, Submaximal**	**Relative, Submaximal**	**Incremental, Maximal**
$V\dot{O}_2$max	-	-	-	Lower
$\dot{Q}$	Lower	Higher	?	Lower
SV	Lower	Lower	Lower	Lower
HR	Higher	Higher	Higher	Similar

Another advantage of the aerobic training is that an atlete reaches a given cardiac output at a lower heart rate, both at rest and during moderate exercise. Therefore, since it is more efficient to increase stroke volume than heart rate, the myocardial metabolic load for any level of activity is reduced.

Regarding the increased O_2 extraction of blood, instead, the factors that contribute to its diffusion between the systemic capillary blood to the *mitochondria*[19] are almost the same to those that influence the diffusing capacity in the lung. A trained muscle experiences a growth of new microvessels (in particular, capillaries) resulting in a greater maximal blood flow. This growth of capillaries (up to 60%), causes an increase in O_2 delivery. It also reduces the diffusion distance for O_2 between the capillary and muscle fibers. In addition, aerobic training increases total capillary length and volume, extends the transiti time of red blood cells along capillaries, enhancing the extraction of O_2 and nutrients from the blood (as well as the removal of waste byproducts). Lastly, aerobic training, maintains an high capillary oxygen partial pressure (P_{O_2}) which, in turn, keeps constant the driving force for O_2 diffusion from capillaries to mitochondria.

Aerobic training, in parallel, increases the mitochondrial content of skeletal muscle fibers by stimulating enzymes and proteins. The biogenesis of the mitochondria increases the O_2 extraction from the blood because mitochondria create the sink for O_2 consumption during the oxidative phosphorylation of ADP to ATP.

2.1.5.7 Responses of children to aerobic exercise

The cardiovascular response in children is similar to that of adult, although children have a lower CO, SV and SBP at both an absolute workload and at maximal exercise. This disparity is mainly due to differences in body size and heart dimension (Table 2.2). Moreover, the rate of improvement in absolute $\dot{V}O_2$max is similar for boys and girls until approximately 12 yr of age; maximal oxygen uptake continues to increase in boys until the age of 18, whereas it remains quite constant in girls between 14 and 18 yr (Fig.2.8). The main difference between adults and children lies in the meaning of $\dot{V}O_{2max}$. In adults, it reflects both physiological function and cardiovascular *endurance* (ability to perform strenous, large-muscle exercise for a prolonged period of time). In children, there is not this relation.

The blood pressure response to incremental exercise test is similar for children and adults, although, for a given level of exercise, a small child responds with a lower SBP and DBP than does an adolescent.

[19] Mitochondria are membrane-bound cell organelles that generate most of the chemical energy needed to power the cell's biochemical reactions. Chemical energy is stored in ATP.

Table 2.2 *Cardiovascular responses to maximal exercise in pre- and postpubescent children [4].*

	Boys		Girls	
Variable	**10 yr**	**15 yr**	**10 yr**	**15 yr**
$\dot{V}O_2 (L \cdot min^{-1})$	1.7	3.5	1.5	2.0
$\dot{Q} (L \cdot min^{-1})$	12	18	11	14
SV $(mL \cdot min^{-1})$	60	90	55	70
HR $(b \cdot min^{-1})$	200	200	200	200
SBP(mmHg)	144	174	140	170
DBP(mmHg)	64	64	64	64
MAP(mmHg)	105	110	103	117.5
TPR(mmHg)	7.0	6.1	9.4	8.4
RPP(mmHg)	290	350	280	340

Likewise, an adolescent responds with lower blood pressure than an adult. The lower blood pressure is consequence of a lower stroke volume response; moreover, boys have an higher peak SBP than girls. This discrepancy is attributable to differences in stroke volume.

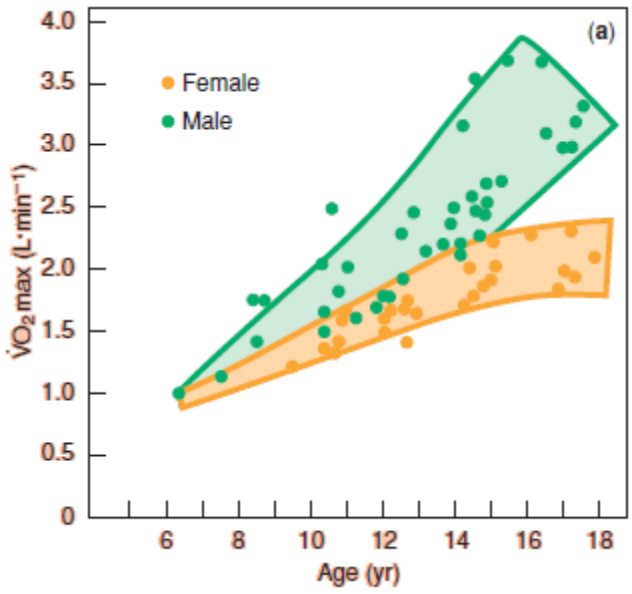

Figure 2.8 *Changes in maximal oxygen consumption in children and adolescents during the ages of 6-18. The dots represent means from various studies. The outer lines indicate normal variability in values [4].*

2.1.5.8 Responses of the elderly to aerobic exercise

The cardiovascular response of the elederly is characterized by a decrease in maximal CO, SV, HR and $V\dot{O}_{2max}$. On the other hand, maximal SBP, DBP and MAP increase. TPR decreases during aerobic exercise, but not with the same extent that it does in younger individuals. The difference is due to the loss of elasticity of the connective tissue in the vasculature. Moreover, older individuals have a lower RPP at maximal exercise than younger individuals because the decrease in maximal HR in older individuals is greater than the increase in maximal SBP when compared with those variables for younger adults.

2.1.6 Cardiovascular responses to static exercise

Static exercise is a common form of physical activity that occurs both during daily activities (such as lifting and carrying heavy objects) and during sports involving this component (such as weight-lifting or racquet sports). In this case, the magnitude of the cardiovascular response mostly depends on the intensity of the muscle contraction held for a specific time period.

2.1.6.1 Intensity of muscle contraction

The intensity of a static contraction is expressed as a *percentage of maximal voluntary contraction (% MVC*). Figure 2.9 shows the cardiovascular response to static contractions of the forearm (handgrip) muscles at 10, 20 and 50% MVC. It should be firstly noted that the contraction could be held for 5 minutes at both 10% and 20% MVC, whereas at 50% MVC, the contraction could be held for only 2 minutes. This means that, likewise aerobic exercise, intensity and duration are inversely related. Furthermore, although the pattern of the response is similar for different muscles, the values may vary depending on the amount of active muscle involved.

Cardiac output increases during static contraction caused by an increase in hert rate. Stroke volume remains quite constant during low-intensity contraction, but decreases during high-intensity contractions. However, in this last case, the stroke volume increases at the cessation of the contraction; this is probably due to a decrease in preload and an increase in afterload. Indeed, the decrease in preload is caused by an increase in intrathoracic pressure which compresses the vena cava and reduces the venous return to the heart; on the other hand, the increase in afterload is caused by the high arterial blood pressure during the contraction, resulting in less blood ejected at a given force of contraction. Also heart rate increases during static exercise; the greater the intensity, the higher the HR.

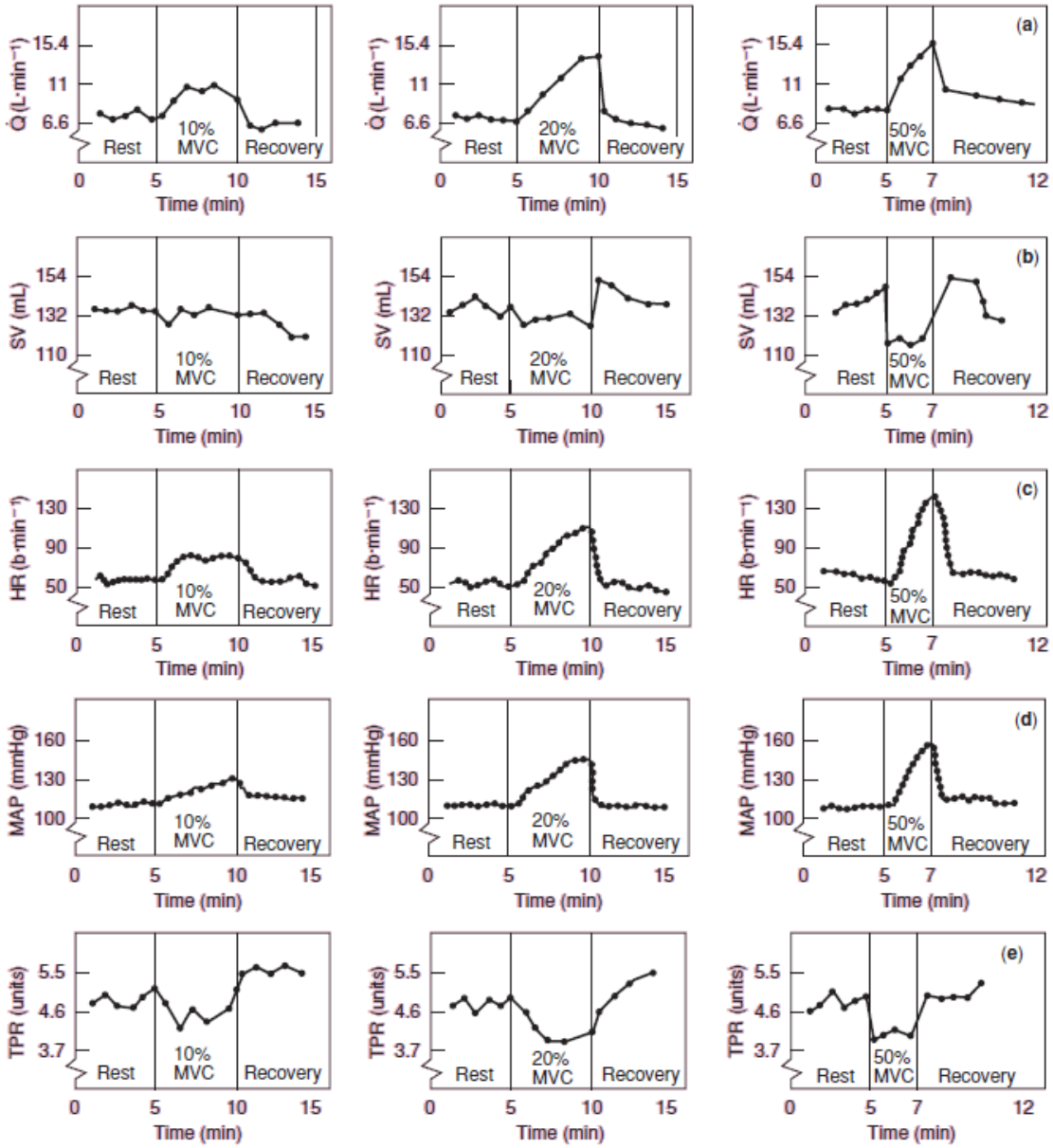

Figure 2.9 *Cardiovascular response to varying intensities of handgrip exercise [4].*

Since static exercise causes a rapid increase in both SBP and DBP (named pressor response), also MAP shows a considerable increase.

TPR decreases during static contractions, although not to the same extent of aerobic exercise. This fact explains the high value of the blood pressure during static exercise. Indeed, this high pressure permits to overcome the resistance to blood flow owing to mechanical occlusion.

Finally, static exercise causes a large increase in myocardial oxygen consumption because both SBP and HR increase.

2.1.6.2 Blood flow during static contractions

Blood flow is impeded during static contarctions because of mechanical constriction of the blood vessel supplying the muscle; the greater the %MVC, the less the blood flow. However, when contraction ceases, the contraction characterized by an higher %MVC shows a greater increase in blood flow with respect that associated toa lower %MVC, suggesting a sort of compensation for the more reduced blood flow during sustained contraction.

Also aerobic exercise is characterized by a mechanical constriction, although the alternating periods of contraction and relaxation allow blood flow, especially through the venous system.

2.1.6.3 Comparison of aerobic and static exercise

Aerobic exercise is said to impose a "volume load" because it is characterized by a large increase in HR (whch contributes to an increase in CO), and a modest increase in SBP and a quite constant or decreased DBP.

On the other hand, static exercise is said to impose a "pressure load" because it is characterized by a modest increase in heart rate, and a dramatic increase in blood pressure (pressor response). Increased MAP means that the heart must pump harder to overcome the pressure in the aorta.

2.1.6.4 Sex differences in responses to static exercise

Heart rate is similar in males and females. However, in case of maximal contraction of handgrip muscles held for 2 minutes (Fig. 2.10), the blood pressures reported for women are significantly lower than those reported for men.

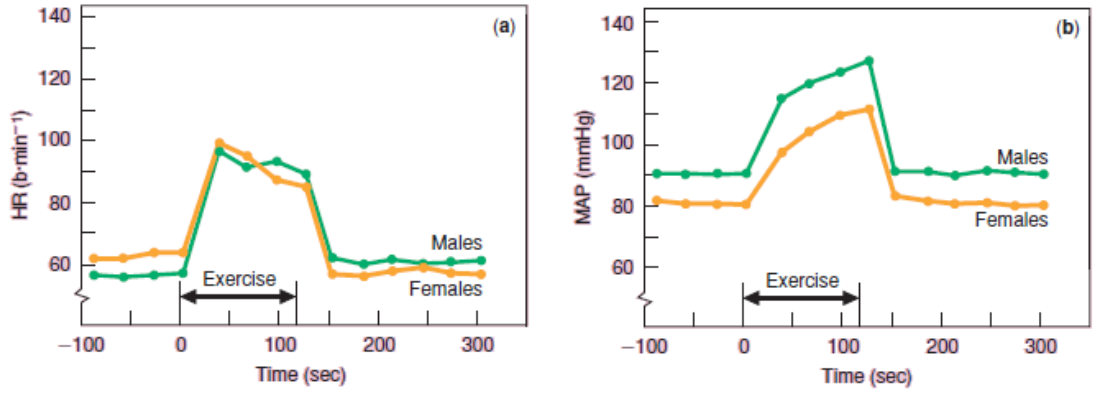

Figure 2.10 *Heart rate and blood pressure response of males and females to static exercise [4].*

2.1.6.5 Cardiovascular responses to static exercise in older adults

Figure 2.11 illustrates the cardiovascular responses of young and old men to sustained handgrip and leg extension exercise over a range of submaximal static workloads. Cardiac output, stroke volume and heart rate are lower for the older men than the younger men at each intensity. The reason is probably the same of the aerobic exercise: the age.related increase in resistance due to a loss of elasticity in the vasculature and a decreased ability of the myocardium to stretch and contract forcibly.

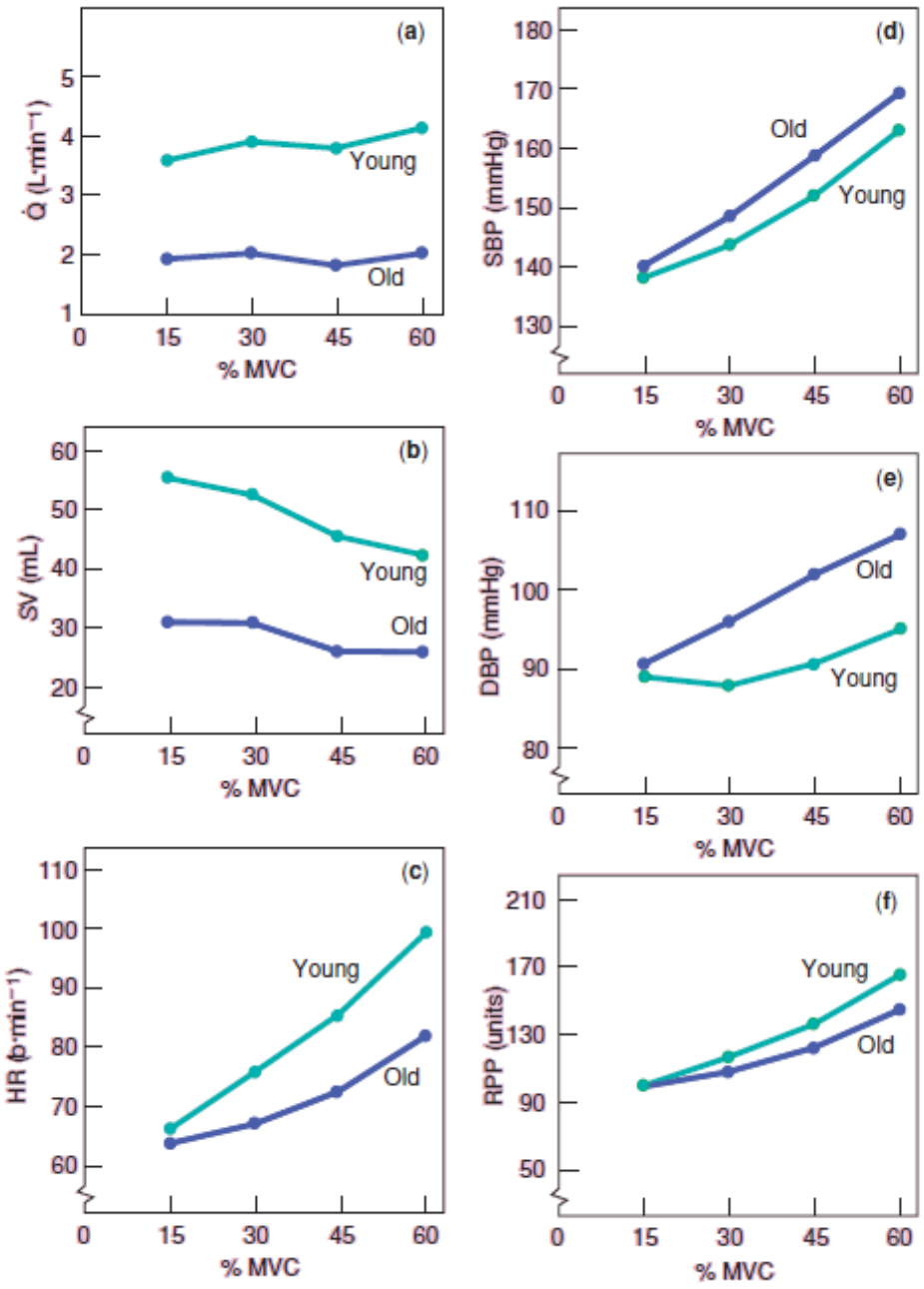

Figure 2.11 *Cardiovascular response of males by age to static exercise [4].*

Moreover, the RPP is higher in the younger men, although the difference is small. The reason is an higher heart rate in younger subjects at each intensity of contraction, which is not completely offset by a lower SBP in the younger men.

2.1.7 Cardiovascular responses to dynamic resistance exercise

Resistance exercise (or weight-lifting) includes both a dynamic and a static contraction. Indeed, at the beginning of the exercise, a static component exists until muscle force exceeds the load to be lifted and movement occurs, which leads to a dynamic component concentric (shortening) contraction. This contraction is followed by a dynamic eccentric (lengthening) contraction during the lowering phase. In addition, there is always a static component corresponding to the gripping of the barbell.
An important difference with respect to aerobic exercise is the dissociation between the energy demand and the cardiorespiratory system. This is mainly due to the fact that much of the energy needed for this kind of exercise comes from anaerobic (without oxygen) sources. Another difference is the mechanical constriction of blood flow due to the static nature of the contraction.
Finally, the magnitude of the response depends on both the intensity of the load (the weight lifted) and the number of repetitions.

2.1.7.1 Constant repetitions/varying load

Of course, the cardiovascular response is greater when the weights to lift are heavier, in case of constant number of repetitions. In particular, the blood pressure is higher at the completion of the heaviest set. Indeed, SBP increases as the intensity increases; however, there is a disagreement among the authors about the DBP: some of them report an increase of DBP and others report no changes. This is probably due to a difference in measurement techniques.

2.1.7.2 Resistance exercise to fatigue

Resistance exercise to fatigue means that the subject performs maximal work regardless of the load. Figure 2.12 illustrates the cardiovascular response at the completion of leg extension exercise performed to fatigue. Subjects perform 50%, 80% and 100% of their one repetition maximum (1 RM) as many times as they could, and responses are recorded at the end of each set. Subjects, obviously, performs the 100% load only one time; on the other hand, they are able to perform the 80% and 50% load an average of 8 and 15 times, respectively. This results in the greatest volume of work performed when the lightest load was lifted the greatest number of times.

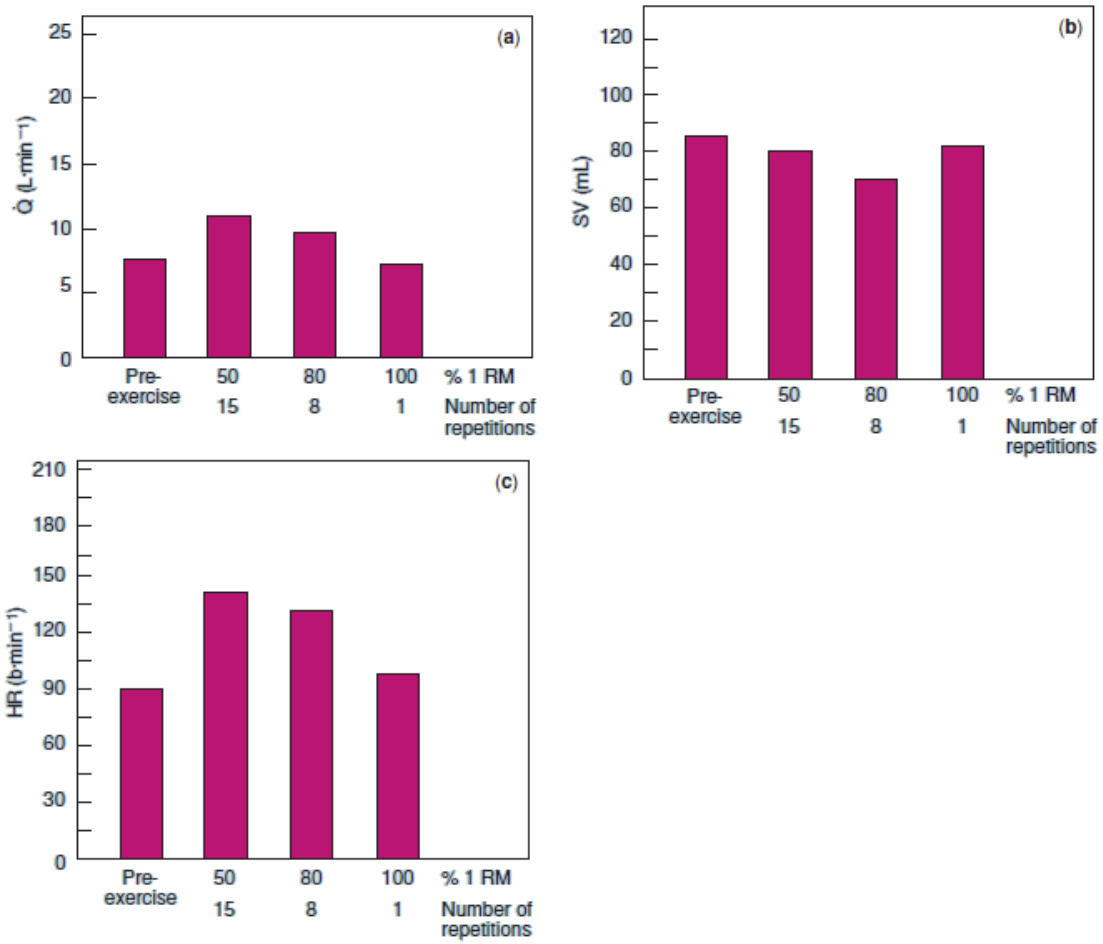

Figure 2.12 *Cardiovascular response at the completion of fatiguing resistance exercise (concentric knee extension exercise) [4].*

The highest cardiac output at the completion of the set is that associated to the lightest load lifted for the greatest number of repetitions. The stroke volume is quite similar in each condition, and slightly below the resting value. This means that the stroke volume, in contrast to dynamic endurance exercise, does not undergo an overload during dynamic resistance exercise. In addition, heart rate and blood pressure attained at fatigue are the same when loads between 60% and 100% of 1 RM are used, regardless of the number of times the load can be performed.

Figure 2.13 shows the MAP (measured intra-arterially) and heart rate during a set of leg press exercise at 95% of 1 RM; both of them increase gradually with succeeding repetitions in a set to failure. The dramatic increase in blood pressure is caused by the mechanical compression on the blood vessels and performance of the *Valsalva maneuver*[20].

[20] The Valsalva maneuver is performed by forceful attempted exhalation against a closed airway.

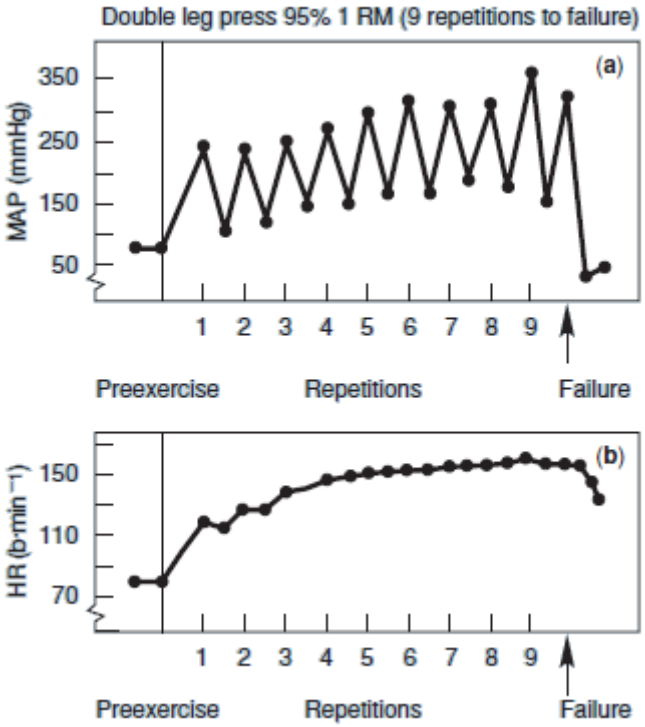

Figure 2.13 *Heart rate and blood pressure response during a set of resistance exercise [4].*

TPR is higher in this kind of exercise rather than during dynamic aerobic exercise because the pressor reflex causes vasoconstriction. Myocardial oxygen consumption and, thus, the RPP reach high values because of the tachycardia and extreme SBP response. This kind of exercise also produces a transient decrease in plasma volume. Finally, the response in children are similar to that of adults, with an increase in heart rate and blood pressure throughout a set. Table 2.3 summurizes the cardiovascular responses to aerobic exercise, static exercise and resistance exercise.

2.1.8 Cardiovascular system after exercise

Recovery from exercise is defined as the period between the end of a bout of exercise and the susequent return to a resting or recovered state. It is characterized by physiological responses which are different from those related to either exercising or resting phases. Indeed, recovery is not simply a return to pre-exercise resting state, but rather a dynamic period during which many physiological changes occur, such as heart adaptations driven by routine physical activity.

Table 2.3 *Cardiovascular responses to exercise*[*]*[4].*

	Short-Term, Light to Moderate Submaximal Aerobic Exercise	Long-Term, Moderate to Heavy Submaximal Aerobic Exercise[†]	Incremental Aerobic Exercise to Maximum	Static[††] Exercise	Resistance[††] Exercise
$\dot{Q}$	Increases rapidly; plateaus at steady state within 2 min	Increases rapidly; plateaus	Rectilinear increase with plateau at max	Modest gradual increase	Modest gradual increase
SV	Increases rapidly; plateaus at steady state within 2 min	Increases rapidly; plateaus; negative drift	Increases initially; plateaus at 40–50% $\dot{V}O_2$max	Relatively constant at low workloads; decreases at high workloads; rebound rise in recovery	Little change, slight decrease
HR	Increases rapidly; plateaus at steady state within 2 min	Increases rapidly; plateaus; positive drift	Rectilinear increase with plateau at max	Modest gradual increase	Increases gradually with numbers of reps
SBP	Increases rapidly; plateaus at steady state within 2 min	Increases rapidly; plateaus; slight negative drift	Rectilinear increase with plateau at max	Marked steady increase	Increases gradually with numbers of reps
DBP	Shows little or no change	Shows little or no change	Shows little or no change	Marked steady increase	No change or increase
MAP	Increases rapidly; plateaus at steady state within 2 min	Increases initially; little if any drift	Small rectilinear increase	Marked steady increase	Increases gradually with numbers of reps
TPR	Decreases rapidly; plateaus	Decreases rapidly; plateaus; slight negative drift	Curvilinear decrease	Decreases	Slight increase
RPP	Increases rapidly; plateaus at steady state within 2 min	Increases rapidly; plateaus; positive drift	Rectilinear increase with plateau at max	Marked steady increase	Increases gradually with numbers of reps

* Resting values are taken as baseline.

† The difference between a plateau during the short-term, light to moderate and long-term, moderate to heavy submaximal exercise response is one of magnitude; that is, a plateau occurs at a higher value with higher intensities.

†† The magnitude of a plateau change depends on the %MVC/load.

Moreover, these changes provide insight into when the cardiovascular system has recovered from prior training and is physiologically ready for additional training stress.
The aim of this paragraph is to investigate the underlying mechanisms occurring in response to acute bouts of aerobic and resistance exercise, with particular attention to the adjustments sustained for more than 20 minutes after exercise.
In particular, the reduction in arterial pressure following the exercise is called *post-exercise hypotension* [5], and it observed after both aerobic and resistance exercise. Therefore, according to equation 1.26, the mechanisms mediating this reduction can be investigated analyzing the cardiac output, the systemic vascular resistance and the central venous pressure.
Finally, as discussed later, it is needed to emphasize that the reduction in blood pressure reflects both obligatory responses to exercise (the primary responses to exercise such as arterial baroreflex resetting or histamine release and receptor activation) and situational responses to exercise (such as reduced preload, elevated body core temperature or changes in body position).

2.1.8.1 Cardiovascular function following aerobic exercise

The whole-body aerobic activity has been performed for at least 20 minutes with moderate intensity. The increase in *systemic vascular conductance* (inverse of the systemic vascular resistance) following the exercise is larger than the elevation in cardiac output; this means that vasodilation is the driver of the pressure reduction. However, during passive recovery (such as upright position), the loss of muscle pump reduces the venous return, central venous pressure and cardiac preload, resulting in a further decrease in pressure leading to severe hypotension and syncope. This vasodilation that occurs after the exercise is called *sustained post-exercise vasodilation*, and lasts several hours. It is mainly due to the vessels of the active muscles, with a lessere contribution of non-active muscles. Indeed, systemic vascular conductance (SVC) in the splanchnic, cutaneous and cerebral vascular beds remains unchanged with respect to pre-exercise values. More precisely, sustained post-exercise vasodilation is mediated by combined central neural mechanisms and local vasodilatory mechanism. The first involve a resetting of the arterial baroreflex with subsequent reduced sympathetic activity despite operating at a lower pressure; this is also associated with changes in recovery of heart rate and its beat-to-beat fluctuations (i.e. *heart rate variability*: see next paragraph). Moreover, the immediate recovery of heart rate (fast phase) from aerobic exercise is due solely to parasympathetic reactivation, whereas the slow phase of recovery is driven by withdrawal of sympathetic outflow lasting up to 90 minutes after exercise.

An important distinction also occurs between active and non-active muscle: vasodilation within non-active muscles occurs via resetting of the arterial baroreflex and the resulting reduction in sympathetic vasoconstrictor tone, whereas vasodilation in active muscles results from combined arterial baroreflex resetting and the release of local vasodilatory substances. Indeed, vasodilation is not dependent on changes in α-adrenergic receptor sensitivity; rather, *histamine*[21] has an obligatory role as a primary mediator of sustained post-exercise vasodilation.

2.1.8.1 Cardiovascular function following resistance exercise

The resistance exercise is constituted by an acute bout of multiple, whole-body strength exercises (e.g. circuit training). it is important to note that the cardiovascular responses from this kind of exercise are different from those follwing a single set of resistance exercise performed by an isolated muscle group.

The arterial blood pressure is reduced for up to several hours following the exercise, although it is not a universal finding. This hypotension is mainly caused by the attenuation in cardiac output which is due, in turn, by a decrease in stroke volume. Furthermore, the

[21] Histamine is an organic nitrogenous compound involved in vasodilation and fall in blood pressure.

SVC is reduced, corroborating the fact that hypotension after exercise is due to central vasodilation (i.e. cardiac hemodynamics) and not to peripheral vasodilation. This is an important difference from the aerobic exercise.
The cardiac output is related to changes in cardiac sympathetic activation and/or in arterial baroreflex sensitivity, whereas the reduced SVC is related to changes in local vasodilator mechanisms within active muscles. There is some overlap in central mechanism; therefore, combined aerobic and resistance exercise does not further reduce arterial pressure compared to aerobic exercise alone. Finally, gender is an important factor because hypotension after exercise is more dependent on vasodilation in women. The reason is still not completely clear, but it may related to the difference in cardiac morphology and/or variations in sex hormone levels.
Non-invasive measures of cardiac vagal tone (i.e. heart rate variability) demonstrate how neural/autonomic mechanisms attenuate the rise in cardiac output and reduce the arterial blood pressure after resistance exercise. However, the reduction in vagal tone and the increase in heart rate are not enough to offset the reduction in stroke volume after resistance exercise. Moreover, the ability of the arterial baroreflex to attenuate the reduction in blood pressure is inhibited by the attenuated vagal baroreflex sensitivity. Overall, the mechanisms associated to the hemodynamic adjustments after resistance exercise are mainly caused by central neural adjustments.

2.1.9 Cardiac autonomic responses using heart-rate variability and systolic time intervals

Heart-rate variability (HRV) is defined as the fluctuations in R-peak to R-peak intervals (RRI), and is considered a useful method by which to monitor the parasympathetic modulation (chronotropic influences) of the cardiac autonomic activity [6]. In particular, monitoring the HRV responses to an exercise test provides insight into both the prediction of cardiovascular disease and the training status of high performance athletes. This paragraph focuses on dynamic aerobic exercise as stress test to investigate the response of HRV. On the other hand, *systolic time intervals* (STI) provide insight into the cardiac sympathetic activity (inotropic influences).

2.1.9.1 Cardiac autonomic regulation during exercise and recovery

Figure 2.14 shows how both cardiac sympathetic neural activity (cSNA) and cardiac parasympathetic neural activity (cPNA) regulate the HR throughout the entire exercise intensity continuum. In particular, cSNA works as a “tone-setter”, and cPNA operates as a “rapid responder/modulator”.

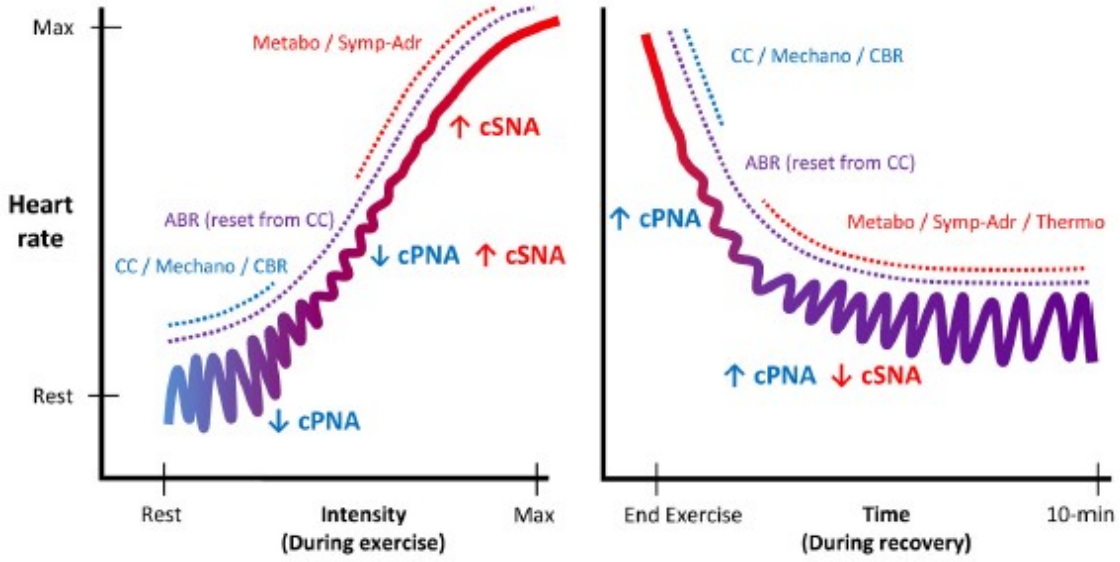

Figure 2.14 *Schematic illustration of autonomic regulation of HR during exercise and recovery. CC, central command; Mechano, mechanoreflex; CBR, central baroreflex; ABR, arterial baroreflex; Metabo, metaboreflex; Symp-Adr, sympatho-adrenal; Thermo, thermoregulatory influences [6].*

As exercise intensity increases further, progressive baroreflex resetting as well as afferent feedback from muscle metaboreceptors trigger further cardiac parasympathetic withdrawal and sympathetic activation, the latter of which is increasingly augmented from moderate to maximal intensity by systemic sympatho-adrenal activation. Upon exercise cessation, the aforementioned processes mediating cardio-acceleration during exercise essentially occur in reverse.

2.1.9.2 Definition and quantification of heart-rate variability

HRV quantifies the variability of HR, although this is a misnomer because HR (bpm) is usually expressed as heart period (milliseconds per beat) before variability is quantified. HRV is measured both in time-domain and frequency-domain.

The two most common time-domain measures of HRV are the *standard deviation of R-R intervals* (*SDRR*), a measure of overall variability; and the *root mean square of successive differences of R-R intervals* (*RMSSD*), a measure of beat-to-beat variability. The latter is sometimes calculated in a different way, which is the *standard deviation of successive differences* (*SDsd*).

Frequency-domain measures of HRV are also useful because different spectral power components of HRV might relate to different elements of cardiac autonomic activity. There are different methods (and multiple sub-variations of methods) utilized to calculate HRV spectra, with the two most common employing a Fourier transform or

autoregressive modelling. Regardless of the method used, the primary components are low frequency (LF, often 0.04–0.15 Hz) and high frequency (HF, often 0.15–0.40 Hz) spectra. Very low frequency spectra (VLF, <0.04 Hz) is seldom reported. Together these constitute total power (TP). These may be expressed as absolute power (ms^2) or as power spectral density ($ms^2 \cdot Hz^{-1}$).

Another method that deserves mention is the *Poincarè plot*, which is based on the *standard deviation 1* (*SD1*); it is used to quantify short-term beat-to-beat HRV (similar to RMSSD).

2.1.9.3 Heart-rate variability during exercise

Figure 2.15 illustrates that, during exercise, HRV undergoes a curvilinear decay as a function of intensity (expresses as $\%VO_{2max}$), which is closely related to heart rate. HRV reaches a near-zero minimum at moderate intensity (associated to the first ventilation/lactate threshold). When intensity increases towards the maximum, HRV slightly increases, although this fact is mediated by mechanical effects of respiration on SA node rather than by neural mechanisms. Regarding the duration, prolonged exercise duration attenuates HRV (although this fact is based on the assumption that HR increase during exercise and HRV does not reach the intensity-dependent minimum). On the contrary, prolonged duration causes a progressive withdrawal of the parasympathetic activity (lower HRV) which, in turn, affects cardiovascular drift. Orthostatic/circulatory conditions (posture, gravity, water immersion) have not substantial effect on HRV. Finally, the mode of contraction (e.g. static or dynamic) is another factor influencing HRV. Indeed, RMSSD decreases with an increase in the exercise load indicating a decrease in vagal modulation of HR with an increase in exercise load [7].

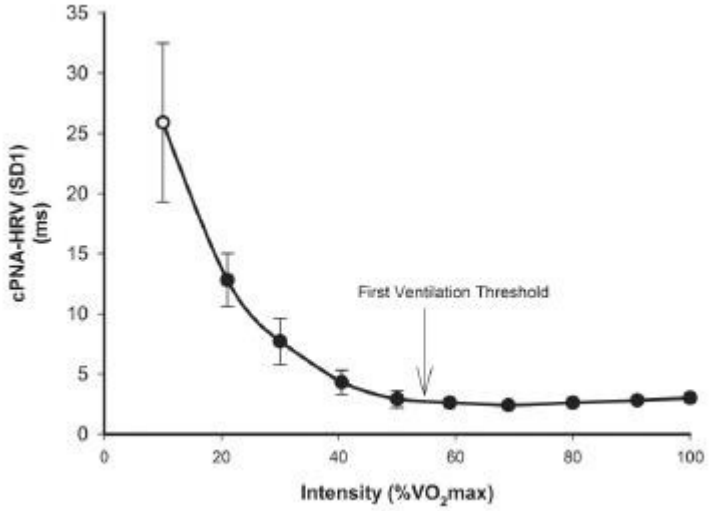

Figure 2.15 *cPNA-HRV (SD1 from Poincarè plot, ms) during rest and incremental exercise. Data are mean ±SD [7].*

2.1.9.4 Heart-rate variability during post-exercise recovery

Figure 2.16 illustrates how exercise intensity has a primary role in the immediate post-exercise recovery of HRV. At the cessation of exercise, HRV shows a recovery that depends on the intensity of the exercise: the higher the intensity, the slower the response. The effect of the exercise duration on HRV is still controversial; some studies report that a 100% in duration does not affect HRV recovery, although one study reports that HRV recovery is slowed in case of 300-400% increase in duration (from 20 to 90 minutes). This fact may suggest the existence of a critical length (relative or absolute) beyond which a possible HRV recovery effect can be seen. Finally, also exercise modality influences post-exercise HRV: indeed, a greater active muscle mass and/or energy expenditure is associated to a slower HRV recovery, at least following maximal incremental exercise.

2.1.9.5 Systolic Time Intervals

The *pre-ejection period* (*PEP*) is the time interval between the electrical depolarization of the left ventricle and the beginning of ventricular ejection; it represents the period of left ventricular contraction with the cardiac valves closed. It is important because it is inversely related to the cardiac sympathetic activity. Systolic Time Intervals (STI) measures are a useful non-invasive indicator of cardiac sympathetic activity.

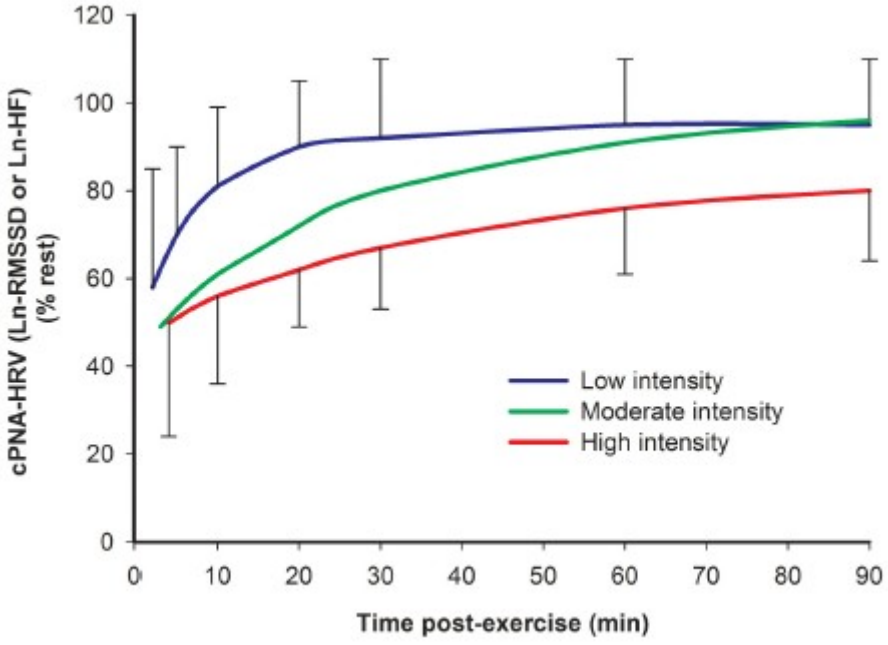

Figure 2.16 *Time course of cPNA-HRV recovery following different intensities of preceding exercise [7].*

2.1.10 Athlete's heart and cardiovascular care of the athlete

During exercise, the heart must normalize the intermittent hemodynamic stress of pressure and volume and meet the systemic demand for an increased blood supply [8]. It performs these tasks, during recurrent exercise, by undergoing *morphological adaptations* which are the result of a change in individual terminally differentiated cardiac myocytes. This adaptive remodeling occurs with preservation or enhancement of contractile function. On the contrary, an adaptation which can proceed to a loss of contractile function and heart failure, is a *pathologic remodeling*.

2.1.10.1 Exercise-induced cardiac remodeling

Already early studies with ECG suggested a left ventricle (LV) enlargement in trained athletes because of an increased cardiac voltage [9]. Subsequent works based on 2D echocardiography confirmed LV hypertrophy and dilation. Pelliccia et al analyzed a group (n=1309) of italian elite athetes from 38 different sports (73% male athletes). They found a marked dilation of LV chambers (>60 mm) in athletes with higher body mass and in those participating in endurance sports [10]. They also analyze the wall thicknesses among 947 italian elite athletes, and found that 1.7% of athletes had LV thicknesses higher than 13 mm (this is a rare finding in healthy athletes, and should be prompt consideration of pathological hypertrophy) and a comcomitant LV cavity dilation. Sharma et al confimed that increased LV wall thickness is associated with increased chamber size in young athletes [11]. Morganroth compared M-mode echocardiographic LV measurements in wrestlers (strength training), swimmers (endurance training) and sedentary control subjects. He found that athletes exposed to strength training demonstrated *concentric LV hypertrophy*[22], whereas endurance athletes demonstrated *eccentric LV enlargement*. This fact underlines that cardiac remodeling depends on the kind of sport (Morganroth hypothesis) [12]. Usually, the magnitude of eccentric hypertrophy resulting from endurance training is typically more pronounced than the concentric hypertrophy resulting from strength training. Several studies show that LV ejection fraction (EF) is generally normal among athletes [13], although one study found that 17% of the athletes participating in the Tour de France demostrated borderline or slightly reduced LV ejection fractions at rest. It has been demonstrated that endurance exercise training leads to enhanced early diastolic LV filling [14]. Moreover, it has been demonstrated that improved LV diastolic function is an essential mechanism of stroke volume preseravtion during exercise. Finally, a study suggested that the concentric LV

[22] Concentric hypertrophy is associated with increased left ventricular wall thickness, whereas eccentric hypertrophy is characterized by dilatation of the left ventricular chamber.

hypertrophy associated with strength training is accompanied by either unchanged or relative impairment of LV relaxation [15].

Exercise-induced cardiac remodeling is not confined only to the LV. Indeed, endurance exercise needs both the LV and right ventricle (RV) to accept and eject a huge amount of blood. A study based on M-mode echocardiography found symmetrical RV and LV enlargement in a small cohort of highly trained endurance athletes [16]. Henriksen et al demonstrates how endurance athletes showed significantly larger RV cavities and a trend toward thicker RV free walls [17]. Scharthag et al confirmed that RV enlargement among endurance athletes [18]. The influence of strength training on the RV is unclear because the data available are limited and inconsistent.

During exercise, also the aorta undergoes a significant hemodynamic load, which depends on sport type. Babaee Bigi and Aslani reported significantly larger aortic dimension at the valve anulus, sinuses of Valsalva, sinotubular junction, and proximal root in the strength-trained athletes [19]. The largest dimension was observed in athletes undergoing longest duration of exercise training. D'Andrea et al found that the aortic root diameter was significantly larger among strength-trained athletes [20]. Vascular remodeling also occurs in the descending abdominal aorta. On the contrary, Pelliccia et al found the largest measurements in endurance-trained athletes [21]. Therefore, making conclusions about the impact of sport-specific exercise training on aortic dimensions is impossible.

Hauser et al demonstrated that a small group of endurance athletes had a larger left atria than sedentary control subjects. Hoogsteen et al [22] found larger dimension in older athletes with respect to younger athletes in cycling. Pelliccia et al demonstrated that the left atrial enlargement was present in 20% of the athletes[23]. D'Andrea et al confirmed a high prevalence of left atrial enlargement in trained athletes and demonstrated an association with endurance exercise training [24].

Exercise-induced cardiac remodeling is similar in male and female athletes, although available data suggest that female athletes exhibit quantitatively less physiological remodeling than their male counterparts. Race is also an important factor, with black athletes tending to have thicker LV walls than white athletes [25].

Chapter 3

Wearable sensors for recording of cardiovascular signals and parameters

"Look at the people you don't love and see them as an exercise for you to open your heart"

[Ram Dass]

3.1 Introduction

Wearable devices are revolutionizing biomedicine through mobile and digital health by monitoring important physiological signs and activities of the athletes in real-time outside the clinic. They also facilitate the development of algorithms for automated health event prediction, prevention and intervention. Some sensors are already being integrated into standard clinical practise, whereas some others exist for use in consumer health and medical research (Fig. 3.1). In addition, they can be further classified into three main categories: mechanical (motion activity monitoring), physiological and biochemical.

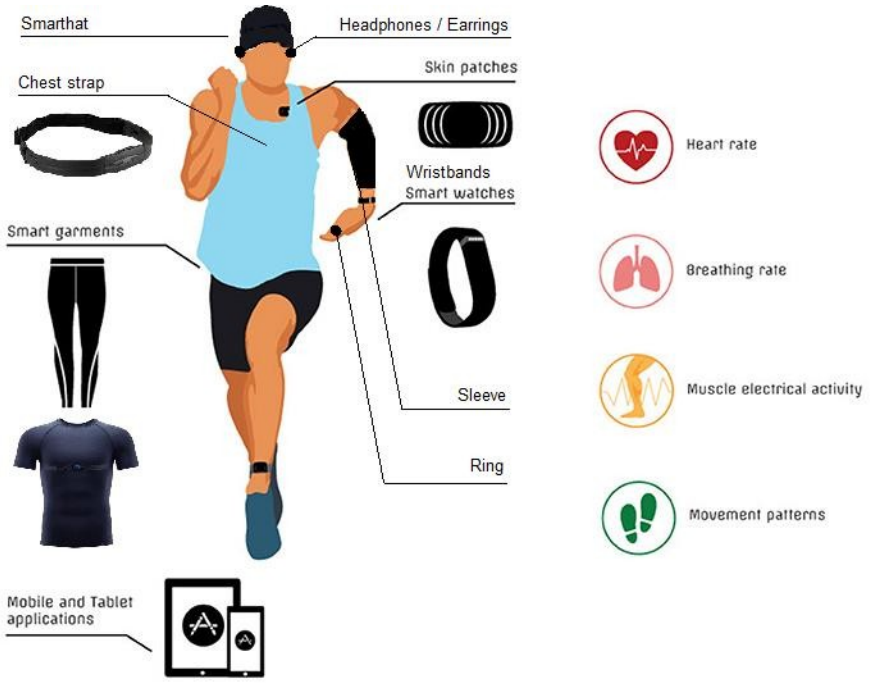

Figure 3.1 *Wearable devices for use in metabolic, cardiovascular and gastrointestinal monitoring; sleep, neurology, movement disorders and mental health; pulmonary health and environmental exposures; CGM, continous glucose monitoring.*

Wearable mechanical sensors usually make use of *inertial measurement units* (*IMUs*) for the estimation of translational and rotational motion, applied forces and sorrounding magnetic field. IMUs are constituted by biaxial or triaxial accelerometers (for 3D movement), gyroscopes (for rotation) and magnetometers.

Physiological sensors comprise optical, electrical, acoustic or thermal sensing components that can be integrated into textile fiber, clothes, and elastic bands or directly attached to the human body. These sensors are capable to measure vital signs and bioelectrical activity such as ECG, electromyogram (EMG), body temperature, electrodermal activity (EDA), electroencephalography (EEG), *arterial oxygen saturation* (SpO_2)[23], blood pressure (BP), respiratory signal and photopletismographic (PPG) signal.

Biochemical sensors combinea chemically sensitive layer and transducer to convert a chemical or biological analyte (glucose, alcohol, electrolyte, pH, oxigenation/gas, humidity) into an electrical signal.

The general structure of wearable health monitoring systems is equipped with a variety of sensors, actuators, wireless communication modules and signal processing units [26]. The general structure of the remote health monitoring system is illustrated in figure 3.2, although it could be different depending on the requirementss of the application. Indeed, the system can comprise several sensors which send data directly to the gateway, or connect each other by means of a body sensor network (BSN) with the central BSN node gathering data from sensors, performing processing and transmitting data to the advanced processing platform.

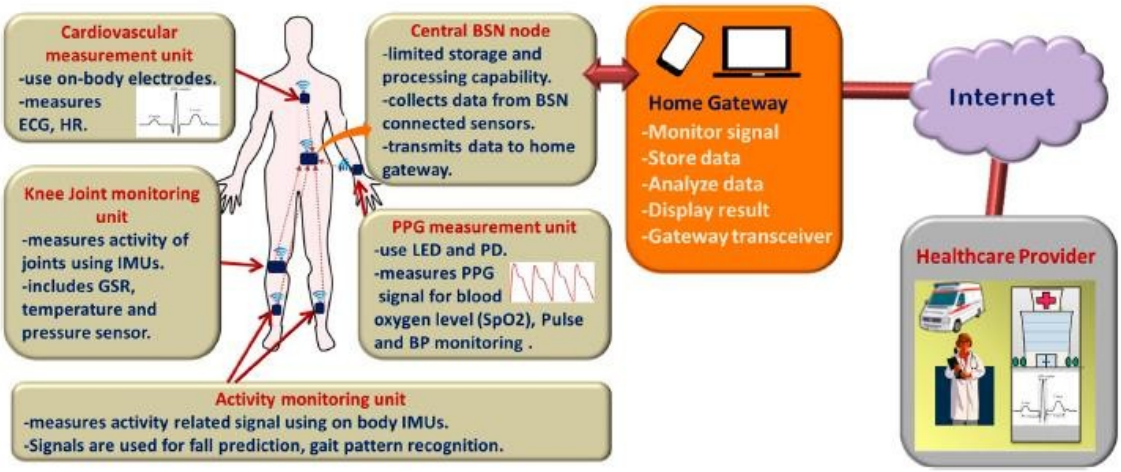

Figure 3.2 *General overview of the remote health monitoring system [26].*

[23] Arterial oxygen saturation is a measure of hemoglobin oxygenation in the arterial compartment of the circulatory system. It is not a measure of the total oxygen content in the arterial blood because a small fraction of oxygen (about 2%) is dissolved in the plasma. It is defined as the ratio of the concentration of oxygenated hemoglobin [HbO_2] and the concentration of total hemoglobin [HbT].

Wearable health monitoring systems also need to satisfy different requirements, covering both medical and ergonomic fields. Indeed, the systems need to be comfortable with their components flexible, small in dimensions, chemically inert, nontoxic and hypoallergenic to the human body. In addition, the dimension of the hardware must be big enough since the central node manages a large amount of data. Also the duration of the battery (power requirements) has a significant impact because long-term use is needed. Finally, a secured communication channel is necessary in order to safeguard the privacy of sensitive personal medical data.
Wearable sensors are also used for providing information on the environment and state of the athlete that can be fed back to improve future performance [27]. In the field of sport, wearability is very specific: that is, a wearable sensor for swimwear has different technical requirements to that of a suit worn for downhill skiing. In addition, sensors must be either integrated or incorporated into the athlete's attire in order to not limiting the freedom of movement required for the activity. The information gathered by the sensors about physiological data, performance and environment cover fundamentally four areas of use: competition, safety and recovery. The great advantage is that data are generated in real time and in field.
For most beginners and amateur athletes or those interested in fitness only, the main field where wearable sensors can be of use is in the training phase. Outside of training, wearable sensors can be useful during competition and during recovery programmes.

3.2 Physiological measurements

One of the most common functions of the wearable sensors is the measurement of physiological parameters. Table 3.1 reports some of the measurable physiological parameters by sensorised garments. The rest of the paragraph focuses on the monitoring of the cardiovascular signals, listing the main wearable technology companies with products applicable towards this field, and sorting them by the product type.

3.2.1 Textile electronics

Hexoskin® Biometric Shirt includes a sensor inserted into pocket at the waist of a comfortable tank top; it monitors HR, HRV, respiratory rate, number of steps, distance traveled, pace, maximal oxygen consumption and calories burned. With a battery life of 12-30+ hours, it allows 600+ hours of standalone recording. Users can visualize data with the connected health platform (iPhone, iPad and Android).

Table 3.1 *Examples of measurable physiological parameters by sensorised garments [27].*

Physiological data	Measured parameters	Description
Cardiac data	ECG	Heart beat profile obtained by measurements of electrical activity of the heart by electrodes placed on the thoracic area; the profile indicates the contractions and relaxations of the cardiac cycles
	Heart rate	Number of the beats per minute (or cycle frequency); can be obtained from ECG data and other pulse measurements
Breathing data	Breathing profile	Thoracic volumetric changes obtained by measuring expansion and contraction of the rib cage
	Pneumography	Measurement of velocity and force of chest movement
Muscle activity	EMG	Measuring electrical activity of the muscles to determine muscle activity and intensity of activity
	Muscle contraction and expansion	Measurements of dimensional changes in muscles during activity
Temperature	Skin temperature	Measuring the temperature at the skin surface
Sweat data	pH	Measuring the pH of sweat during activity
	Skin conductivity	Measuring skin conductivity to characterise sweat-gland activity
Oxygenation	Oxymetry	Oxygen saturation level in the blood, obtained by emitting light onto the skin and measuring the reflected light

Athos® is a leader in the development of smart apparel allowing the measurement of HR, respiratory rate, and muscle activity. The Athos system is designed for casual athletes as well as those who are trying to maximize their fitness and looking for any possible edge to get ahead of their competition. The shirt is based on a small electronic device inserted into an integrated pocket at chest. There are about 12 EMG sensors and 2 heart rate sensors embedded in the shirts to keep track of muscle activities and heart rate (Fig. 3.3); similarly, the shorts also have a pair of 8 EMG and 4 heart rate sensors. Athos uses also a six-axis accelerometer, but muscle activity tracking is what makes Athos stand out from a field of accelerometer-based competitors. Users can look at the Athos® App Live View on their phones via Bluetooth to see real time stats.

Figure 3.3 *From left to right: Athos shirt, Athos core interpreting and transmitting biosignals from the garment, Athos app.*

Heapsylon LLC (or Sensoria®) commercializes both compression shirts and bras for the monitoring of the HR. They comprise electronic snaps onto the garment at the chest and provide accurate and consistent measures without the hassle of wearing a strap; in particular, the electrodes need to be moistened before the use. The shirt offers a comfortable and close-to-body feel. Users can visualize real time metrics on their smartphones (Sensoria Run v2.0 app) or smartwatches. The t-shirt can be used with most Bluetooth Smart heart rate monitors with standard snaps (Fig. 3.4).

Smartex® Wearable Wellness System includes a sensorized garment (bra or shirt), an electronic device inserted into a front pocket at the chest (dedicated to the acquisition, the processing and the storage of data), and a complete software kit to be used in order to manage and visualize the acquired data and to configure the electronic device (Fig. 3.5). The electronic device elaborates the acquired signals to extract several parameters such as HR, respiration rate, HRV, posture and activity classification (lying, standing, walking, running), estimation of energy exprenditure and steps/min.

Figure 3.4 *From left to right: Sensoria shirt and app, Sensoria bra, Sensoria smartwatch.*

Figure 3.5 *From left to right: Smartex bra, Smartex software (top), Smartex device (bottom), Smartex shirt.*

In addition, the device is able to save data on a Flash Memory (microSD), transmit data via Bluetooth, and save and transmit them simultaneously, without losing information in case of interruption of Bluetooth transmission. The storage capability can reach up to 30 hours. Data can also be transmitted via wireless to any host device equipped with Bluetooth (such as desktop PC, Notebook, Smartphone) to analyse in real-time the monitored physiological parameters.

OMsignal® system consists of a garment (OMbra for women and OMshirt for men) with integrated sensors and an electronic device (acquisition module for data recording and processing) positioned under the chest line under the arm (Fig. 3.6). The garment contains 3 silicone-based electrodes that are in contact with the skin, recording a single-lead ECG; two electrodes are situated just below the major pectoral muscles, left and right, providing a modified V5-lead signature. The electrode located at the bottom of the left scapula acts as a right leg lead. A woven wire at the ribcage level records respiratory inductance plethysmography. The ECG sensors are connected to the acquisition module through 5 snaps. OMsignal® system monitors HR, respiratory data, distance and speed, cadence and movement intensity. Collected data are conveyed via bluetooth to a smartphone (OMrun app) to see insights in real time. The acquisition module has the capacity to save or process ECG signals for offline analysis or real-time monitoring. Data transfer from the acquisition module to a computer simply requires a USB cable.

Figure 3.6 *A, OMshirt (men);B,OMbra (women); C, acquisition module; D, five snaps.*

In addition, the acquisition module can also be configured for direct data transfer into a web-based cloud, offering theoretically unlimited recording/storage capacity and direct long-term remote monitoring.

Numetrex®/Textronics Inc.®/Adidas® miCoach is available as bras, tank tops and shirts for HR monitoring (Fig. 3.7). They include electronic device clips into a pocket at chest. The electrodes need to be moistened prior to use and be in close contact. Data are sent to Runtastic app.

Kymira® shirt (Fig. 3.8) is designed to lower the risk of heart attacks for athletes. Electrodes are printed onto the shirt's fabric feed and wirelessly transmit single lead ECG data to the cloud via bluetooth.

Figure 3.7 *From left to right: Numetrex/Textronics Inc./Adidas miCoach shirt, Numetrex/Textronics Inc./Adidas miCoach bra, Runtastic app.*

Figure 3.8 *Kimira shirt.*

There, Kymira's proprietary algorithms process and clean the data to remove noise and movement artefacts in order to accurately detect irregular heartbeats such as arrhythmia heart beats.

3.2.2 Chest straps and patches

MC10® BioStamp RC™ is an epidermal sensor supported by 25 validated wear locations on the body, among which the chest (Fig. 3.9). Its clinically validated algorihtmic interpretation of raw physiological data delivers clinical insights into vital signs, activity, posture, sleep, and the relationships among them: HR and HRV (in both time and frequency domain), respiratory, activity, EMG and posture (Fig. 3.10).

Figure 3.9 *From left to right: BioStampRC sensor, 25 validated wear locations on the body.*

Figure 3.10 *From left to right: BioStamp sleep, posture, activity insights; BioStamp vital signs insights.*

Health Care Originals® ADAMM-RSM is a chest patch which allows continuous monitoring of HR, respiration, adventitious breath events, temperature, cough and activity. Overall, the system (Fig. 3.11) also consists by a smartphone app (which monitors the symptoms, sets notifications and reminders, and shares data with caregivers and healthcare providers), and a web portal (where the user can manage his data in complete privacy and security).

iRhythm® Zio patch (Fig. 3.12) enables an uninterrupted ECG signal, giving the assurance of reliable data with minimal artifact. This patch is used for ambulatory cardiac monitoring.

Figure 3.11 *From left to right: Health Care Originals app, web portal, patch.*

Figure 3.12 *From left to right: Zio patch, body location, ZioSuite portal.*

The advantage is that there are no batteries to charge and electrodes to reposition: this translates into longer wear times and an astounding 98% subject compliance. It also means faster time to diagnosis. Zio report is the product of a FDA[24]-cleared deep-learning algorithm together with meticulous review by Certified Cardiographic Technicians; physicians agree with the findings of the report 99.9% of the time. With the clinician portal, ZioSuite, it is possible to interpret reports, manage subjects, and even track subject devices, with very high efficiency. Moreover, it is possible to do it all from your computer or while on the go with the mobile app.

Preventice BodyGuardian® Heart (Fig. 3.13) is a small, discrete, wireless monitor that attaches to the chest via strip, with the medical-grade adhesive and electrode gel. Users can continously monitor ECG and other vital parameters on their smartphones via bluetooth.

Figure 3.13 *Preventice BodyGuardian Heart.*

[24] Food and Drug Administration (FDA) is a Federal agency of the Department of Health and Human Services responsible for telling which foods, drugs and medical devices are safe to use.

VitalConnect VitalPatch® (Fig. 3.14) is a chest patch (containing electrodes) that monitors eight physiological measurements continously in real time: single-lead ECG, HR, HRV, respiratory rate, body temperature, body posture, fall detection, activity. In particular, the sensor contains ECG electrodes, 3-axes MEMS accelerometers, and thermistors. The zinc air battery has a 168 hours life (about 7 days duration), with the possibility of real-time 10 hours of storage.
Zephyr™ BioHarness 3.0 is able to monitor physiological parameters by means of three different modalities: a chest strap with integrated sensors, a compression shirt with embedded sensors, and a flexible support which can be connected to the standard ECG electrodes (Fig. 3.15). It monitors ECG (250 Hz), HR (240 bpm ±1 bpm), respiratory frequency (0-120 bpm ±1 bpm), skin temperature (10-60 °C ±2°C), activity (standing, walking, running), acceleration (3-axes accelerometer at 100 Hz up to 16g), position/posture (±180°), and calories. Electrodes need to be lightly moistened prior to use to capture heart data; electronic device snaps into place on the side or front of strap/garment. The battery has a duration of about 35 hours in recording-modality, and about 28 hours in continuous transmission. It can store data of up to 500 hours. The wireless communication is given by Bluetooth combined with Zigbee [25]. BioHarness 3.0 is equipped with the software Omnisense which is composed by two modules: Omnisense Live for the real-time monitoring, and Omnisense Analysis for analysis of the recorded data. In particular, Omnisense Live allows to manage the apparatus assigning them to the various users, and monitor the weared and activated BioHarness devices. The software has a display which shows the combined data on the user's personal dashboard in real-time. It is possible to set alarm-thresholds on the aerobic or cardiovascular parameters; every overcoming of these thresholds emits an acoustic signal, and the user's dashboard changes colour at the correspondance of the level of exceedance of the threshold (green, orange or red). It is possible to manage up to 55 users at the same time with the same system. The new software Omnisense 3.0 has also the possibility to monitor the trainings of the athletes. For each user, the trainer can decide to carry out a personalized/customized training according to the objectives to reach.

Figure 3.14 *From left to right: VitalConnect VitalPatch sensor, body application area, app.*

[25] Zigbee is an IEEE 802.15.4-based specification for a suite of high-level communication protocols.

Figure 3.15 *From left to right: BioHarness 3.0 chest strap; body application area of the chest strap; BioHarness 3.0 compression shirt; BioHarness 3.0 flexible support; body application area of the flexible support.*

Indeed, the software has about a hundred of "workout models which can be automatically inserted into the training program of the athlete or, alternatively, it is possible to personalize/customize a specific training model. The training areas are distinguished by colours correspondant to the values of the percentage of the cardiac frequency in relation to the anaerobic threshold. The software, therefore, is able to show the intensity of the training carried out by the athlete (Fig. 3.16). The software for analysis allows to visualize all the parameters recorded on the apparatus in graphical format, to elaborate data and to compare different sessions in order to obtain a complete profile of the user. It is possible to show the trend of the single vital parameters or the combination of several parameters. The software can generate automatic reports for each user o for a team, comparing performances of each athlete of the team. Nowadays, BioHarness 3.0 is available also for the use with GPS terminals. GPS data are sent to the apparatus which store them; they can be successively downloaded and used for analyses and comparisons. Data stored during a training or a recording, with the joint use of the GPS, can be successively exported as .kml files and displayed on Google Map: doing so, a great dataset si obtained comprising position, velocity, elevation, cardiac frequency and respiratory frequency. This function is very useful for tracking the psycho-physical behaviour of the athlete during a training or simply during a walk of a user. GPS and psycho-physical data can be reproduced in form of exportable Excel table (Fig. 3.17).

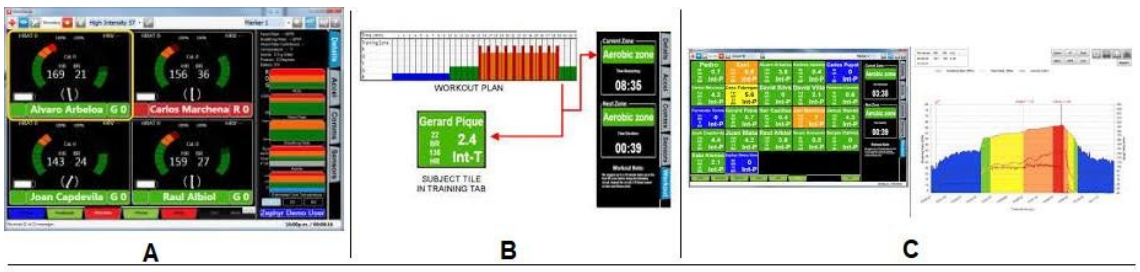

Figure 3.16 *Panel A, multiusers monitoring display; Panel B, training areas, correspondant colours and timings; Panel C, multiusers training models and table (the table of each athlete assumes the colour in correspondance of the training area).*

Nowadays, the BioHarness 3.0 has a new hybrid transmission method, called ECHO, which combines Bluetooth and Zigbee technologies. This new solution allows to have additional boosters in order to cover entire football fields or athletics grounds. Indeed, ECHO system, with only one booster, ensures minimum coverage radius of approximately 100 meters (300 yards). Regarding the mobile monitoring, BioHarness 3.0 can connect via Bluetooth to an Android smartphone, on which the softwares ZephyrME or ZephyrLife have been installed. Data transmitted by the apparatus are displayed on the smartphone screen in graphical-numeric format. The user must connect to the web site www.Zephyranwhere.com from his smartphone, after creating an account and a password, to send data. The web page shows a dashboard from which it is possible to visualize in real-time the cardiac frequency, respiratory frequency, activity, posture, temperature and ECG tracing. In addition, with the new BioHarness 3.0, it is possible to associate a SpO_2 detector, a weight-scale, and a pressure monitoring system. for each user, it is possible to create a web page with data storage and recording available for a coach or cavegiver.

Corscience® CorBelt (Fig. 3.17) is an intelligent chest strap equipped with an algorithm for the recognition of atrial fibrillation with the aid of HRV. It continuously measures and analyzes a 1-channel ECG, and it can be used also as an event recorder. Indeed, the CorBelt has a storage function: it analyzes the ECG and, if arrhythmia occurs, records a 2-minute ECG (1 minute before the arrhythmia and 1 minute after the arrhythmia). Currently, only rhythmological pathologies are detected: ventricular tachycardia, ventricular fibrillation, bradycardias, absolute arrhythmias, pauses. The ECG recording is done by two hard electrodes made of stainless steel. The memory capacity is about 20 minutes or 10 events. The recorded ECG measurements are sent to an intermediate relay station (usually a cell phone, personal digital assistant or modem) via Bluetooth, and are further transmitted to a rescue dispatch center or clinic. Therefore, data can almost be transmitted live with the CorBelt mobile software. The batteries are rechargeable. The entire package includes: CorBelt device, mobile phone, transmission software installed in the mobile phone, mobile phone charger, two chest straps (small and large), two chargeable batteries, CorBelt suitcase.

Figure 3.17 *From left to right: CorBelt chest strap, mobile phone, body application area.*

The Equivital EQ02 LifeMonitor senses, records and processes data measured from the person, and is able to transmit this over a wireless or wired interface. LifeMonitor has two components: the Sensor Electronics Module (SEM) and the Sensor Belt, which positions the SEM on the left side of the chest (Fig. 3.18). It can output the following channels of data simultaneously: two-lead ECG (256 Hz), HR (25-240 bpm), RR-interval, respiratory rate (0-70 breaths per minute), skin temperature (0°C to 60°C ±0.3°C), 3-axes accelerometer (±2, ±4, ±8, ±16g), body position (all orientations with fall detection and motion). A wide selection of wired or wireless sensors integrate with LifeMonitor, which can also measure the following channels of data: oxygen saturation (including photoplethysmography at 16-bit resolution), galvanic skin response, core temperature capsule, dermal temperature patch, and GPS. Data are sent, in real-time, to any EQView software suite app: this includes EQView Mobile (smartphone app compatible with RIM and Android operating systems). The battery has a duration up to 48 hours. LifeMonitor has a memory of 8 GB for up to 50 days of continuous data logging.
Piezologist is a cardiorespiratory monitoring system comprising a patch-type sensor worn at the chest, and a mobile application. The sensor utilizes piezoelectric material as the signal sensing component, and MetaWearC board as the signal acquisition unit. Piezoelectricity is the electric charge that accumulates in solid materials in response to an applied mechanical stress. The board also comes with Bluetooth support. The monitored parameters are HR, respiration rate, cycles, but ECG waveform and blood pressure data were also extracted using the same sensor. The first developed model included the sensor on the top of the case: a circular plate held the double face adhesive tape. This plate was attached to the case via winding. Nowadays, the sensor is distant from the skin in order to obtain a small signal-to-noise ratio (SNR), and is placed on the top of the case. Moreover, the adhesive tape is attached to the sensor surfaces (Fig. 3.19). The entire Piezologist system consists of the above-described piezoelectric sensor together with a desktop application for remote medical data analysis and risk detection, and mobile-based data presentation and activity analysis.

Figure 3.18 *From left to right: Equivital EQ02 LifeMonitor CorBelt SEM, chest strap.*

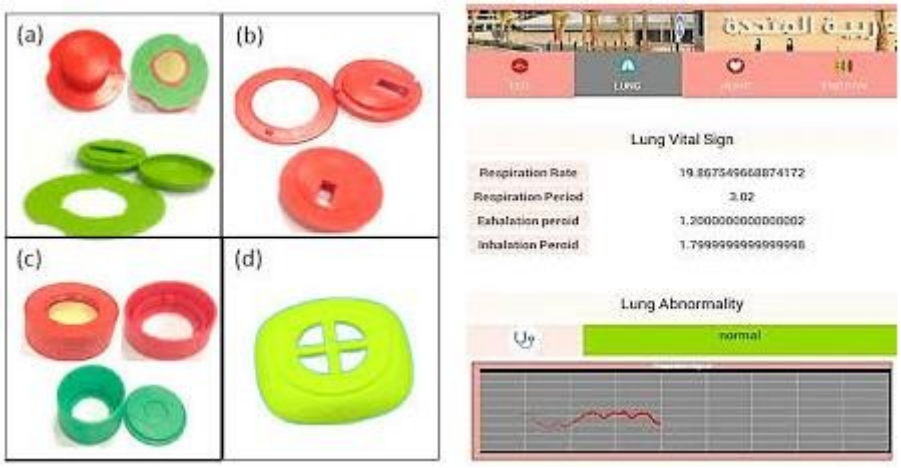

Figure 3.19 *Left: Piezologist case design and prototype evolution: a) first model, b) second model (reduced plate size and snap-fit enclosure), c) third model (sensor distant from the skin, removal of the plate, and small led back case that snap-fit into the top case), d) fourth and final model. Right: Mobile Application prototype.*

3.2.3 Smartwatches and wristbands

Jawbone UP3® Fitness Tracker (Fig. 3.20) is a wristband that monitors parameters such as HR, sleep stages, food and liquid intake, number of steps, distance traveled and running. It communicates via bluetooth with smartphones and has a battery duration of about 7 days. UP3 is based on a multisensor platform which comprises a 3-axes accelerometer, two bioimpedance sensors, and two sensors for the temperature (skin and environment)

Striiv® Fusion Bio Fitness Tracker (Fig. 3.21) is a smartwatch with the following features: continuous HR monitoring, activity tracking (number of steps, distance, burned calories), journaling (possibility to log and journal daily habits like diet, weight, medication, hydration directly on the band screen), caller ID & text alerts, app notification, alarm & reminder, and support (it works flawlessly with Android, Apple, and any standard phone supporting Bluetooth 4.0).

Figure 3.20 *Jawbone UP3.*

Figure 3.21 *Striiv Fusion Bio.*

Striiv Fusion Bio has a battery duration of about 5 days with a single charge; sometimes, depending on the usage, it can hold the charge for a week.
Fitbit Charge HR™ Fitness Tracker (Fig. 3.22) is a smartwatch monitoring HR, calories burned, sleep quality, food and liquid intake, number of steps, elevation, climbing and running. It has a battery duration of about 5-7 days. Unfortunately, there is no any integrated GPS which, however, can be found in the model Fitbit Surge. Many GPS-integrated devices focus on running and cycling, and ignore the posisbility to monitor also the gym workout. However, Fitbit Charge HR is useful also for the gym; indeed, the optical HR monitor, using a luminous LED, can "see" the blood pulsing on the wrist. Thanks to the smartphone app, it is possible to monitor also the quality and the quantity of the sleep. The app shows a broad overview of all day data and statistics, incuding steps, HR, run distance, burned calories, training minutes, and sleep monitoring. Fitbit Charge 3 is the last natural heir of the Fitbit Charge HR, and comprises also a sensor for the blood oxygen saturation level (SpO_2) monitoring.
Garmin Vivosmart® HR (Fig. 3.23) is a smartwatch that monitors HR, calories burned, sleep quality, number of steps, climbing, running and swimming. It has a battery duration of about 5 days, and the allowed wireless platforms are bluetooth and ANT+.

Figure 3.22 *Left: Fitbit Charge HR Fitness Tracker; Right: Fitbit app.*

Figure 3.23 *From left to right: Garmin Vivosmart HR fitness tracker (anterior and posterior view, respecitively), Garmin Connect app.*

With the January 2016 update, Garmin Vivosmart HR is able to monitor HR for many activity profiles in addition to the running one; the updated version of May 2016 is the Garmin Vivosmart PLUS with integrated GPS. As has been said, the HR monitoring is continuous, but Vivosmart HR offers two different modalities: training modality and resting modality. In the first one, the HR and the frequency range are displayed in real-time, whereas, in the second one, a touch on the screen is needed to visualize the resting HR. Indeed, Vivosmart HR displays the HR as well as the frequency range within which the athlete is training. allowing to increase or decrease the training intensity. Data from the sensor can be saved and recorded on the Garmin Connect by means of Garmin Connect Mobile app or Garmin Express on PC. Garmin Forerunner 645 music is the last heir of the Garmin smartwatches family; its hallmark is the possibility to save more than 1000 music tracks on the 4GB memory importing them from PC or through Garmin Express software, or through Media Player or iTunes. A very important characteristic is also the independence and autonomy of the smartwatch which, at the end of each training, evaluates the results and analyzes them by means of Firstbeat (VO_2max, performance condition, Training Status, Training Effect). Another very useful function is LiveTrack which, connecting to the GPS signal, allows to share its position in real-time during a training. Training Status function permits to verify the efficacy of the training, whereas Training Load function allows to calculate the intensity of the training for a period of 28 days. Regarding the gym, Forerunner 645 Music has pre-set profiles for cardio-workout, strength-training, indoor-rowing, and many other. For outdoor enthusiasts, there are profiles for snowboard, ski, cycling, swimming, and rowing.

Adidas® miCoach Fit Smart (Fig. 3.24) is a smartwatch monitoring HR and distance.

Figure 3.24 *From left to right: Adidas miCoach Fit Smart (anterior and posterior view, respecitively), Adidas miCoach Train & Run app.*

It comprises the optical heart monitor Mio continuous and an accelerometer. Through the miCoach Train & Run app, it is possible to choose up to 15 different training options, set personal daily and weekly objectives, and receive notifications. The results are shown on a smartphone or tablet via Bluetooth 4.0, and also on PC synchronizing at personal Adidas account. The memory supports up to 10 hours of training. The smartwatch is water-resistant allowing the use also for swimmers.

Apple® Watch (Fig. 3.25) monitors HR, distance and ECG; Apple® Watch Series 4 have several other sensors monitoring acceleration, ambient light, rotations, GPS, barometric altitude and PPG HR (photopletismography HR). Indeed, the smartwatch is able to generate a single-lead ECG. Electrodes detecting the electrical signals from the heart are placed on the posterior part and in the Digital Crown of the Apple Watch Series 4. By pressing a button, it is possible to obtain an ECG in only 30 seconds. This means that the app is able to understand if the heart rate is regular (sinusal rhythm) or if there are signals of atrial fibrillation or other heart rhythm alterations.

Figure 3.25 *From left to right: Apple Watch Series 4, Apple Health app.*

The recorded data are saved and stored on Apple Watch Series 4 Health app. Moreover, this app are shareable with the personal physician.

Polar® A360 (Fig. 3.26) is a smartwatch monitoring HR and tracks performance. It can be used also by swimmers, because it is water-resistant up to 30 meters. The smartwatch contains an optical sensor developed by the same Polar. The usage of the sensor is very simple: just activate the training mode, and the HR is continuously monitored in each activity (gym, running, swimming-pool, football, walking). The added value is represented by the Training Benefit function, which gives feedback about the training and suggests how to change or alternate the intensity of the training. Polar offers morethan 100 modalities of sport profiles. It is possible to customize each sport activity in Polar Flow app or on Flow Web service. The Smart Calories function allows to estimate the quantity of the burned calories during the day. Sleep monitoring modality is automatically activated. The battery has a life of about 12 days, but with disabled notifications. Polar Vantage M is the last heir of the A360; it integrates the presence of the HR monitor, the GPS GLONASS, and the Bluetooth with lower battery-consumption impact. Its trademark is the Polar Precision Prime sensor, which integrates 4 bioimpedance sensors and optical sensors with green and red wavelengths able to penetrate much more deeper the skin in order to obtain a more accurate measure of the blood flow. It comprises more than 130 sport profiles which can be also customized using Polar Flow. Training Load Pro function allows the measurements of the effort produced each training session, with the possibility to set a daily activity objective, and to keep track of the burned calories, the steps, the run distance thanks to the dedicated functionalities of Activity Tracking of Polar M. The measurement of VO_2max is obtained through Running Index. The battery of the Vantage M ensures a duration up to 30 hours with enabled training mode.

Samsung® GearFit 2 is a smartwatch monitoring HR, calories, number of steps, and sleep quality (Fig. 3.27).

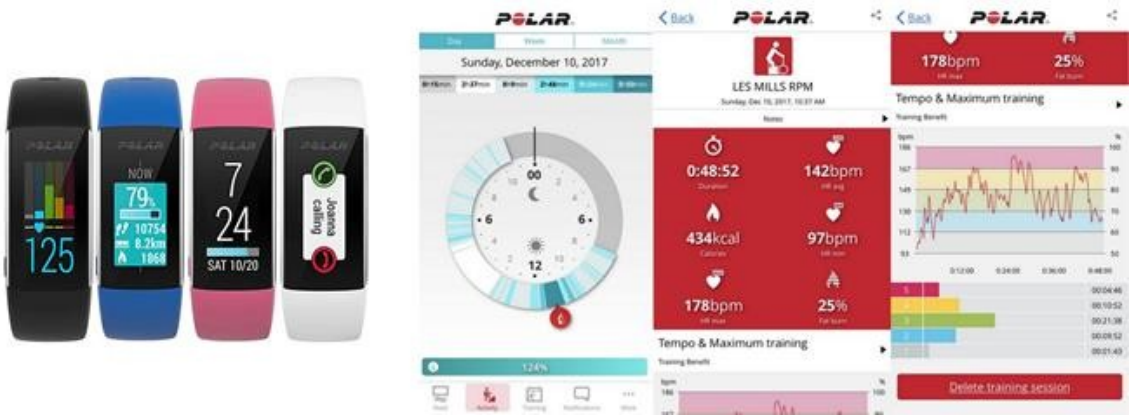

Figure 3.26 *From left to right: Polar A360, Polar Flow app.*

Figure 3.27 *From left to right: Samsung GearFit2 smartwatches, Samsung Health app.*

An important distinction is that it is not a device for swimmers. In addition, it adapts its metrics to the kind of sport it recognizes. GearFit2 monitors HR every 10 minutes, but the detection becomes continuous as soon as one available activity tracking is enabled. A disadvantage is that the accuracy is poor: it ranges between 2-5 bpm at rest, and up to 10 bpm during prolonged activities. Therefore, Samsung is positioned behind Garmin and Fitbit in terms of accuracy of the HR monitor sensor. GearFit2 comrises also GPS, gyroscope, barometer and accelerometer. Through the GPS, it is possible to display an interactive map of the path. Samsung Health app diplays all the steps, calories, sleep graphs. The battery duration ranges between 2-4 days.
Under Armor® HTC® Grip (Fig. 3.28) is a wristband monitoring HR, calories burned and distance traveled (it has an integrated GPS). It has battery with a duration of about 5 hours with the GPS enabled, and about 2 days with normal usage.
Huawei® Honor Band A1 and Band 3 Pro (Fig. 3.29) are two smartbands monitoring cardio-respiratory fitness.

Figure 3.28 *Under Armor HTC Grip wristband and app.*

Figure 3.29 *From left to right: Huawei Honor Band A1, Huawei Band 3 Pro, Huawei Health app.*

In particular, the Band 3 Pro is suitable also for swimmers (SWOLF is an index that evaluates the efficacy of the swims and the number of the strokes). For the other kinds of training, there are functionalities for the calculation of the recovery time, VO_2max, and burned calories. Recorded data are displayed on Huawei Health app. The duration of the battery is another strong point of this smartwatch: the autonomy declared by Huawei for a normal daily use is 14 days, whereas it reaches up to 20 days in stand-by mode.
Xiaomi® Mi Band 3 (Fig. 3.30) monitors HR, time and number of steps. Xiaomi Mi Fit app allows to visualize the performed steps, burned calories and run distance.
AliveCor® Kardia Band (Fig. 3.31) is a wristband monitoring ECG. Indeed, it is possible to record a single-lead ECG by simply touching the integrated sensor which communicates with the Watch app. Kardia's algorithm is able to instantly detect the presence of atrial fibrillation (AF).

Figure 3.30 *Left:Xiaomi Mi Band; right: Xiaomi Mi Fit app.*

Figure 3.31 *Left: AliveCor Kardia Band; right: Kardia Mobile app.*

In addition, it includes the Normal Detector which indicates whether the HR and rhythm are normal, and the Unreadable Detector which tells whether the ECG has to be repeated. Moreover, Kardia integrates seamlessly with Apple's Health app to include ECG data. AliveCor has also re-introduced its first device, AliveCor Mobile ECG, under the new Kardia brand name as Kardia Mobile app.

Ava Science Inc.® Wristband (Fig. 3.32) monitors PPG HR, accelerations, electrodermal activity (EDA) and temperature.

Omron® Heart Guide (Fig. 3.33) is a smartwatch that monitors PPG HR, oscillometric blood pressure and accelerations. It synchronizes to the HeartAdvisor app.

Figure 3.32 *Ava Science wristband and app.*

Figure 3.33 *Left: Omron Heart Guide smartwatch; right: HeartAdvisor app.*

Sentio Solutions® Feel (Fig. 3.34) is a wristband comprising four integrated sensors which monitor a variety of physiological signals such as: PPG HR, skin temperature, blood volume pulse, electrodermal activity. In particular, the HRV is measured through a Blood Volume Pressure (BVP) sensor, the electrodermal response (EDR) is measured through a Galvanic Skin Response (GSR) sensor, movement and activity are measured with Inertial Measurement Unit (IMU). In addition, Sentio Feel is water-proof. The Feel mobile app tracks the signals throughout the day.

Withings® Steel HR, Activitè, Go, Pulse O_2 (Fig. 3.35) are bands monitoring HR and distances.

Stirfit® band monitors HR, blood oxygen, body mass index, calories burned, distance, fatigue and sleep.

Figure 3.34 *Sentio Feel wristband and Feel Mobile app.*

Figure 3.35 *Left: Withings Steel HR; right: Withings Pulse O2.*

3.2.4 Other applicable products

LifeBEAM® (Fig. 3.36) is a smart hat that monitors HR. It is based on electro-optical technology (dynamic light scattering) which samples pulse in high frequency, calories and skin temperature.
Komodo Technologies Inc.® AIO Smart Sleeve (Fig. 3.36) monitors ECG, HR and sleep stages.
BioSensive Technologies Inc. ® Joule (Fig. 3.37) are earrings monitoring HR, calories burned, steps taken and overall activity level.
Jabra® Sports Pulse Wireless Headphone (Fig 3.37) monitors HR and accelerations.
Motiv® Ring (Fig. 3.37) monitors PPG HR and accelerations.
Oura® Ring (Fig. 3.37) monitors PPG HR, accelerations, rotations and skin temperature.

Figure 3.36 *Left: LifeBEAM smarthat; right: Komodo Technologies Inc. AIO Smart Sleeve.*

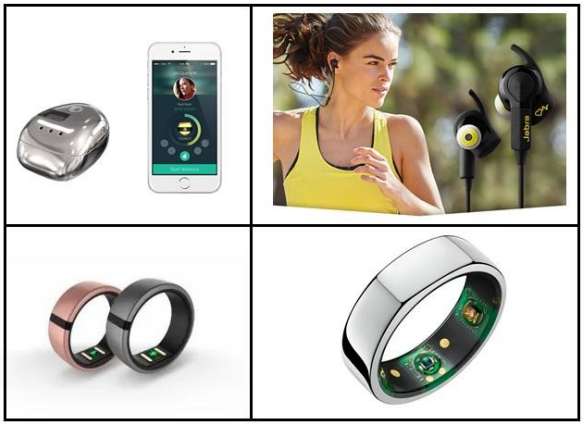

Figure 3.37 *Top left corner: BioSensive Technologies Inc. Joule; top right corner: Jabra Sports Pulse Wireless Headphone; bottom left corner: Motiv Ring; bottom right corner: Oura Ring.*

3.2.5 Chronotropic competence indices

Chronotropic incompetence (CI) is defined as the inability of the heart to increase its rate commensurate with increased activity or demand. Therefore, CI relies on heart rate response to exercise. According to Fick equation (1.19):

$$VO_{2\,max} = (HR \cdot SV) \cdot (C_{(a-v)}O_2) \tag{3.1}$$

Thus, CI parameter could be a surrogate for oxygen consumption in measuring cardiopulmonary response to exercise. The following four indices are defined for the quantitative measurement of the overall profile of heart rate response during the exercise test:

- Resting Heart Rate (HR_{rest}): it is defined as the HR when a person is awake, in a neutrally temperate environment, and has not been subject to any recent exertion or stimulation, such as stress or surprise;
- Chronotropic Rate (CR): it represents the rate at which the HR increases as exercise intensity increases; it is measured as amount of HR increase in response to every unit of metabolic equivalent (MET) exercise intensity increase:

$$CR = \frac{(HR_{stage} - HR_{rest})}{(MET_{stage} - 1)} \tag{3.2}$$

- Chronotropic Limit (CL): it represents the maximal HR a person can reach without severe problems through exercise stress. It is measured as Heart Rate Reserve (HRR) and calculated as:

$$CL = HRR = \frac{(HR_{max} - HR_{rest})}{(HR_{PredM} - HR_{rest})} \quad (3.3)$$

where HR_{max} is the maximal HR one achieves during exercise test, and HR_{PredM} is the predicted maximal HR usually calculated as 220-Age. Maximal HR is usually obtained when reaching peak exercise, which is easily identified during cardiopulmonary exercise testing (CPET). In this case, the normal range of CL is between 0.8 and 1.3. However, if peak exercise is not achievable, normal CL values can be estimated from various types of exercise. For example, in a 6-minutes walking test, CL equal to 0.4 for a 60-year old person should be considered normal. With a resting HR of 75 bpm, CR would be 10 beats per MET, and the maximal HR would be 109 bpm with an exercise intensity of 4.4 MET.

- Heart Rate Recovery at 1 minute after exercise ($HR_{recovery}$): it is defined as the reduction in HR at maximum during exercise and the rate as measured at 1 minute after stopping exercise.

Cardiac Chronotropic Competence Testing (3CT) is a device produced by SmartHealth Electronics Ltd.® and designed to measure the chronotropic competence indices (CCI). It consists of a wearable device, a smartphone app, and a workstation. The wearable device is an ECG patch with embedded 3D accelerometer and 3D gyroscope to collect activity signals. The collected ECG signals and activity signals are sent to the smartphone app via bluetooth. The app processes signals and derives HR, estimates walking step length, number of steps and walking speed, and calculates exercise intensity in terms of METs. The app, then, sends all data and testing information to the workstation, where the clinician can observe all signals and status. The report consists of a table with the CCI values, together with curves of heart rate variation against exercise intensity (Fig. 3.38).

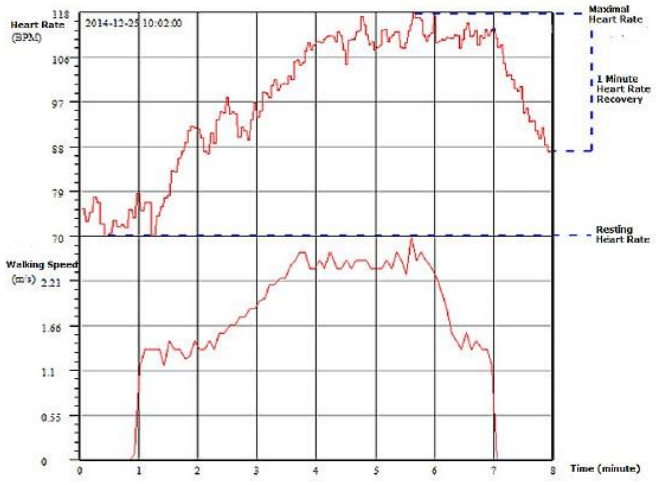

Figure 3.38 *Curves of HR variations against intensity during the 8-minute walking test [28].*

Chapter 4

Algorithms for the automatic identification of the exercise phases

"When we love, we exercise our hearts"
[Akeelah Fallah]

4.1 Heart Rate Varability for automated identification of exercise exertion levels

4.1.1 Introduction

Analysis of Heart Rate Variability (HRV) has been demonstrated to potentially help in estimating activity of autonomous nervous system (ANS) and level of exertion [29]. Despite there are several methods to analyse HRV, it has been shown that short-term sequences of beat-by-beat heart rate data in time domain are very effective in continuous monitoring of levels of physiological stress. Therefore, short-term HRV analysis in time-domain is used for automated identification of exercise exertion level during exercise.

4.1.2 Description of the method

ECG signals are extracted from subjects that undergo a 13-minute exercise constituted by three phases: rest, exercise and recovery. More precisely, the exercise is constituted by two 5-minutes periods with different leg exercise levels (1.5 and 2.5 miles/hour leg cycling); before, between and after these two periods, volunteer takes 1-minute rest. Data are extracted from the first minute of the exercise (that represents the rest), the 1$1^{th}$ to 12^{th} minute of the exercise (that represents the height of exercise), and the 12^{th} to 13^{th} minute of exercise (that represents the recovery). Each subject carries out the exercise several times, and extracted datasets are analyzed by HRV analysis software (Kubios HR, University of Eastern Finland), which produces all time-domain HRV variables (Table 4.1).
After that, three statistical analyses are performed: *paired t-tests*[26], *bivariate correlation*[27] and *discriminant function analysis*.

[26] A paired t-test is used to analyze the difference between two variables for the same subject.
[27] Bivariate correlation is an analysis that measures the strength of relationship between two variables.

Table 4.1 *HRV variables [29].*

HRV Variable	Definition
Mean RR	Mean of RR intervals
SD RR	Standard deviation of RR intervals
RMSSD	Square root of the mean squared difference between successive RR intervals
NN50	Number of successive RR interval pairs that differ more than 50 ms
pNN50	NN50 divided by the total number of RR intervals
RR tri	The integral of the RR interval histogram* divided by the height of the histogram
TINN	Baseline width of the RR interval histogram

**RR histogram: number of intervals over RR duration*

Paired t-tests find significant changes between rest and highest of exertion for mean RR, SD RR, RMSSD, RR tri, between highest of exertion and recovery for mean RR, SD RR, RR tri, TINN, and between rest and recovery for mean RR, SD RR, RR tri.
The relationship between each two variables is studied to check the possibility of reduction of the time-domain variables in a predictive model using values for each time-domain HRV variable from each subject. This bivariate correlation finds out a significant correlation both between SD RR and TINN, and between NN50 and pNN50).
All values of HRV variables from the volunteers are used to compose two *discriminant functions*[28] (Function 1 and Function 2) based on linear parameter combinations, and to build a predictive model for discrimination among three exertion categories (rest, highest of exertion, and recovery).

4.1.3 Results and conclusions

The classification of the study sample with a model derived from the whole sample results in 80.0% of rest, 100.0% of highest of exertion, and 86.7% of recovery cases correct classification; thus, overall 88.9% of original grouped cases are correctly classified with two developed canonical discriminate functions. *Cross-validated classification*[29] performed using leave-one-out method results in 80.0% of rest, 100.0% of highest of exertion, and 80.0% of recovery cases correct classification; thus, overall 86.7% of original grouped cases are correctly classified (Fig. 4.1).

[28] Discriminant function analysis (DFA) is a statistical procedure that classifies unknown individuals and the probability of their classification into a certain group.
[29] Cross-validation assesses how the results of a statistical analysis generalize to an independent data set.

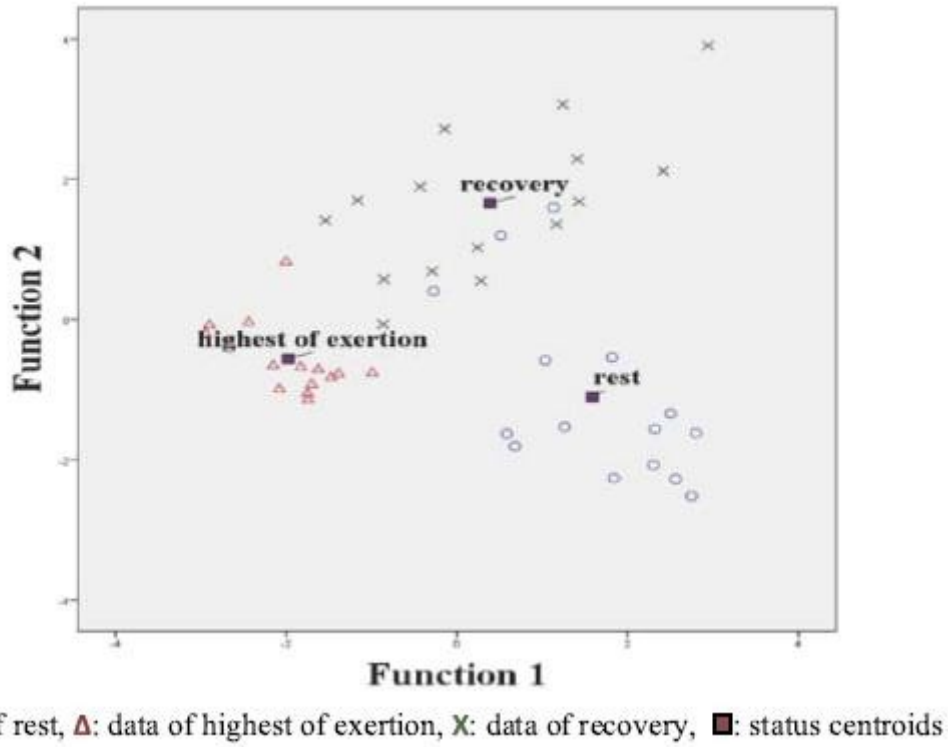

Figure 4.1 *Classification status graph [29].*

In conclusion, comparative analysis of HRV during exercises demonstrates responsiveness of time-domain indices to different levels of an exercise exertion and their potential in monitoring autonomic balance and stress levels.

4.2 Dynascope: a software tool for the analysis of Heart Rate Variability during exercise

4.2.1 Introduction

Analysis of HRV can be used, beyond as a predictor for mortality in presence of cardiovascular pathologies, as a tool for the identification of the success of any training program of athletes [30]. HRV is analysed in the three dynamic conditions (prior, during and after the exercise) and with different techniques (such as *Poincaré plots*, analysis of HR sudden increase and reduction).

The Poincaré plot analysis is a geometrical and nonlinear method to assess the dynamics of HRV. It is a diagram in which each R-R interval is plotted as a function of the previous R-R interval where the values of each pair of successive R-R interval define a point in the plot.

Dynascope is a Windows-based C++ software tool that estimates RR changes during physical onset, offset, and initial recovery stage. In particular, the onset and offset stages are defined as HR increase (HRI) and HR recovery (HRR) respectively.

4.2.2 Description of the method

ECG signal is continuously recorded for the whole exercise test, constituted by pseudo-resting, exercise and recovery phases; the recording may contain one or more resting-exercise-recovery episodes. The *tachogram* (the time-series of RR intervals) is automatically extracted from the ECG tracing by HeartScope (algorithm developed by AMPS Ilc, New York, NY). The tool indistinctly works with two modalities of recording: single bout (RR recording contains a single episode of exercise) and multiple bouts (RR recording contains two or more episodes of exercise). After the opening of the RR file, the tool automatically divides all the exercise episodes in HRI and HRR phases (Fig. 4.2). The parameters initially detected by Dynascope are: *HRI start*, *HRI end*, *HRR start*, and *HRR end*. After that, the RR series (expresses in milliseconds) of HRI and HRR are filtered (*FiltRR*) using a median-filter (with a window length of 15 beats), used both for filtering the series and calculating the variance of RR (*VarRR*). The slopes of HRI (*TachySlope1* and *TachySlope2*) and HRR (*BradySlope*) are estimated applying the least squares method to FiltRR and taking the time as X-axis.

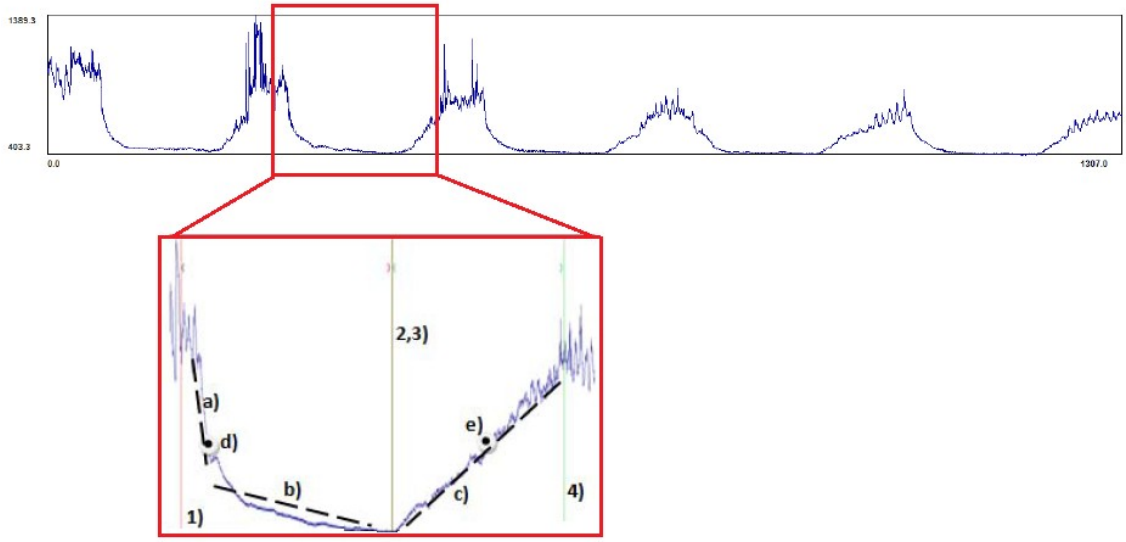

Figure 4.2 *Upper panel: view of a five-bouts RR series in Dynascope. Lower Panel: representation of parameters detected by Dynascope: 1) HRI start; 2) HRI end; 3) HRR start; 4) HRR end; dashed lines represent the slopes, respectively a) TachySlope1, b) TachySlope2, c) BradySlope; d) and e) are the points where TachySpeed and BradySpeed were detected [30].*

Figure 4.2 shows that HRI has two different descending phases: the first one is associated to the beginning of the physical activity and is of higher magnitude with respect to that of the second phase. In addition, the maximum speed for exercise (*TachySpeed*) and the maximum speed for recovery (*BradySpeed*) are estimated filtering further FiltRR with a mean-filter and deriving the resulting signal (*DRR*).
Moreover, the part preceding the first exercise (*Baseline*) and all the recovery phases are extracted from the original RR-series. Indeed, these series are associated with corresponding RR_{N+1} series to construct Poincaré plots, one representing the Baseline and one for each recovery episode.

4.2.3 Results and conclusions

The visualization of the Poincaré plots gives a qualitative analysis of the trend of RR series (Fig. 4.3). The parameters extracted by Dynascope describe the quality of the response to an exercise evaluating HRI ("Tachy" parameters) and HRR ("Brady" parameters) phases. "TachySlope" and "TachySpeed" parameters are aimed to estimate the speed of the simultaneous vagal deactivation and sympathetic activation, combined, when the heart is under stress. The "slope" parameter indicates the speed whereby the HR increase and "speed" parameter indicates the maximum speed of this process. Likewise, BradySlope and BradySpeed describe the quality of recovery and the speed of the vagal tone reactivation. Poincaré area estimates the quality of the vagal recovery, its value depending on variance and RR changes.

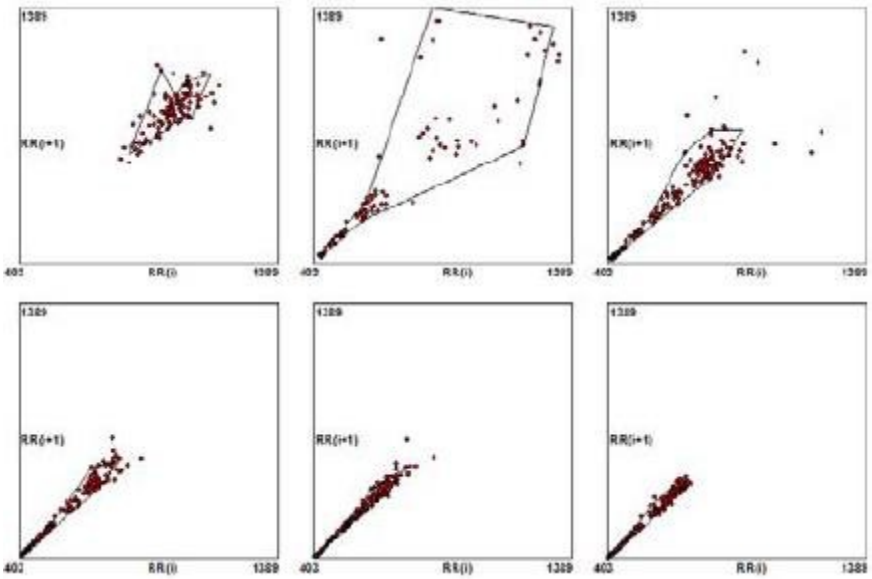

Figure 4.3 *Poincaré plots view of a 5-bouts recording. The upper left corner plot represents the Baseline, the other plots represents (from left to right) the Poincaré plots of recovery phases [30].*

A small study on 10 healthy subjects was conducted in order to validate Dynascope. Volunteers underwent three subsequent 5-minutes bouts of exercise on a supine-bicycle with three different loads (50W, 100W, 150W) separated by 5 minutes rest phases. The aim is to evaluate how Dynascope may estimate different response to exercise between different bouts.

The parameters automatically calculated by Dynascope are shown in Table 4.2. It can be seen that the results are consistent with the physiological adaptations described in chapter 2. In particular:

- All parameters decrease with increasing load and successive bouts of exercise;
- the reduction of Max RR reflects an incomplete recovery of HR with successive bouts (suggesting an after effect as memory), BradySlope decreases with successive bouts linearly with increasing of recovery duration;
- TachySpeed and BradySpeed have a significant reduction and this could indicate a reduction in the capacity of the HR control system (both autonomic and humoral) to respond to exercise;
- TachyVar and BradyVar decrease partially reflecting a reduction in vagal tone caused, in turn, by an incomplete recovery;
- The decrease of Poincaré area provides information to HRV during the offset phases of rest after successive bouts: a greater value of this area could suggest an increased vagal reactivation after exercise;
- The trend of these results describes the effects of exercise within different loads and the subsequent series of exercises on HRV and reflects the dynamics of the onset and offset of HR regulatory systems during subsequent bouts of submaximal exercise.

Table 4.2 *Several parameters computed by Dynascope for the study population. Results are given by mean ± std. Kruskal-Wallis test: (*) significant, p-value<0.05 (N) non-significant, p-value>0.05 [30].*

	Exercise Load			p-value
	50W	**100W**	**150W**	
Max RR [ms]	948±56	853±60	735±52	*
TachySlope1 [ms/s]	1.74±0.52	1.59±0.37	1.64±0.23	N
BradySlope [ms/s]	4.94±0.69	3.51±0.53	2.51±0.51	*
TachySpeed [ms/s]	17.70±2.21	13.05±1.95	9.27±0.78	*
BradySpeed [ms/s]	12.53±1.18	10.08±1.37	7.35±1.63	*
TachyVar [ms^2]	12203±3679	8749±3413	2501±812	*
BradyVar [ms^2]	10281±5319	3583±1460	2508±1405	N
Poincaré Area [ms^2]	82047±33161	63430±30485	35309±23782	*

In conclusion Dynascope is a tool that, by means of the estimation of HR changes between different episodes of exercise, is useful both in evaluating exercise capacity and the efficiency of a specific training program, and in monitoring clinical conditions of subjects and the efficacy of therapy.

4.3 A fully automatic algorithm for the analysis of heart rate changes during exercise

4.3.1 Introduction

The post-exercise HR recovery and HRV are non-invasive methods used for the determination of cardiovascular autonomic function. Regarding the sport testing, HRV analysis is used for evaluating modifications of autonomic cardiovascular functions during exercise or after a training period [31]. The method illustrated in this paragraph makes an analysis of the exercise based on the information on HR recovery and HR variability changes.

4.3.2 Description of the method

Volunteers are recorded at standing resting position for almost 5 minutes, then in walking condition for an additional 3 minutes. Then, the *Bruce protocol* [30]takes place; in the last 30 seconds of the protocol, the subject is positioned in supine position starting the recovery phase, whose duration is approximately 5 minutes long.
RR series are automatically extracted from the recorded ECGs thanks to HeartScope (AMPS Ilc, New York, NY); from these RR series, the three experimental conditions (rest, exercise, recovery) are automatically detected. Then, the tachogram is filtered by a moving-average filter with a window size of 20 subsequent RRs (F_{RR}). F_{RR} is further filtered with a derivative filter in order to obtain dF_{RR}. Var_{RR} is obtained averaging dF_{RR} series at fixed time points with a moving-average filter and the computation of the variance of predefined windows at the same fixed time points of the tachogram. RR, dF_{RR} and Var_{RR} are normalized (Var_{RRn} and dF_{RRn}) using maximum and minimum values for enahnace the comparison. Finally, the area in the phase plane (RR-VarRR) and (RR-dRR) are quantified. For statistical analysis, Kruskal-Wallis test on median is used, p-value<0.05 is considered significant level, p-value<0.1 is also marked.

[30] The Bruce protocol is a standard test in cardiology and is comprised of multiple exercise stages of three minutes each. At each stage, the gradient and speed of the treadmill are elevated to increase work output (called METs).

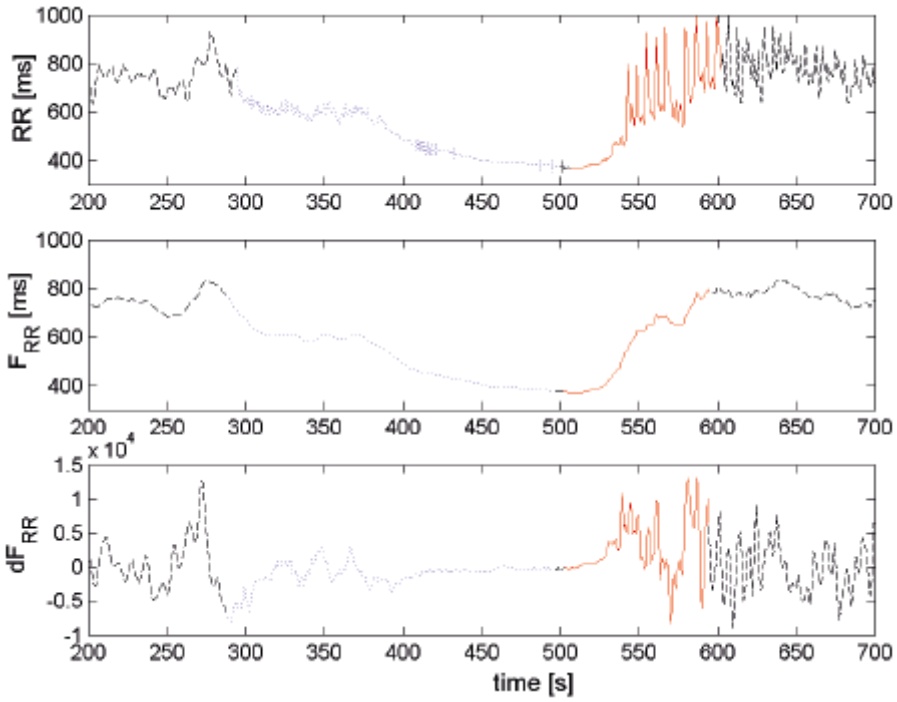

Figure 4.4 *The tachogram, the filtered tachogram and dF RR-RR for an healthy individual. The two exercise phases are visualized differently: dotted line for exercise and solid line for recovery phase [31].*

Figure 4.4 shows a clear reactivation a minute into recovery phase (sudden RR interval increase and appearance of marked dF RR oscillations). In addition, the variance in the recovery phase is much higher than the exercise phase or rest phase.
Figure 4.5 shows that, during the exercise phase (blue dotted line), VarRR is dramatically reduced, whereas it rapidly increases after 20 seconds from the beginning of the recovery phase (solid red line) . Moreover, dRR reflects a decrease in RR during late exercise phase, and a monotonic RR increase starting with the beginning of recovery.

4.3.3 Results and conclusions

The above-described plots of figure 4.5 illustrate that, at a given RR interval, the variance is larger during recovery than during exercise and even during rest. These results are consistent with the physiological adaptations described in chapter 2. Indeed, they suggest that tonic control of heart rate (seting the mean value of RR interval) and dynamical control (setting the level of HRV) should be regarded as different autonomic regulations.
In conclusion, this technique is useful for quantifying fitness level.

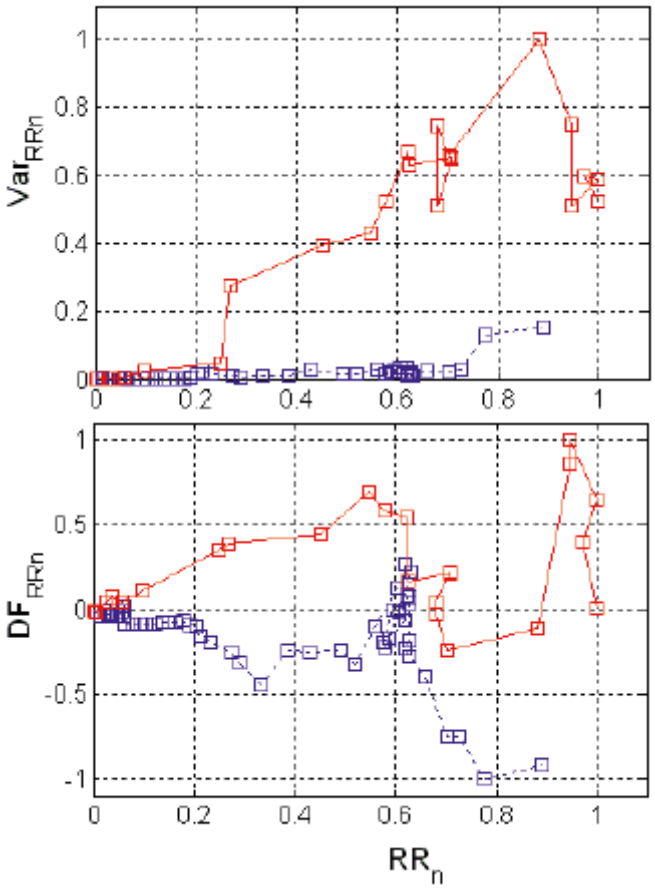

Figure 4.5 *Example of normalized Var_{RR}-RR (upper) and d_{RR}-RR (lower) plots for an healthy individual [31].*

4.4 HeartScope: a software tool addressing Autonomic Nervous System regulation

4.4.1 Introduction

HeartScope is a Windows-based computer program written in C++ that works on ECG, arterial pressure (AP), respiratory volume (RESP) and sympathetic nerve activity directed to muscle (MSNA) [32].

4.4.2 Description of the software tool

HeartScope opens the previously recorded beat-to beat series of the above-mentioned parameters; in particular, these raw signal may not be calibrated (i.e. quantized representation from the A/D board) and a calibration is needed in order to obtain meaningful values of the parameters (Fig. 4.6).

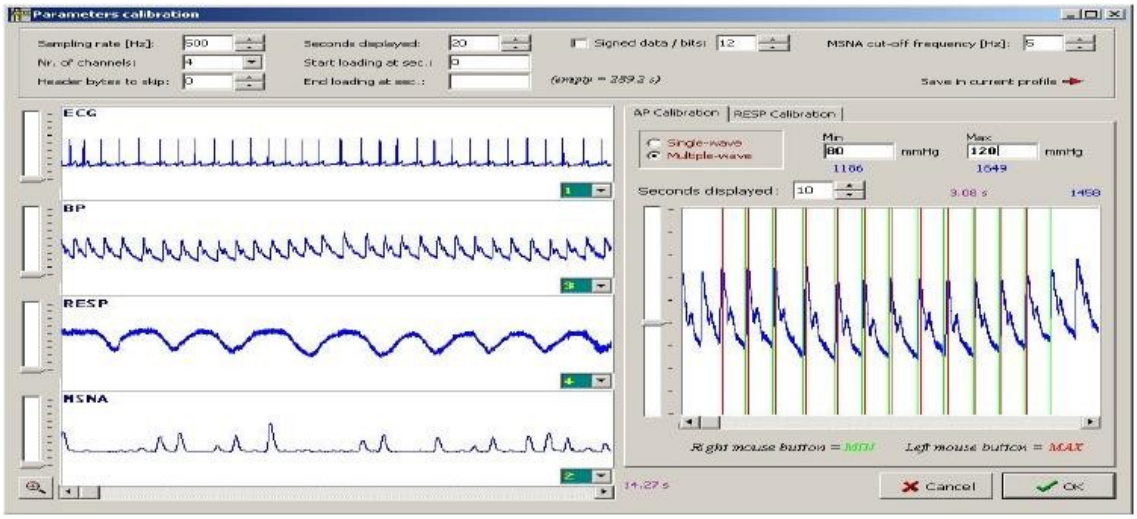

Figure 4.6 *Parameters-calibration window comprising ECG, BP, RESP and MSNA [32].*

After this calibration-step, HeartScope performs the evaluation of the cardiovascular variables on the beat-to beat basis: the heart period (HP) as the temporal distance between two successive QRS complexes (or two successive diastolic points on AP if ECG is not present), systolic AP (SAP) as the AP maximum inside the current HP, diastolic AP (DAP) as the AP minimum after the current SAP, mean MSNA in the current HP, respiratory volume sampled once per cardiac beat at the beginning of the current HP.
The beat-to-beat variability time series are shown in a dedicated interactive window (Fig. 4.7), where the segment boundaries (vertical segments) can be inserted/deleted by the user by clicking the right mouse button on the graph. Another mouse-driven popup menu can enable/disable the analysis of a selected segment.

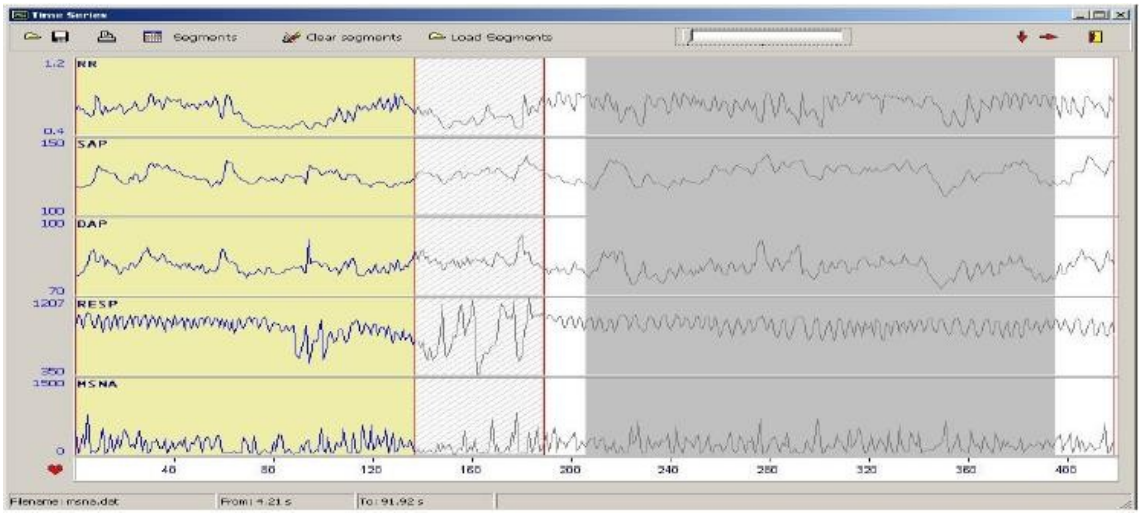

Figure 4.7 *Beat-to-beat variability series window [32].*

Chapter 5

A new algorithm for the identification of training phases

"I have always considered sport as the perfect metaphor for life. Having played football for 25 years, in fact, taught me how exercise tests our skills, our hearts, but above all our ability to bounce back after setbacks. This represents the most intimate soul of sport, and I am sure it is the real secret of life. I owe everything to exercising: perhaps also the fact of being still alive. That's why I love sport so much: it makes me feel alive"
[Alessio Scalese]

5.1 Database used for the algorithm

5.1.1 Database description

The database used for the validation of this new algorithm comprises 126 cardiorespiratory datasets (CRD) from 81 athletes while performing 10 different sports [33]. The database has a tree-like structure (Fig. 5.1), where the main directory (*SportDB*) contains a folder for each sport: *AER* for aerial skills, *BAS* for basketball, *CRO* for CrossFit, *FIT* for fitness, *JOG* for jogging, *MID* for middle-distance running, *RUN* for running, *SOC* for soccer, *TEN* for tennis, and *ZUM* for Zumba. Each sport folder, in turn, contains a subfolder for each athlete performing that sport (*S*$_n$, with n=1,2,…). Lastly, each subfolder comprises a sub-subfolder for each acquisition performed by that athlete (*CRD*$_m$, with m=1,2,…).
In addition, inside each CRD$_m$ sub-subfolder, there are a demographic data file (*Dem.txt*), a cardiorespiratory data MATLAB structure (*Data.mat*), and a training note file (*TrNote.txt*). The demographic data gathers information about gender (male: 0; female: 1), age (years), weight (Kg), height (cm), smoking habit (no: 0; yes: 1), alcohol consumption (no: 0; sometimes: 1), and weekly training rate (integer from 1 to 7); missing data are indicated with 'NA'. The cardiorespiratory data structure gathers the recorded cardiorespiratory signals during the acquisition, and comprises four fields:

- *Data.ECG*, containing the raw electrocardiogram (ECG);
- *Data.HR*, containing the raw heart-rate (HR) series;
- *Data.RR*, containing the RR-interval series;
- *Data.BR*, containing the raw breathing-rate (BR) series.

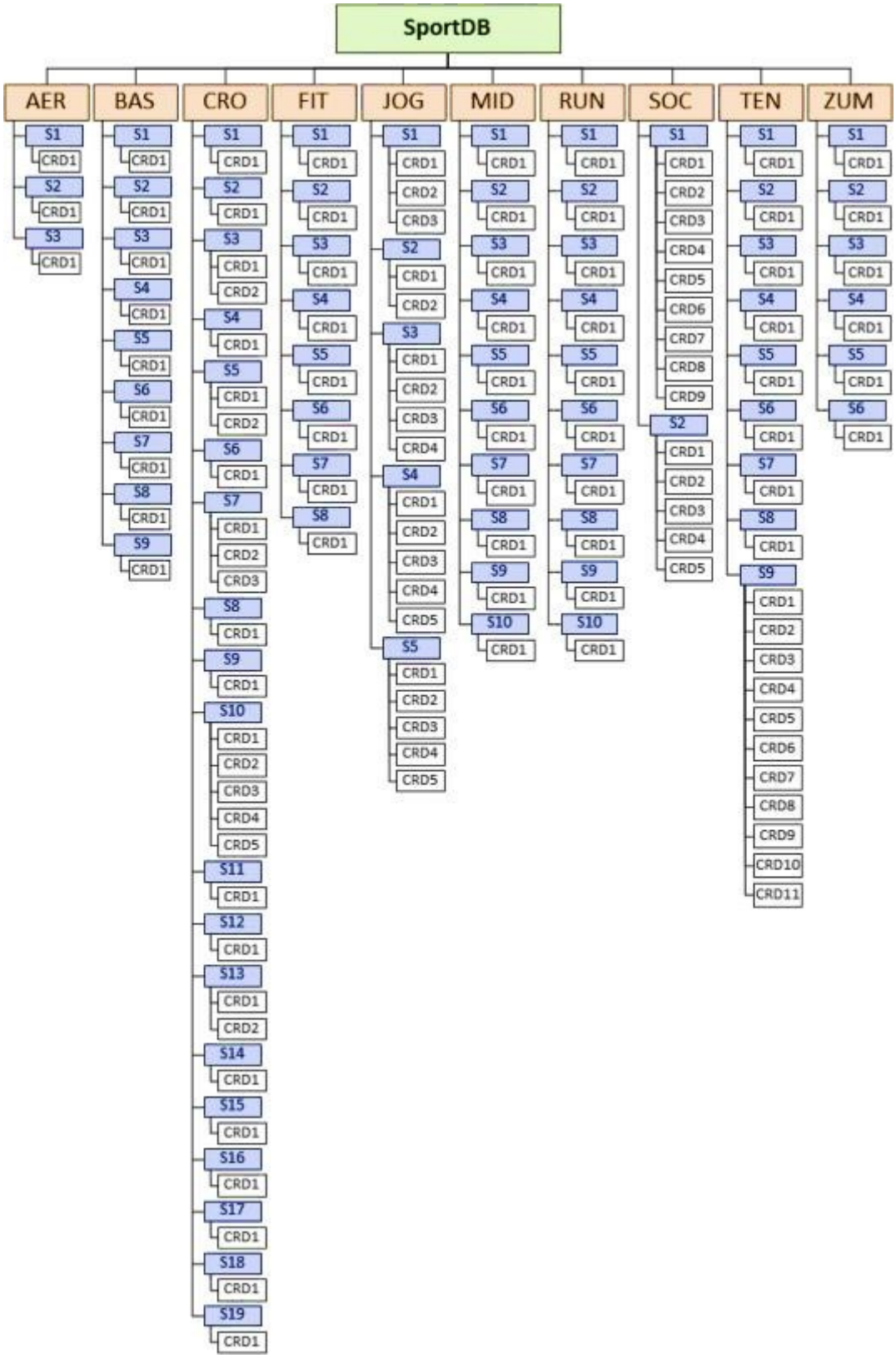

Figure 5.1 *Sport Database tree structure [33].*

The training-notes file gathers information about duration of the three training phases (pseudo-resting, exercise, recovery) during the acquisition and annotations about the sport-related acquisition protocol; in particular, training phases not practised by the subject are annotated as '*none*'.

For the new algorithm described in this chapter, only the middle-distance running subjects were taken into consideration because their performances gave rise to well-defined phases with very elevated HR and recovery clearly visible (not affected by so much noise). Tables 5.1 and 5.2 illustrate the demographic data and the training notes respectively of Sport Database concerning only the middle-distance running subjects.

Characteristics of the cardiorespiratory signals (sampling frequency, amplitude range, and data-loss index) are shown in Table 5.3.

Table 5.1 *Demographic data of Sport Database concerning only middle-distance running (MID) subjects [33].*

	Number of CRD	Gender (0/1)	Age (years)	Weight (Kg)	Height (cm)	Smoking (0/1)	Alcohol consumption (0/1)	Weekly Training rate
S1	1	0	48	70	170	0	0	4
S2	1	0	55	69	180	0	1	3
S3	1	0	41	65	180	0	0	5
S4	1	0	44	90	175	1	1	2
S5	1	0	49	70	180	0	1	4
S6	1	0	54	76	178	0	1	4
S7	1	0	21	67	174	0	1	6
S8	1	0	18	65	179	0	1	5
S9	1	0	18	65	178	0	1	5
S10	1	0	21	65	175	0	1	3

Table 5.2 *Training notes of Sport Database concerning only middle-distance running (MID) subjects [33].*

	Pseudo-resting phase	Exercise phase	Recovery phase
S1	from 00:00:00 to 00:03:55	from 00:03:55 to 00:12:19	from 00:12:19 to 00:21:02
S2	from 00:00:00 to 00:03:44	from 00:03:44 to 00:13:22	from 00:13:22 to 00:18:06
S3	from 00:00:00 to 00:03:22	from 00:03:22 to 00:09:52	from 00:09:52 to 00:14:30
S4	from 00:00:00 to 00:03:02	from 00:03:02 to 00:12:00	from 00:12:00 to 00:16:32
S5	from 00:00:00 to 00:03:24	from 00:03:24 to 00:12:52	from 00:12:52 to 00:16:22
S6	from 00:00:00 to 00:02:08	from 00:02:08 to 00:12:30	from 00:12:30 to 00:16:01
S7	none	from 00:00:00 to 00:11:07	none
S8	from 00:00:00 to 00:02:17	from 00:02:17 to 00:09:30	from 00:09:30 to 00:14:02
S9	from 00:00:00 to 00:03:23	from 00:03:23 to 00:10:29	from 00:10:29 to 00:15:53
S10	from 00:00:00 to 00:04:04	from 00:04:04 to 00:11:11	from 00:11:11 to 00:18:24

Table 5.3 *Characteristics of the cardiorespiratory signals [33].*

Signal	Sampling Frequency	Amplitude Range	Data Loss
ECG	250 Hz	0.25 – 15 mV	0 mV
HR	1 Hz	25 – 240 bpm	0 bpm
RR	1 Hz	250 – 2400 ms	Inf
BR	1 Hz	3 – 70 cpm	6553.5 cpm

5.1.2 Data collection and acquisition

All middle-distance running subjects were supposed healthy (i.e. without previous history of cardiorespiratory diseases and not taking any drug) during the acquistion period, even after a clinical evaluation performed by *CaRiSMA* software [34].
All subjects gave their informed consent prior to data collection and acquistions, which were undertaken in compliance with the ethical principles of Helsinki Declaration and approved by the institutional expert committee.
Demographic data, cardiorespiratory signals and training notes of each CRD folder were gathered during the same acquisition. In particular, demographic data were collected by survey. The recordings of the cardiorespiratory signals were performed through the chest strap BioHarness 3.0 by Zephyr described in section 3.2.2. This wearable device directly records the ECG (mV; raw data), and automatically calculates the HR series (bpm; processed data) and the BR series (cpm; processed data).
Table 5.3 reports the characteristics of these signals. More precisely, the chest strap was slightly moistened before each acquisition in order to optimize electrical conductivity. After that, the sensor was placed under the left arm (Fig.5.2), as suggested by guidelines described in the user manual.

Figure 5.2 *User manual guidelines for the correct application of the BioHarness 3.0 sensor (https://www.zephyranywhere.com/media/download/bioharness3-user-manual.pdf).*

The RR-interval series (ms) were indirectly calculated from HR series by means of the following formula:

$$RR = \frac{60}{HR} \cdot 1000 \quad (5.1)$$

Lastly, all information about duration of the training phases (pseudo-resting, exercise, recovery) during each acquisition and details about the acquisition protocol were manually annotated in the training note file.

5.1.3 Acquisition protocol

The acquisition protocol comprises several phases, whose startings and durations were varying and measured using a stopwatch and reported in the training note file.
More precisely, the middle-distance running acquisition protocol is constituted by an initial phase of pseudo-resting, a phase of exercise and a final phase of recovery. During the pseudo-resting phase the subject sits courtside. The exercise phase requires that the subject performs a standard *Conconi's test* [35] running for 2 km in a standard 400 m track and indipendently increasing his/her speed every 200 m. During the recovery phase, the subject sits courtside again.

5.2 Algorithm and statistical method

5.2.1 Description of the automatic algorithm

The software used for the development of the algorithm is *Matlab R2017b*. The algorithm takes as input both HR and RR time-series. In particular, the HR time-series is characterized by an almost constant trend during the pseudo-resting phase, an increasing trend during the exercise phase, and a decreasing trend followed by an almost constant trend (with a return to the pseudo-resting values of HR) during the recovery phase. Consequently, according to formula 5.1, the RR time-series is characterized by an almost constant trend during the pseudo-resting phase, a decreasing trend during the exercise phase, and an increasing trend followed by an almost constant trend (with a return to the pseudo-resting values of RR) during the recovery phase.
The idea behind the automatic algorithm is to produce an index based on the slope time-series associated to both HR and RR time-series. The determination of each slope value associated to HR is performed taking a 60-beats windows (thus, the window dimension is 59 beats long) translating along the entire HR time-series. More precisely, the window

starts taking the first and the sixtieth beat of the HR time-series; then, the angular coefficient (slope) associated to this first window is determined by the following formula:

$$m = \frac{y_2 - y_1}{x_2 - x_1} \tag{5.2}$$

where y_2 is the sixtieth value of HR, y_1 is the first value of HR, x_2 is the is the time-instant associated to the sixtieth value of HR (it corresponds to the sixtieth second since sampling frequency is 1 Hz), x_1 is the time-instant associated to the first value of HR (it is equal to the first second). Then, the window moves one beat on, taking the second and the sixty-first beat of the HR time-series, calculating the angular coefficient associated to this window, and so on until the last value of the HR time-series. This means that the slope time-series associated to HR is constituted by $t - 59$ values, where t is the length of the HR time-series (duration of the subject acquisition). According the above-described HR trend, the course of the slope associated to HR (m_1) is characterized by (Fig. 5.3):

- an initial almost linear tract (corresponding to the almost linear section of HR associated to the pseudo-resting phase);
- a positive "wave" (corresponding to the increase and reduction-in-increase of HR associated to the beginning of the exercise phase);
- a central almost linear tract (corresponding to the almost linear section of HR associated to the exercise phase);
- a negative "wave" (corresponding to the decrease and reduction-in-decrease of HR associated to the ending of the exercise phase);
- a final almost linear tract (corresponding to the almost linear section of HR associated to the recovery phase.

Similarly, the course of the slope associated to RR (m_2) is characterized by (Fig. 5.4):

- an initial almost linear tract (corresponding to the almost linear section of RR associated to the pseudo-resting phase);
- a negative "wave" (corresponding to the decrease and reduction-in-decrease of RR associated to the beginning of the exercise phase);
- a central almost linear tract (corresponding to the almost linear section of RR associated to the exercise phase);
- a positive "wave" (corresponding to the increase and reduction-in-increase of RR associated to the ending of the exercise phase);
- a final almost linear tract (corresponding to the almost linear section of RR associated to the recovery phase.

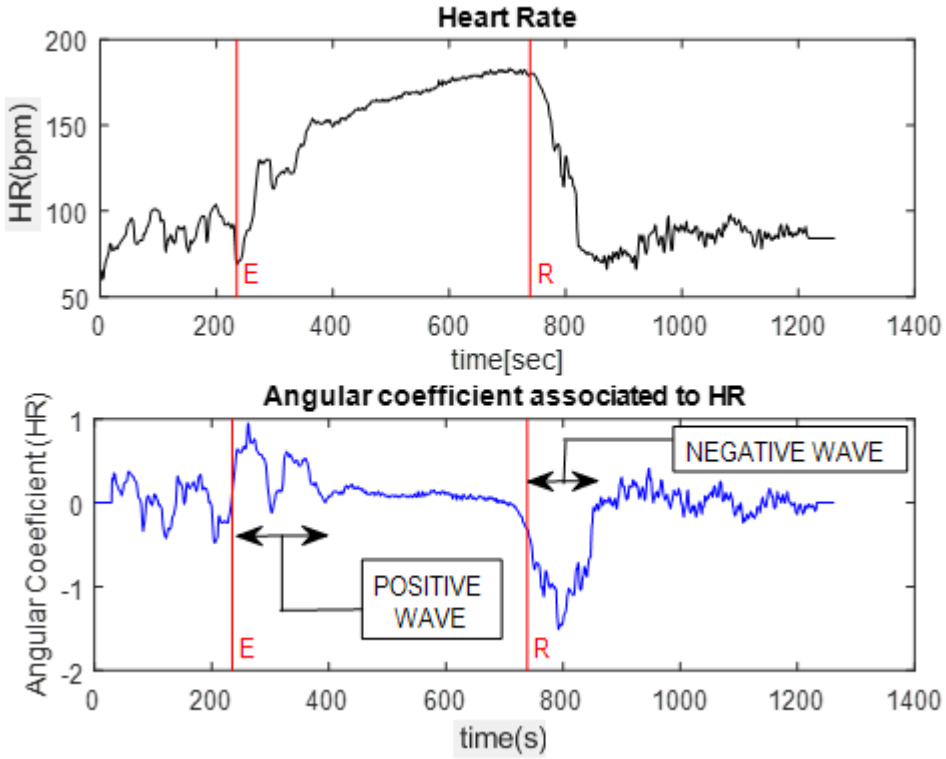

Figure 5.3 *Example of comparison between HR and angular coefficient associated to HR. The red vertical lines labelled with letters 'E'and 'R' represent the time instants of the beginning of the exercise phase and of the beginning of the recovery phase measured with the stopwatch, respectively.*

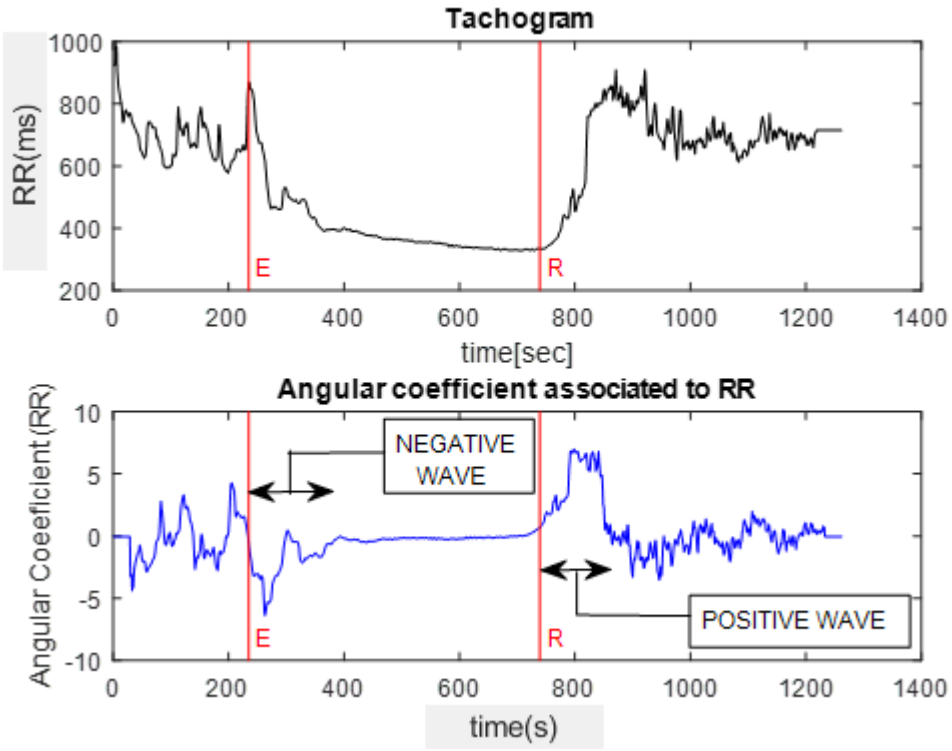

Figure 5.4 *Example of comparison between RR and angular coefficient associated to RR.*

From figures 5.3 and 5.4 it is possible to note that an initial and a final *zero-padding* has been performed on both the angular coefficient associated to HR and the angular coefficient associated to RR. The aim of this operation is twofold:

- make possible a time comparison between HR and its angular coefficient, and between RR and its angular coefficient;
- make possible a time comparison between the angular coefficients and the time instants measured by the stopwatch (represented with red vertical lines).

Therefore, the first point allows to better undestand how the angular coefficient changes depending on the HR – or RR – signal (time courses described in page 112); the second point is necessary for the final validation of the algorithm, because the time instants of the beginnings of both exercise and recovery phases calculated by the algorithm will be compared with the same instants measured by the stopwatch.

Without these two zero-paddings, the signals of the two angular coefficients would consist of 59 fewer values (peer to the dimension of the moving window). More precisely, the initial zero-padding is constituted by 29 values, whereas the final zero-padding comprises 30 values, making the first calculated value of the angular coefficient coincide with the centre of the first window (starting from the first value and ending at the sixtieth value of the HR – or RR – signal).

On the other hand, figures 5.3 and 5.4 show how both angular coefficients exhibit a significant variability, especially on the theoretical linear tracts. For this reason, it has been decided to merge the two angular coefficients into a single index simply called "*angular coefficient*" (m):

$$m = m_2 \cdot |m_1| \tag{5.3}$$

As figure 5.5 illustrates, the angular coefficient (m) exhibits a considerably reduced variability, because by means of formula 5.3 the variabilities of both m_1 and m_2 compensate each other. Moreover, since the absolute value is performed on the angular coefficient associated to HR (m_1), the time-course of the angular coefficient (m) is similar to that of the angular coefficient associated to RR (m_2), with the meaningful difference that the signal emphasizes both the negative and the positive wave shown in figures 5.3 and 5.4.

Therefore, the angular coefficient (m) is the base-signal on which the algorithm automatically identify the the three training phases (pseudo-resting, exercise, and recovery), and the two transition phases (from pseudo-resting to exercise, and from exercise to recovery).

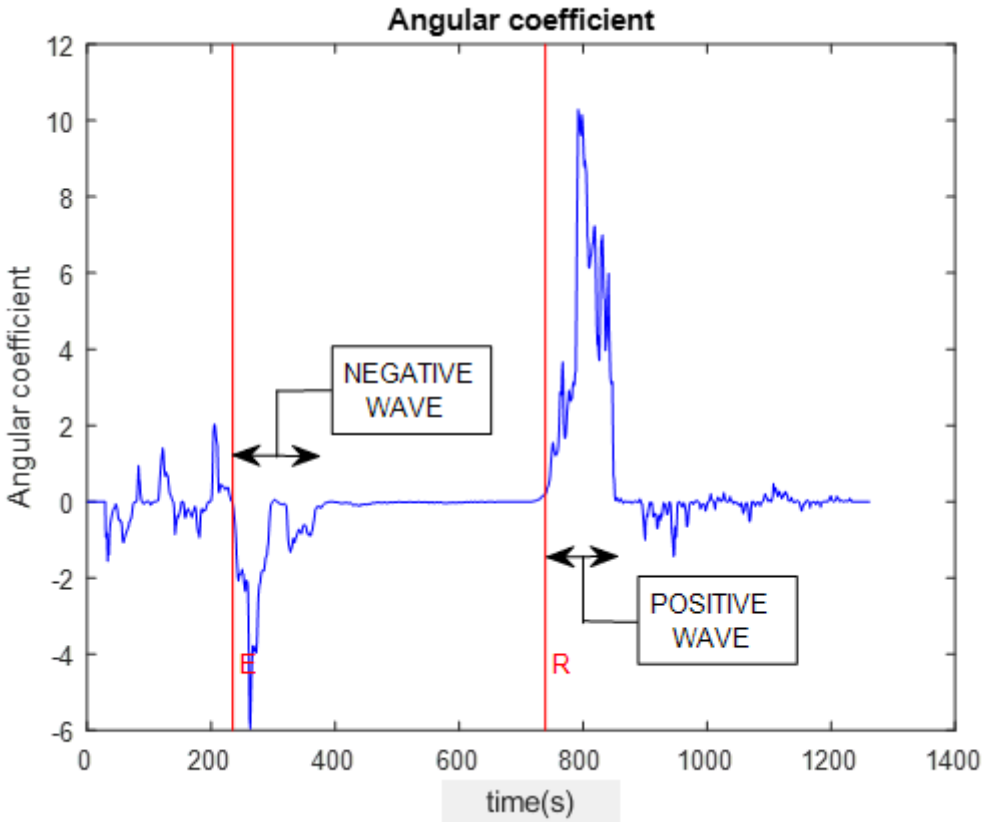

Figure 5.5 *Angular coefficient (m) resulting from the application of formula 5.3 on the angular coefficients (m_1 and m_2) of figures 5.3 and 5.4.*

The first step is the determination of the time-instant of the beginning of the exercise phase (that is equal to the time-instant of the ending of the resting-exercise transition phase). The underlying idea is to search for the first linear tract on the angular coefficient signal constituted by, at least, 30 successive values theoretically peer to zero. However, since the values of the linear tract are not actually equal to zero, it is preferred to choose a *range* (between -0.1 and +0.1) instead of a unique value equal to zero. Once the linear tract has been identified, the time-instant of the beginning of the exercise phase corresponds to the first value of this linear tract. This step is transduced in the software Matlab R2017b applying a moving window along the angular coefficient (m), composed by 30 values, starting from the third value and ending on the third last value of the signal in order to evade both the initial and the final zero-paddings. The initial and the final instants are determined for each window. Then, if the standard deviation of the signal throughout each window multiplied by 4 is within the range, the algorithm stores the first value of the window into an array. Lastly, the algorithm takes the first value of the array. This instant of the beginning of the exercise phase is highlighted in figure 5.6 by a red asterisk.

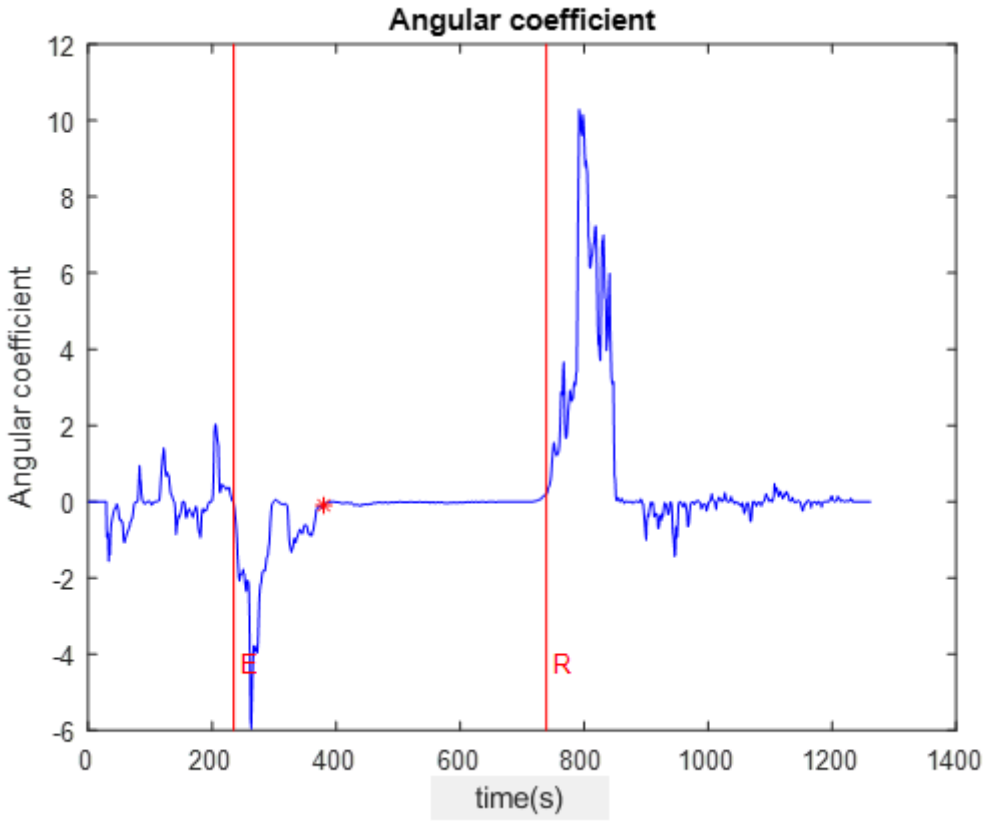

Figure 5.6 *Angular coefficient (m) and instant of the beginning of the exercise phase marked by a red asterisk.*

The second step is the determination of the time-instant of the beginning of the resting-exercise transition phase. Since this transition phase, as has been explained previously, is associated with the negative wave of the angular coefficient, the underlying idea is to find the global minimum from the beginning of the signal up to the instant of the beginning of the exercise phase, and to go back until the signal goes above the inferior limit of the range (equal to -0.1) for the first time. However, as figure 5.7 illustrates, the problem is that the signal could have another "fake" global minimum between the beginning of the signal and the beginning of the exercise phase, which would falsify the identification of the beginning of the resting-recovery transition phase. For this reason, a particular version of the *findpeaks*-function in Matlab R2017b has been used that finds local-minimum peaks guaranteed to have a vertical drop of more than a certain threshold from the peak on both sides without encountering either the end of the signal or a larger intervening peak. Moreover, the threshold of the findpeaks-function (*Thr*) is determined multiplying the global minimum (*thr1*) in the tract before the beginning of the exercise phase by a coefficient, called *Coeff1*, that is a sort of index of the variability of the signal in the first 100 values of the signal:

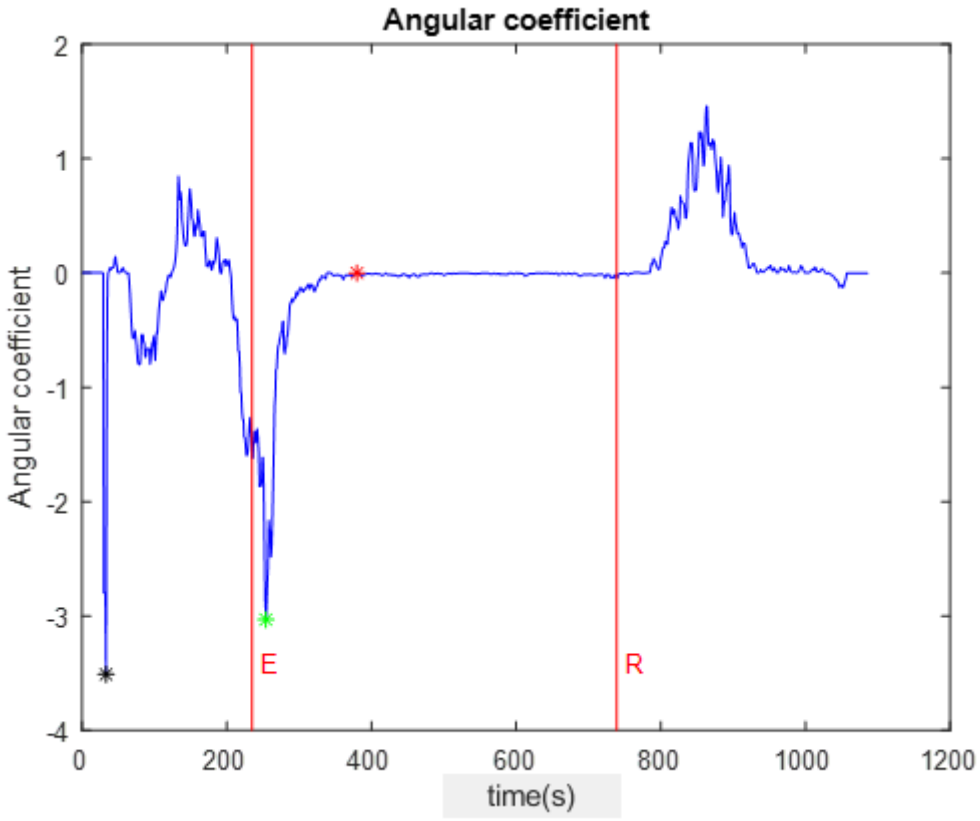

Figure 5.7 *Blue, angular coefficient (m); red asterisk, instant of the beginning of the exercise phase; black asterisk, "fake" global minimum; green asterisk, global minimum determined by the findpeaks-function.*

$$Thr = Coeff1 \cdot |thr1| \tag{5.4}$$

The variability of the signal is determined by the standard deviation in the tract under observation. From a theoretical point of view, the flatter the signal in that tract, the lower its standard deviation, the higher is the threshold of findpeaks-function, and the higher is Coeff1. Viceversa, the more variable the signal in that tract, the higher its standard deviation, the lower is the threshold of findpeaks-function, and the lower is Coeff1 (Fig. 5.8). In particular, Coeff1 assumes the following values:

- 0.75 if standard deviation of the first 100 values of the signal is lower than 0.5;
- 0.50 if standard deviation of the first 100 values of the signal is between 0.5 and 1;
- 0.19 if standard deviation of the first 100 values of the signal is higher than 1.

The reference values of the standard deviation (0.5 and 1) have been chosen based on a statistics on the standard deviations in this tract of the 10 subjects under investigation.

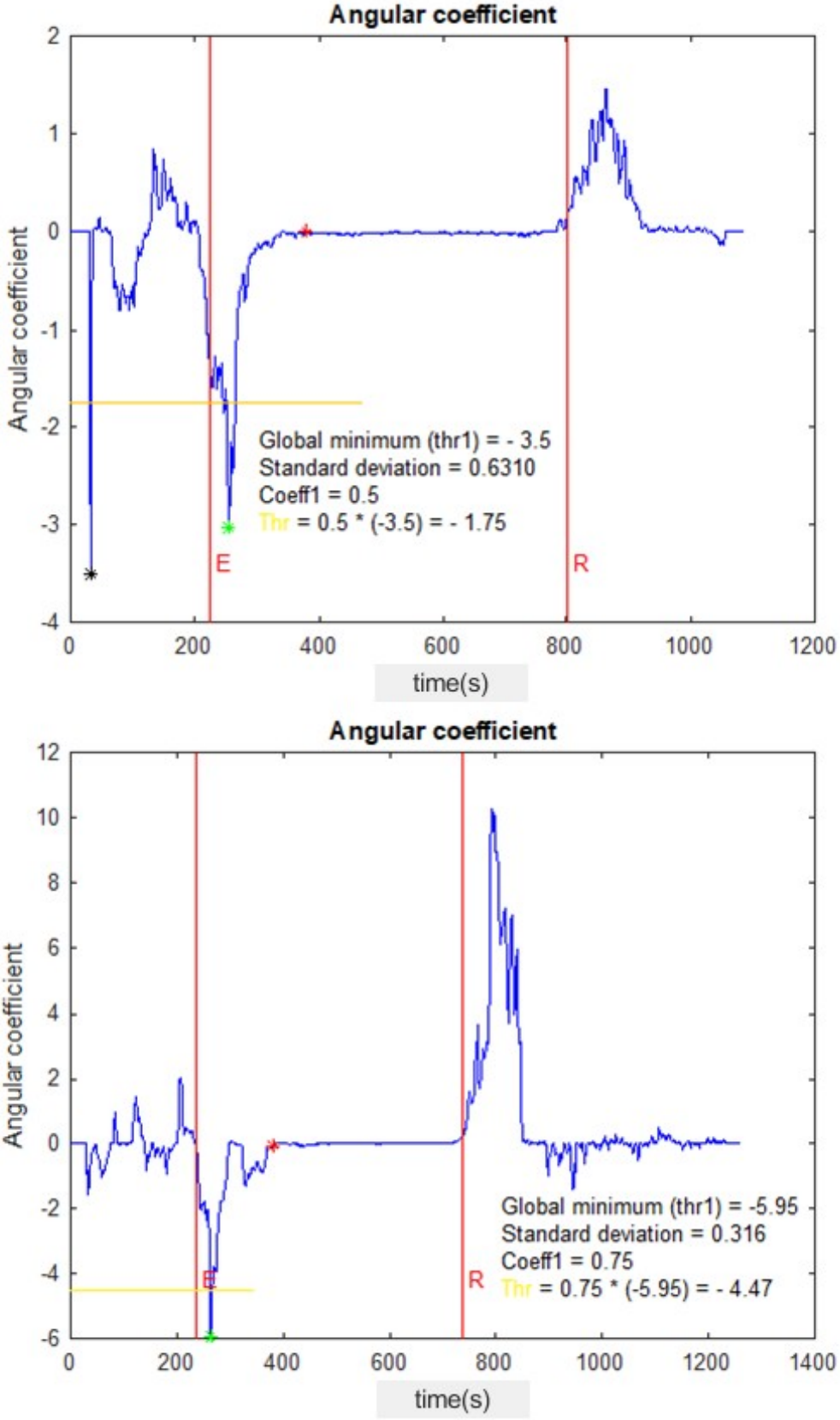

Figure 5.8 *Comparison between two different thresholds (in yellow) computed for the findpeaks-algorithm. Lower Panel: red asterisk, beginning of the exercise phase; green asterisk, thr1 (also reference global minimum).*

The three values of Coeff1 has been chosen experimentally applying several values until the algorithm reaches its best performance. Lastly, the algorithm takes the final value of the series of the local-minimum peaks calculated by findpeaks-function (the leftmost one).
As has already been said, the beginning of the resting-exercise transition phase is determined going back from the reference global minimum, and taking the first value above the inferior limit of the range, equal to -0.1.
The third step is the determination of the time-instant of the beginning of the exercise-recovery transition phase (that is equal to the time-instant of the ending of the exercise phase). The process is similar to that described for the second step. Determination of the reference global maximum (in this case, it has to do with the positive wave) by means of the findpeaks-function from the beginning of the exercise phase until the end of the signal: also in this case, the threshold of the findpeaks-function (*THR*) is determined multiplying the global maximum (*thr2*) in this new tract by a coefficient, called *Coeff2*, that is a sort of index of the variability of the signal in the tract going from the beginning of the exercise phase to the end of the signal:

$$THR = Coeff2 \cdot |thr2| \tag{5.5}$$

The variability of the signal is again determined by the standard deviation in the tract under observation. In particular, Coeff2 assumes the following values:

- 0.75 if standard deviation of the first 100 values of the signal is lower than 0.5;
- 0.50 if standard deviation of the first 100 values of the signal is between 0.5 and 1;
- 0.22 if standard deviation of the first 100 values of the signal is higher than 1.

Likewise, the three values of Coeff2 has been chosen experimentally applying several values until the algorithm reaches its best performance. The only difference is that the algorithm takes the first value of the series of the local-maximum peaks calculated by findpeaks-function (the leftmost one). the beginning of the exercise-recovery transition phase is determined going back from the reference global maximum, and taking the first value below the superior limit of the range, equal to +0.1 (Fig. 5.9).
The fourth and last step is the determination of the ending of the exercise-recovery transition phase (that is equal to the time-instant of the beginning of the recovery phase). In this case, the instant of the beginning of the recovery phase is equal to the first value below the superior limit ot the range (equal to +0.1) starting from the reference global maximum and going towards the end of the signal (Fig. 5.9).
At this point, all the reference instant needed for the identification of the three training phases and the two transition phases, are determined.

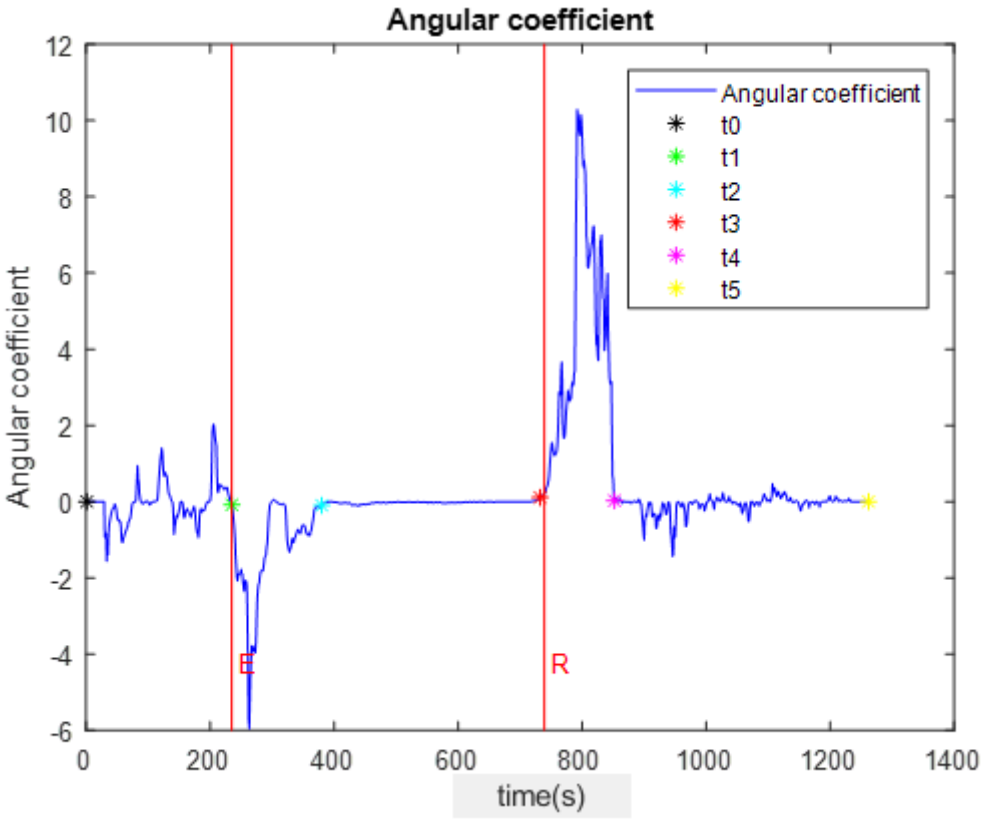

Figure 5.9 *Blue, angular coefficient; black asterisk, beginning of the pseudo-resting phase; green asterisk, beginning of the resting-recovery transition phase; cyan asterisk, beginning of the exercise phase; red asterisk, beginning of the exercise-recovery transition phase; magenta asterisk, beginning of the recovery phase.*

In summary:

- t_0 is the time-instant of the beginning of the pseudo-resting phase (equal to the time-instant of the beginning of the test);
- t_1 is the time-instant of the beginning of the resting-exercise transition phase (equal to the time-instant of the ending of the pseudo-resting phase);
- t_2 is the time-instant of the ending of the resting-exercise transition phase (equal to the time-instant of the beginning of the exercise phase);
- t_3 is the time-instant of the beginning of the exercise-recovery transition phase (equal to the time-instant of the ending of the exercise phase);
- t_4 is the time-instant of the ending of the exercise-recovery transition phase (equal to the time-instant of the beginning of the recovery phase);
- t_5 is the time-instant of the ending of the recovery phase (equal to the time-instant of the ending of the test).

In figure 5.10, the resting-exercise transition phase is represented by a red patch, whereas the exercise-recovery transition phase is represented by a green patch. In this figure, are still graphed the red vertical lines associated to the time-instants of the beginning of the resting-exercise transition phase (labelled with letter 'E') and of the beginning of the exercise-recovery transition phase (labelled with letter 'R') measured with the stopwatch.

5.2.2 Statistical method

The error (err_1) between the time-instant of the beginning of the resting-exercise transition phase measured by the stopwatch (E) and the time-instant of the beginning of the resting-exercise transition phase calculated by the algorithm (t_1) is defined as:

$$err_1 = |E - t_1| \tag{5.6}$$

The error (err_2) between the time-instant of the beginning of the exercise-recovery transition phase measured by the stopwatch (R) and the time-instant of the beginning of the exercise-recovery transition phase calculated by the algorithm (t_3) is defined as:

$$err_2 = |E - t_3| \tag{5.7}$$

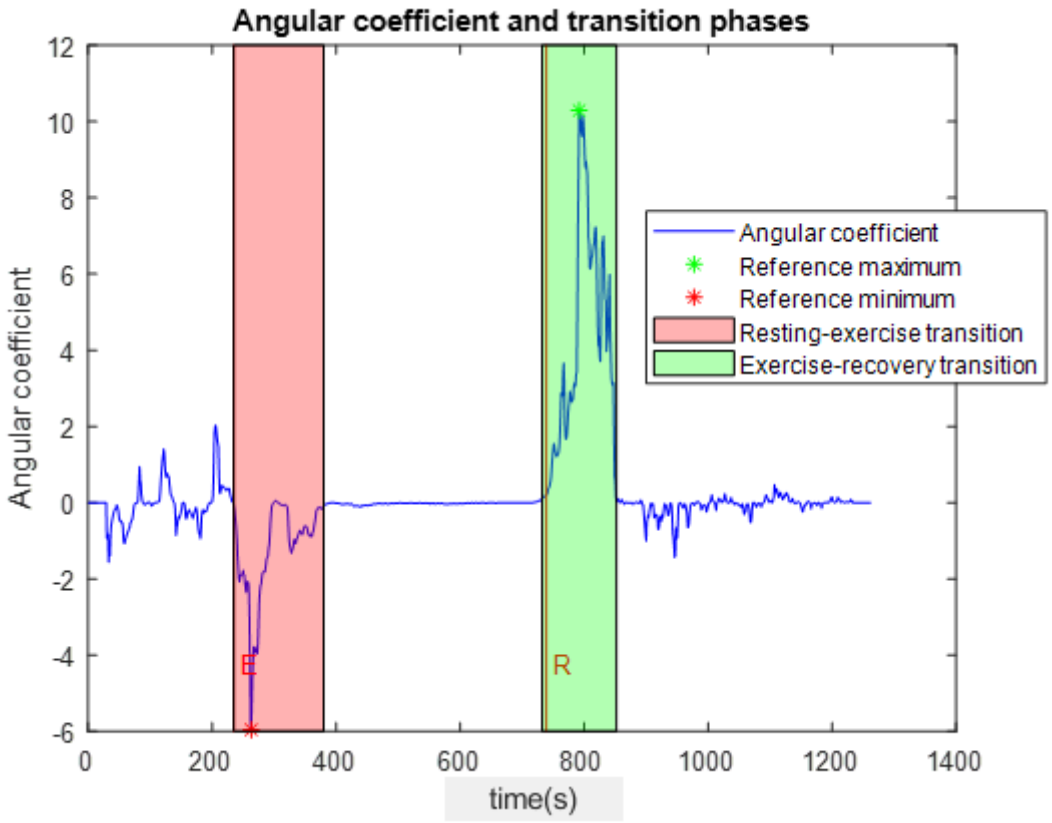

Figure 5.10 *Angular coefficient with both resting-exercise and exercise-recovery transition phases.*

The percentage error err_1 (%) is defined as:

$$err_1(\%) = \frac{err_1 \cdot 100}{t_5 - t_0} \tag{5.8}$$

The percentage error err_2 (%) is defined as:

$$err_2(\%) = \frac{err_2 \cdot 100}{t_5 - t_0} \tag{5.9}$$

The duration of the pseudo-resting phase (d_{rest}) is defined as the time-difference between the time-instant of the beginning of the resting-exercise transition phase (t_1) and the time-instant of the beginning of the test (t_0):

$$d_{rest} = t_1 - t_0 \tag{5.10}$$

The duration of the resting-exercise transition phase ($d_{rest-exe}$) is defined as the time-difference between the time-instant of the ending of the resting-exercise transition phase (t_2) and the time-instant of the beginning of the resting-exercise transition phase (t_1)

$$d_{rest-exe} = t_2 - t_1 \tag{5.11}$$

The duration of the exercise phase (d_{exe}) is defined as the time-difference between the time-instant of the beginning of the exercise-recovery transition phase (t_3) and the time-instant of the beginning of the exercise phase (t_2)

$$d_{exe} = t_3 - t_2 \tag{5.12}$$

The duration of the exercise-recovery transition phase ($d_{exe-rec}$) is defined as the time-difference between the time-instant of the ending of the exercise-recovery transition phase (t_4) and the time-instant of the beginning of the exercise-recovery transition phase (t_3)

$$d_{exe-rec} = t_4 - t_3 \tag{5.13}$$

The duration of the recovery phase (d_{rec}) is defined as the time-difference between the time-instant of the ending of the test (t_5) and the time-instant of the ending of the exercise-recovery transition phase (t_4)

$$d_{rec} = t_5 - t_4 \tag{5.14}$$

The mean value of the heart-rate over a certain period is calculated by means of the command *mean(HR)* on Matlab R2017b specifying the time reference duration. The standard deviation of the heart-rate over a certain period is calculated by means of the command *std(HR)* on Matlab R2017b specifying the reference duration. For the sake of simplicity, there are reported only the mean value and the standard deviation of the heart-rate over the pseudo-resting period called mean(HR_{rest}) and std(HR_{rest}) respectively:

$$mean(HR_{rest}) = mean(HR(t_0: t_1)) \quad (5.15)$$
$$std(HR_{rest}) = std(HR(t_0: t_1)) \quad (5.16)$$

Similarly:

- mean($HR_{rest-exe}$) and std($HR_{rest-exe}$) are the mean value and the standard deviation of the heart-rate over the resting-exercise transition phase, respectively;

$$mean(HR_{rest-exe}) = mean(HR(t_1: t_2)) \quad (5.17)$$
$$std(HR_{rest-exe}) = std(HR(t_1: t_2)) \quad (5.18)$$

- mean(HR_{exe}) and std(HR_{exe}) are the mean value and the standard deviation of the heart-rate over the exercise phase, respectively;

$$mean(HR_{exe}) = mean(HR(t_2: t_3)) \quad (5.19)$$
$$std(HR_{exe}) = std(HR(t_2: t_3)) \quad (5.20)$$

- mean($HR_{exe-rec}$) and std($HR_{exe-rec}$) are the mean value and the standard deviation of the heart-rate over the exercise-recovery transition phase, respectively;

$$mean(HR_{exe-rec}) = mean(HR(t_3: t_4)) \quad (5.21)$$
$$std(HR_{exe-rec}) = std(HR(t_3: t_4)) \quad (5.22)$$

- mean(HR_{rec}) and std(HR_{rec}) are the mean value and the standard deviation of the heart-rate over the recovery phase, respectively

$$mean(HR_{rec}) = mean(HR(t_4: t_5)) \quad (5.23)$$
$$std(HR_{rec}) = std(HR(t_4: t_5)) \quad (5.24)$$

The mean value of the tachogram over a certain period is calculated by means of the command *mean(RR)* on Matlab R2017b specifying the time reference duration. The

standard deviation of the tachogram over a certain period is calculated by means of the command *std(RR)* on Matlab R2017b specifying the reference duration. For the sake of simplicity, there are reported only the mean value and the standard deviation of the tachogram over the pseudo-resting period called mean(RR_{rest}) and std(RR_{rest}) respectively:

$$mean(RR_{rest}) = mean(RR(t_0: t_1)) \quad (5.25)$$
$$std(RR_{rest}) = std(RR(t_0: t_1)) \quad (5.26)$$

Similarly:

- mean($RR_{rest\text{-}exe}$) and std($RR_{rest\text{-}exe}$) are the mean value and the standard deviation of the tachogram over the resting-exercise transition phase, respectively;

$$mean(RR_{rest-exe}) = mean(RR(t_1: t_2)) \quad (5.27)$$
$$std(RR_{rest-exe}) = std(RR(t_1: t_2)) \quad (5.28)$$

- mean(HR_{exe}) and std(HR_{exe}) are the mean value and the standard deviation of the tachogram over the exercise phase, respectively;

$$mean(RR_{exe}) = mean(RR(t_2: t_3)) \quad (5.29)$$
$$std(RR_{exe}) = std(RR(t_2: t_3)) \quad (5.30)$$

- mean($HR_{exe\text{-}rec}$) and std($HR_{exe\text{-}rec}$) are the mean value and the standard deviation of the tachogram over the exercise-recovery transition phase, respectively;

$$mean(RR_{exe-rec}) = mean(RR(t_3: t_4)) \quad (5.31)$$
$$std(RR_{exe-rec}) = std(RR(t_3: t_4)) \quad (5.32)$$

- mean(HR_{rec}) and std(HR_{rec}) are the mean value and the standard deviation of the tachogram over the recovery phase, respectively

$$mean(RR_{rec}) = mean(RR(t_4: t_5)) \quad (5.33)$$
$$std(RR_{rec}) = std(RR(t_4: t_5)) \quad (5.34)$$

5.3 Results

Figures from 5.11 to 5.19 show the three training phases (pseudo-resting, exercise, and recovery) and the two transition phases (resting-exercise and exercise-recovery) of each subject. The algorithm was not applied on the seventh subject since the acquisition protocol was not respected missing resting and recovery phase.
The time-course of the angular coefficient is represented in blue. The reference maximum is represented by a green asterisk. The reference minimum is represented by a red asterisk. The resting-exercise transition phase is represented by a red patch. The exercise-recovery transition phase is represented by a green patch. The red vertical line labelled with letter 'E' represents the time-instant of the beginning of the resting-exercise transition phase measured by the stopwatch. The red vertical line labelled with letter 'R' represents the time-instant of the beginning of the exercise-recovery transition phase measured by the stopwatch.

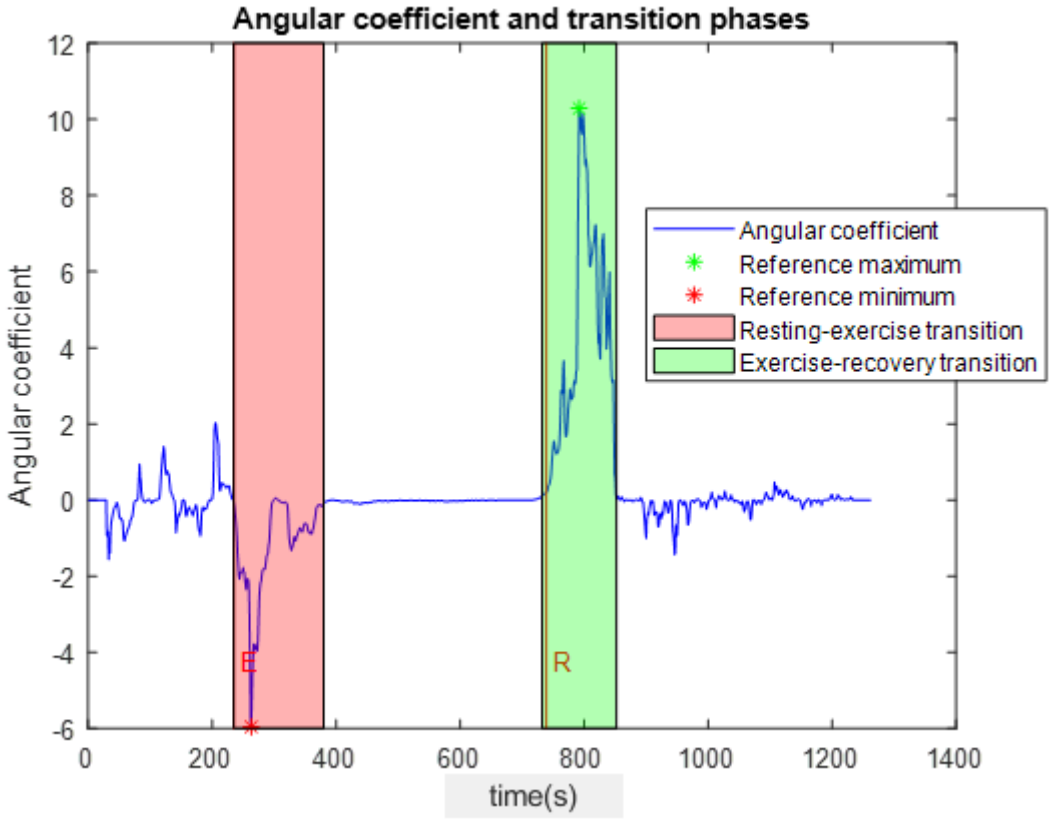

Figure 5.11 *First subject.*

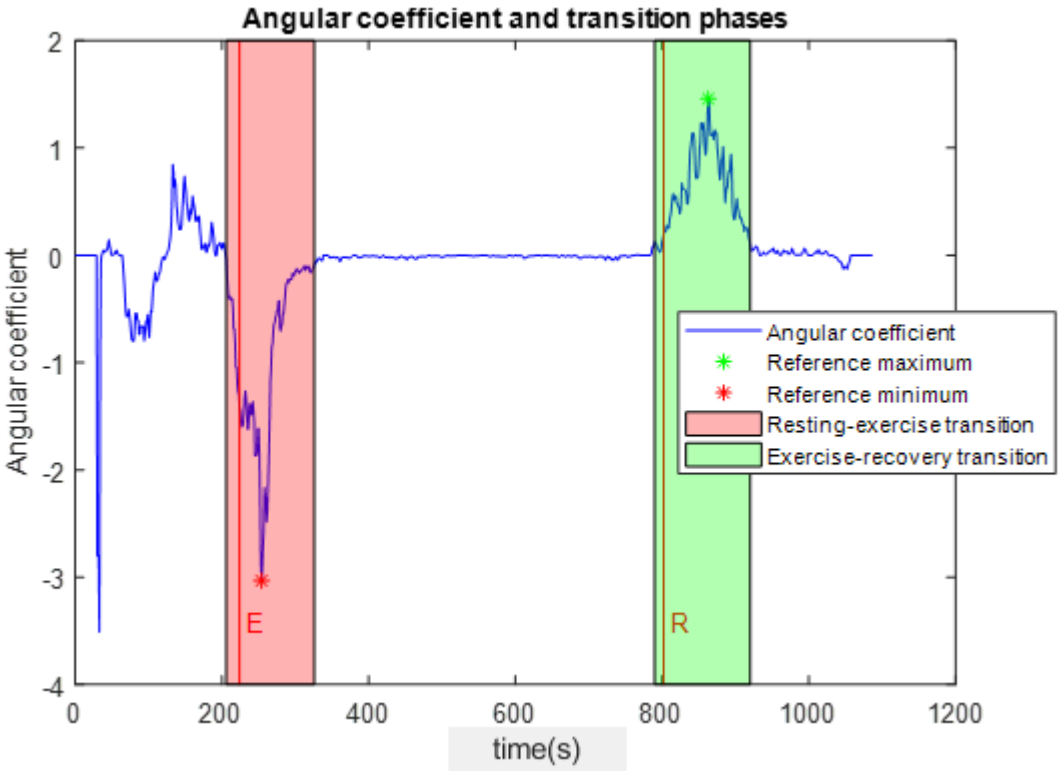

Figure 5.12 *Second subject.*

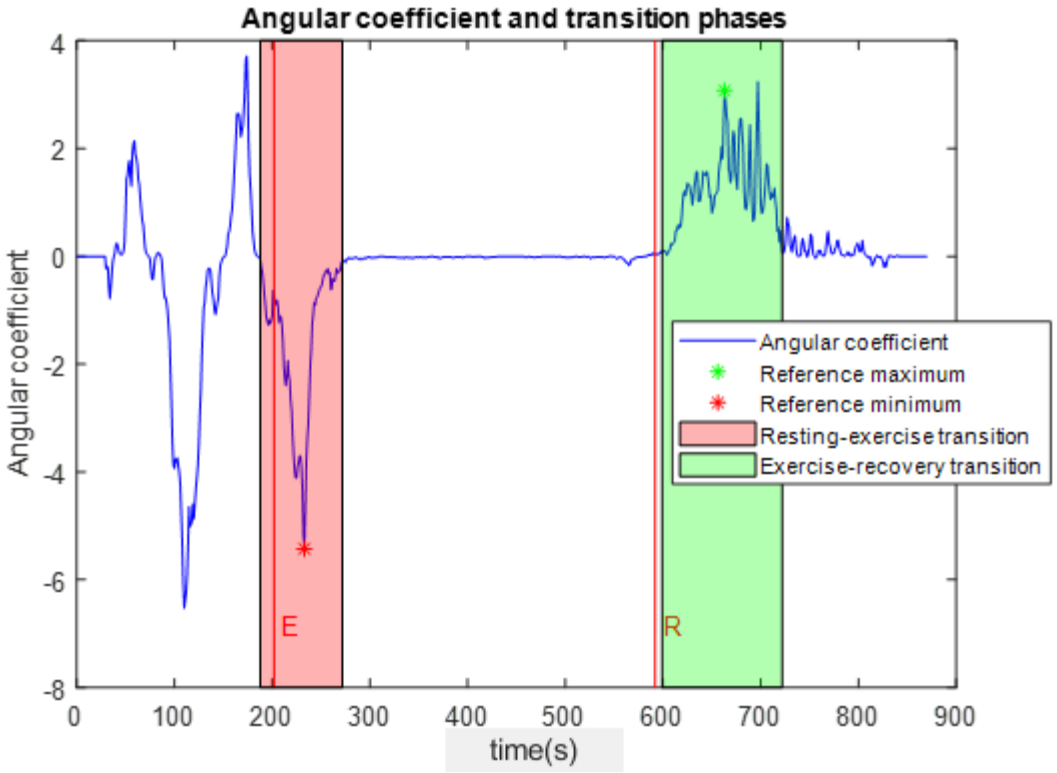

Figure 5.13 *Third subject.*

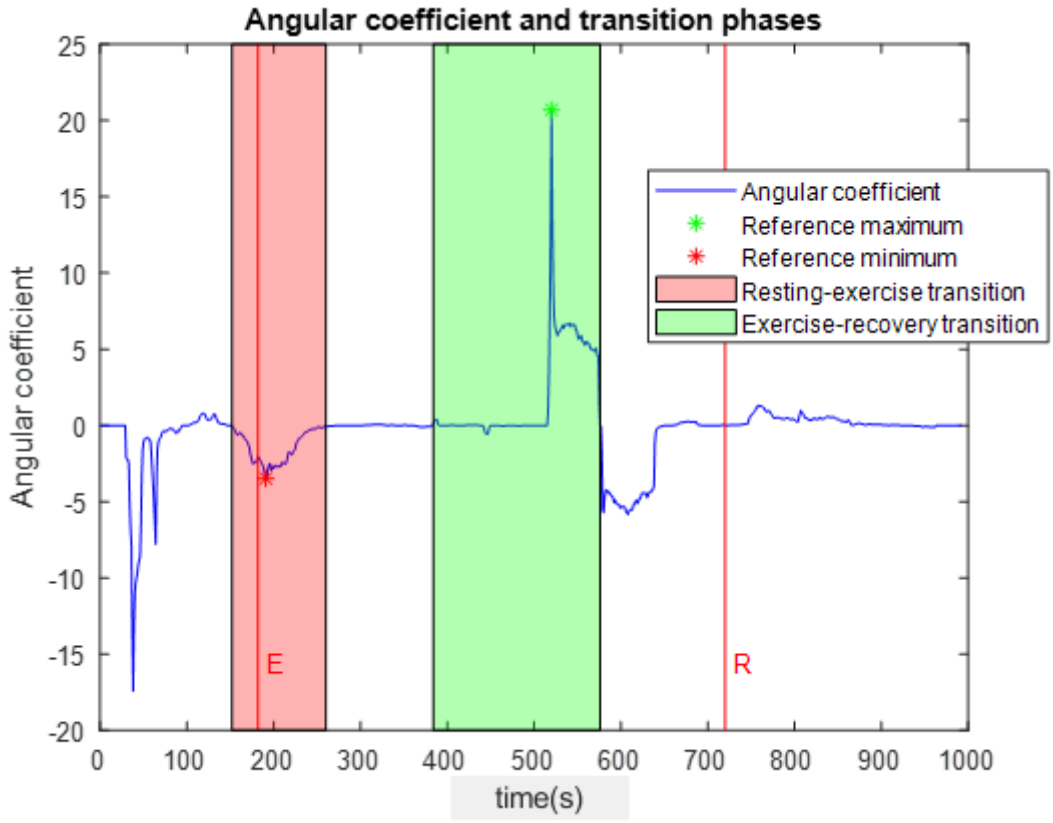

Figure 5.14 *Fourth subject.*

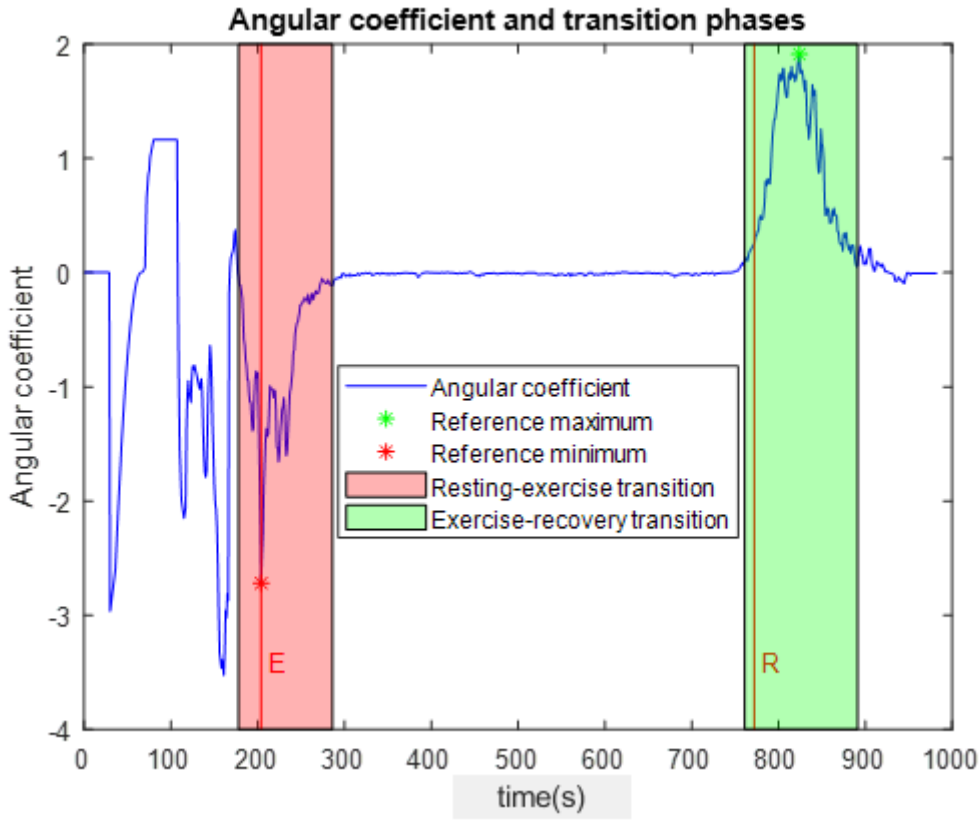

Figure 5.15 *Fifth subject.*

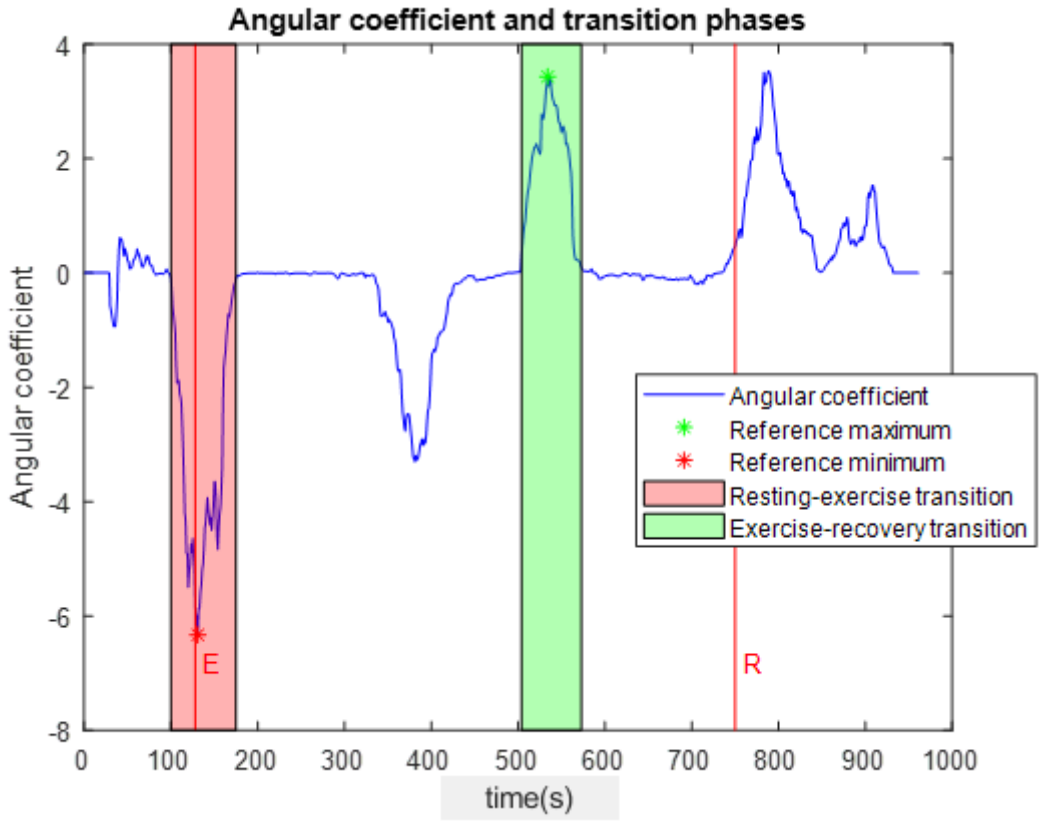

Figure 5.16 *Sixth subject.*

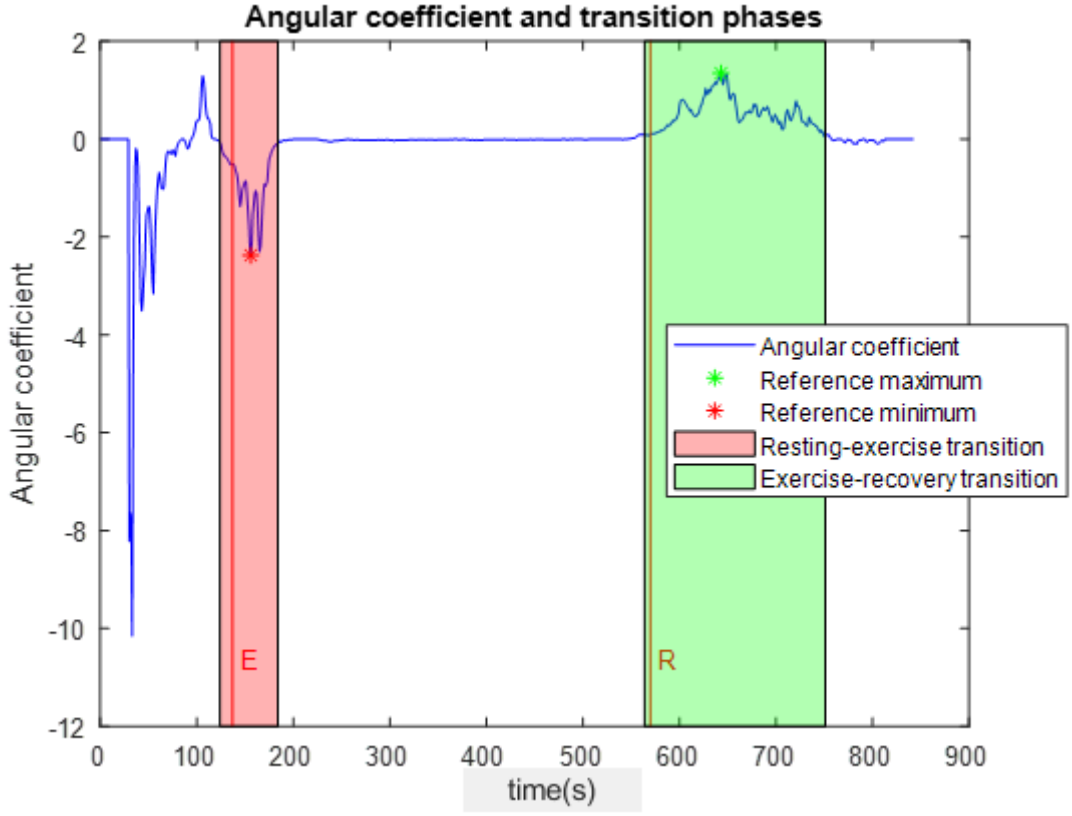

Figure 5.17 *Eighth subject.*

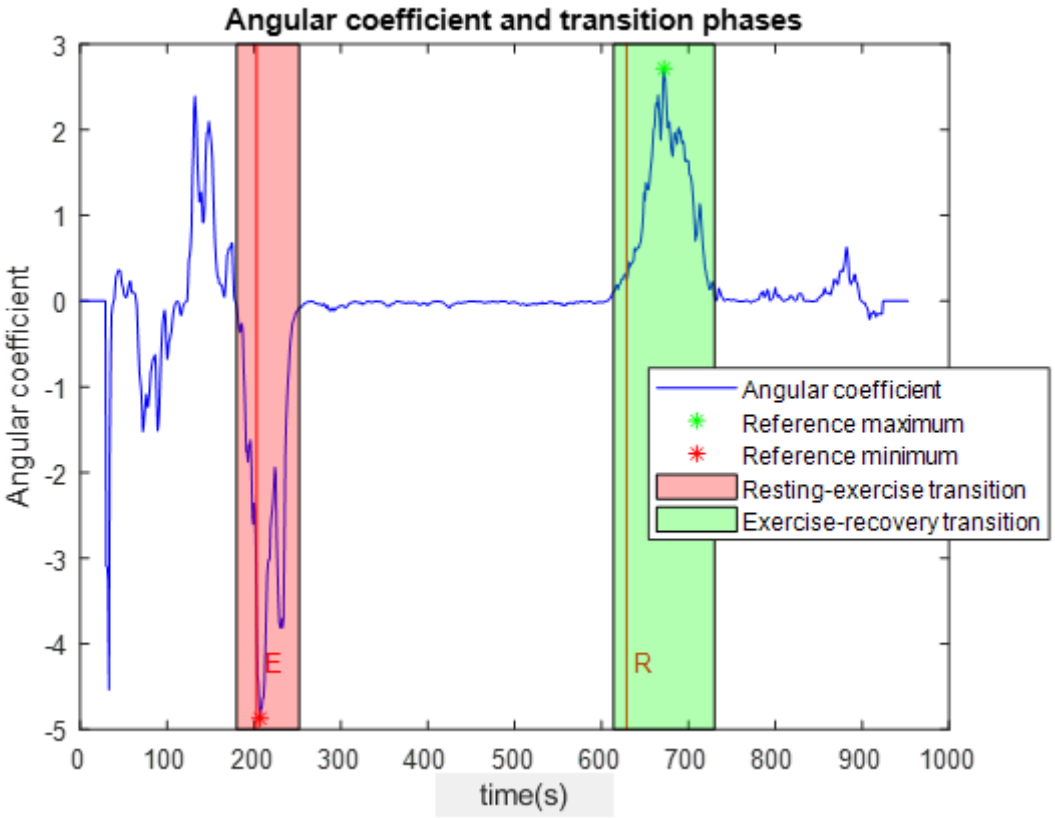

Figure 5.18 *Ninth subject.*

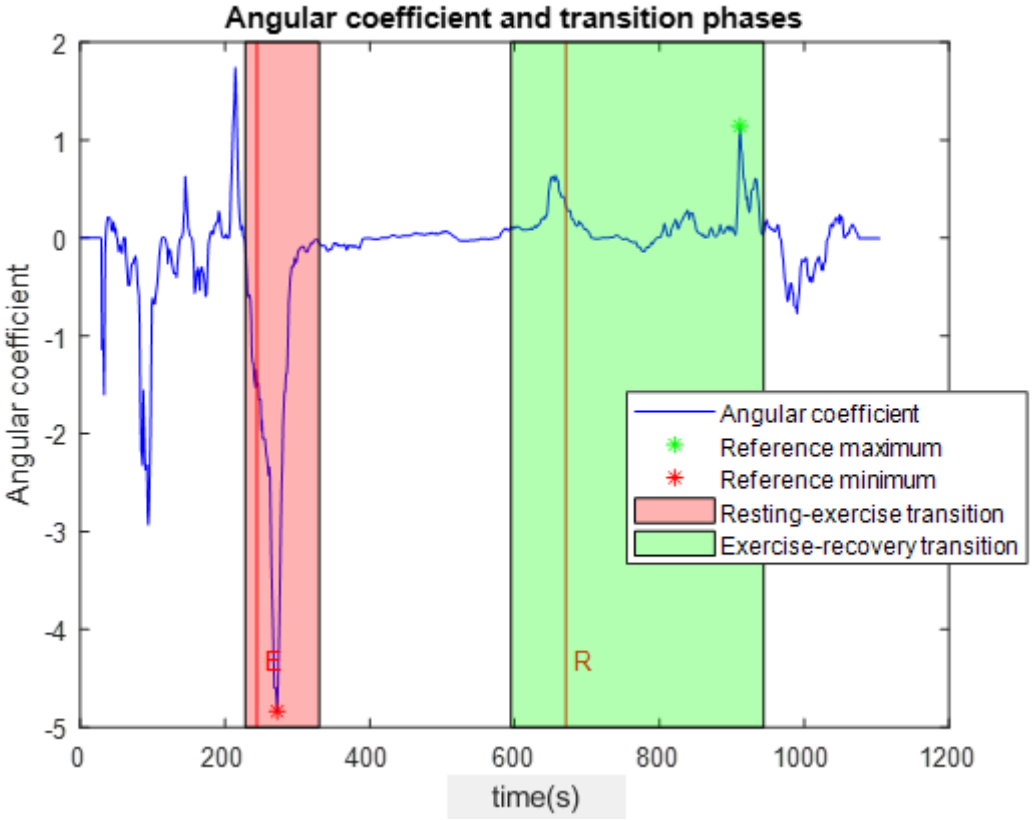

Figure 5.19 *Tenth subject.*

Table 5.4 *Comparison between time-instants relative to the beginnings of both resting-exercise and exercise-recovery transition phases measured with the stopwatch and those automatically determined by the algorithm of each subject.*

Subject	E (s)	R (s)	t_1(s)	t_2 (s)	err_1 (s)	err_2 (s)	err_1(%)	err_2(%)
1st subject	235	739	235	732	0	7	0	0.55
2nd subject	224	802	206	790	18	12	1.66	1.10
3rd subject	202	592	188	599	14	7	1.61	0.80
4th subject	182	720	152	384	30	336	3.02	33.87
5th subject	204	772	178	761	26	11	2.65	1.12
6th subject	128	750	100	504	28	246	2.91	25.60
8th subject	137	570	124	564	13	6	1.54	0.71
9th subject	203	629	180	614	23	15	2.41	1.57
10th subject	244	671	228	595	16	76	1.45	6.88

E[s], beginning of the resting-exercise transition phase measured by the stopwatch in seconds; R[s], beginning of the exercise-recovery transition phase measured by the stopwatch in seconds; t_1[s], beginning of the resting-exercise transition phase determined by the algorithm in seconds; t_2[s], beginning of the exercise-recovery transition phase determined by the algorithm in seconds; err1 [s], absolute value of the time-difference between E[s] and t1[s]; err2 [s], absolute value of the time-difference between R[s] and t2[s]; err1(%), err1 expressed in percentage;err2(%), err2 expressed in percentage.

Table 5.5 *Duration of the three training phases (pseudo-resting, exercise, recovery) and the two transition phases (resting-exercise and exercise-recovery) of each subject determined by the algorithm.*

Subject	d_{rest}(s)	$d_{rest\text{-}exe}$(s)	d_{exe}(s)	$d_{exe\text{-}rec}$(s)	d_{rec}(s)
1st subject	235	145	352	120	410
2nd subject	206	120	464	130	166
3rd subject	188	84	327	123	148
4th subject	152	108	124	192	416
5th subject	178	108	475	130	91
6th subject	100	75	329	69	388
8th subject	124	60	380	187	91
9th subject	180	72	362	116	223
10th subject	228	102	265	349	160

d_{rest}[s], duration of the pseudo-resting phase in seconds; $d_{est\text{-}exe}$[s], duration of the resting-exercise transition phase in seconds; d_{exe}[s], duration of the exercise phase in seconds; $d_{exe\text{-}rec}$[s], duration of the exercise-recovery transition phase in seconds; drec[s], duration of the recovery phase.

Table 5.6 *Mean value ± standard deviation of heart-rate of the three training phases (resting,exercise, recovery) determined by the algorithm.*

Subject	(HR_{rest}) (s)	(HR_{exe}) (s)	(HR_{rec}) (s)
1st subject	87.68±9.08	169.46±9.88	84.18±6.50
2nd subject	103.11±9.79	164.40±8.41	114.27±3.20
3rd subject	87.37±16.51	147.70±6.53	85.36±3.84
4th subject	96.45±19.46	165.12±3.38	130.40±25.25
5th subject	89.01±14.59	164.93±7.69	107.29±3.28
6th subject	78.92±6.58	165.55±40.91	138.58±34.32
8th subject	129.92±20.72	187.94±9.70	118.17±3.83
9th subject	115.42±15.42	173.99±10.52	110.76±6.53
10th subject	101.92±13.12	164.83±4.73	116.25±7.97

mean(HR_{rest}) [s], mean value of heart-rate of pseudo-resting phase; std(HR_{rest}) [s], standard deviation of the heart-rate of resting phase; mean(HR_{exe}) [s], mean value of heart-rate of exercise phase; std(HR_{exe}) [s], standard deviation of the heart-rate of exercise phase; mean(HR_{rec}) [s], mean value of heart-rate of recovery phase; std(HR_{rec}) [s], standard deviation of the heart-rate of recovery phase.

Table 5.7 *Mean value ± standard deviation of heart-rate of the two transition phases (resting-exercise and exercise-recovery) determined by the algorithm.*

Subject	($HR_{rest-exe}$) (s)	($HR_{exe-rec}$) (s)
1st subject	121.46±23.18	129.45±39.09
2nd subject	126.49±19.16	147.53±20.87
3rd subject	113.76±19.53	124.73±22.18
4th subject	134.50±24.42	155.73±28.09
5th subject	131.41±16.23	140±24.06
6th subject	102.76±22.79	190.63±32.33
8th subject	153.08±19.24	154.88±27.68
9th subject	130.42±25.23	154.12±27.03
10th subject	135.73±22.65	134.47±12.31

mean($HR_{rest-exe}$) [s], mean value of heart-rate of resting-exercise trainsition phase; std($HR_{rest-exe}$) [s], standard deviation of the heart-rate of pseudo-resting phase; mean($HR_{exe-rec}$) [s], mean value of heart-rate of exercise-recovery transition phase; std($HR_{exe-rec}$) [s], standard deviation of the heart-rate of exercise-recovery transition phase.

Table 5.8 *Mean value± standard deviation of tachogram of the three training phases (resting,exercise, recovery) determined by the algorithm.*

Subject	(RR_{rest}) (ms)	(RR_{exe}) (ms)	(RR_{rec}) (ms)
1st subject	692.27±77.94	355.29±21.32	717.32±59.22
2nd subject	587.92±65.72	365.92±18.84	525.46±14.69
3rd subject	709.99±125.81	407±17.75	704.28±31.33
4th subject	662.52±206.68	363.52±7.56	477.25±89.46
5th subject	702.49±116.53	364.57±16.91	559.73±16.99
6th subject	765.68±66.17	382.92±83.57	465±131.99
8th subject	477.93±107.55	320.11±16.73	508.26±16.64
9th subject	530.41±84.08	346.12±21.21	543.70±33.90
10th subject	599.12±83.29	364.31±10.51	518.59±36.19

mean(RR_{rest}) [ms], mean value of tachogram of pseudo-resting phase; std(RR_{rest}) [ms], standard deviation of the tachogram of resting phase; mean(RR_{exe}) [ms], mean value of tachogram of exercise phase; std(RR_{exe}) [ms], standard deviation of the tachogram of exercise phase; mean(RR_{rec}) [ms], mean value of tachogram of recovery phase; std(RR_{rec}) [ms], standard deviation of the tachogram of recovery phase.

Table 5.9 *Mean value ± standard deviation of tachogram of the two transition phases (pseudo-resting -exercise and exercise-recovery) determined by the algorithm.*

Subject	($RR_{rest\text{-}exe}$) (ms)	($RR_{exe\text{-}rec}$) (ms)
1st subject	516.86±124.04	515.69±179.33
2nd subject	486.51±81.44	415.09±60.08
3rd subject	545.34±106.59	497.04±91.96
4th subject	461.78±87.99	408.14±119.43
5th subject	464.08±61.52	441.11±74.03
6th subject	614.50±140.97	323.84±54.60
8th subject	398.45±52.80	399.83±70.61
9th subject	478.70±98.40	401.78±72.32
10th subject	456.71±89.22	449.93±41.43

mean($RR_{rest\text{-}exe}$) [ms], mean value of tachogram of resting-exercise transition phase; std($RR_{rest\text{-}exe}$) [ms], standard deviation of the tachogram of pseudo-resting phase; mean($RR_{exe\text{-}rec}$) [ms], mean value of tachogram of exercise-recovery transition phase; std($RR_{exe\text{-}rec}$) [ms], standard deviation of the tachogram of exercise-recovery transition phase.

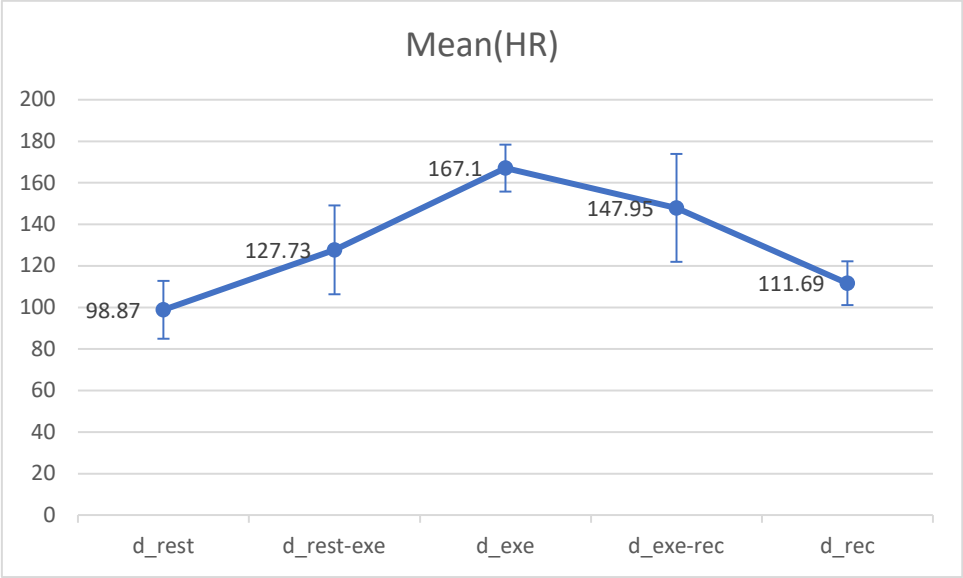

Figure 5.20 *Average values of both mean(HR) and std(HR) of the study population.*

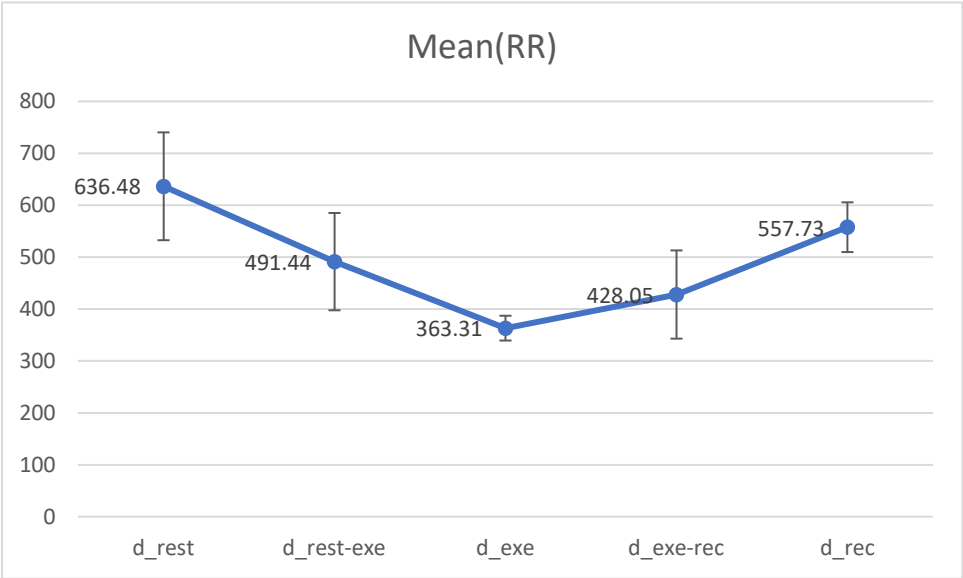

Figure 5.21 *Average values of both mean(RR) and std(RR) of the study population.*

5.4 Discussion

Figures from 5.11 to 5.19 shows that the algorithm has correctly identified both transition phases (from pseudo-resting to exercise and from exercise to recovery), and consequently the three training phases in 7 out of 9 subjects. This is visually assessed by the red patch (associated to the resting-exercise transition phase) has its left and right margins very close to the beginning of the descending tract and to the ending of the ascending tract, respectively, of the first negative wave before the almost linear tract of the exercise phase. Similarly, also the green patch (associated to the exercise-recovery transition phase) has its left and right margins very close to the beginning of the ascending tract and to the ending of the descending tract, respectively, of the first positive wave after the almost linear tract of the exercise phase. This is supported also by Table 5.4 which shows the percentage of error regarding the determination of the time-instant of the beginning of the resting-exercise transition phase ranges from a minimum of 0% (first subject) to a maximum of 3.02% (fourth subject). On the other hand, the algorithm has not been able to correctly identify the recovery transition phase in subject 4 and subject 6, assesable just observing their green patche, which appears before the red vertical line labelled with letter 'R' associated to time-instant of the beginning of the exercise-recovery transition phase. This is confirmed, in Table 5.4, by a percentage of error reaching peaks of 33.87% in the fourth subject and of 25.60% in the sixth subject. As will be discussed in the conclusions, this wrong behaviour of the algorithm is due to a well-founded reason. However, taking this two percentages out, the percentage of error regarding the determination of the time-instant of the beginning of the exercise-recovery transition phase ranges from a minimum of 0.55% (first subject) to a maximum of 1.57% (ninth subject), although subject 10 shows a percentage of error equal to 6.88. But, looking at figure 5.19 in detail, it can be note how the red vertical line labelled with letter 'R' is placed on the descending tract of the positive wave, rather than on the ascending tract. This could suggests a wrong timekeeping by the stopwatch or an incorrect report of the manual annotation. Therefore, table 5.4 is also useful for a sort of skimming of successive statistical data: patients 4 and 6 are taken into consideration except for the exercise phase onwards.

The most interesting data of table 5.5 is the duration of the exercise-recovery phase ($d_{exe-rec}$) which represents the real recovery from the exercise, since the last phase (d_{rec}) can be considered a second resting phase. Subject 9 shows the fastest recovery with a duration of 116 seconds whereas, excluding subject 10, patient 8 shows the slowest recovery with a duration of 187 seconds. From a physiological point of view, it could be said that the duration of the recovery is dependent on the age of the patient and on its weekly training rate. This assumption is confirmed in the case of patient 9 who is 18 years old and has a

weekly training rate equal to 5. Patients 1, 2, and 4, whose ages and weekly training rates range from 48-55 and 3-4 respectively, show longer, and similar to each other, recoveries. The only example against the trend is Subject 8 which, although is 18 years old and has a weekly training rate equal to 5, has a recovery duration of 187 seconds. Since, for this subject, err_2(%) is equal to 0.71% (so an optimal identification of the beginning of the recovery phase by the algorithm), there are several possible conclusions to be drawn either an effective long recovery period despite the high weekly training rate, or a wrong behaviour of the algorithm. Concerning this last hypothesis, the unexpected long recovery is due to a wrong identification of the ending time-instant of the exercise-recovery phase by the algorithm, in particular to the range [-0.1, +0.1] chosen for the determination of the time instants described in page 120. Effectively, looking at the green patch of figure 5.17, it is possible to note how, from the reference maximum, the signal shows a clear decrement until half of the patch, and then an almost linear tract until the right margin of the patch (despite a lot of variability). The problem lies in the fact that the clear descending tract before the almost linear tract does not go below the superior limit of the range (equal to +0.1).

Analyzing in more detail subject 4, its starting signal is affected by data loss (the signal comprises values equal to zero). Since data loss is lower than 10%, a correction of the zero-values has been applied, but without taking into consideration the calibration of the sensor from the instant it gets the signal back. Therefore, the artefact is not completely eliminated, with the consequence of the wrong identification of the recovery. Future works can be addressed to the improvement of a more accurate algorithm.

This problem holds also for subject 6, whose recovery phase is wrongly identified because there are variations of velocity in the execution of the exercise with consequent HR variations. Therefore, another possible future improvement of the algorithm is its application on not-completely aerobic sports, with athletes having variable velocities and phases during the same exercise (such as football, volleyball, etc).

The algorithm is also able to identify the transition phases. The exclusion of these phases from the signal permits a reliable analysis of the HRV and of the signal in frequency-domain, avoiding non-stationary phases. Table 5.9 is important for the evaluation of the HRV. Overall, with reference to figures 5.20 and 5.21, it can be noted how the highest standard deviation of RR is on the pseudo-resting period (equal to 103.75 s), whereas the lowest standard deviation of RR is on the exercise phase (equal to 23.82 s). Moreover, also the two transition phases show elevated values of RR-standard deviation (93.66 s for the resting-exercise transition and 84.86 s for the exercise-recovery transition). This result is consistent with the fact that in an healthy situation (like all the ten subjects object of this study), HRV increases during relaxing activities (such as meditation or sleep, since

the parasympathetic nervous system dominates), and decreases during stressful activities (such as exercise, since the elevated sympathetic activity helps the body to keep up with the demand). Therefore, HRV is typically higher when the heart is beating slowly, and it is lower when the heart starts to beat faster, as indeed happens during exercise.

Conclusions

"Your heart beats approximately
104,000 times in a day
and each one of those heartbeats
is far too valuable to waste
on comparing yourself to another.

You were given your heart's
unique rhythm to dance
to your very own beat.
Not to the beating of anyone
else's heart.
Just your own"

[Nikita Gill]

The present work has wanted to provide a tool for athletes and sports professionals able to enhance the performance, but always having, as necessary condition, the safety of the health status of the athlete. Indeed, only by recording the heart-rate from a wearable sensor, the algorithm automatically detect the transition phases resting-exercise and exercise-recovery and, therefore, also the pseudo-resting, exercise and recovery phase. Already at this point, it is possible to perform an evaluation of the training status of the athlete simply looking at the duration of the exercise-recovery transition phase, which represents the real recovery from fatigue of the exercise. This data serves the sports professionals – in particular fitness coaches and trainers – to have a response of their training programmes and to monitor the progresses of this parameter over time. It has been demonstrated, indeed, that the optimization of the athlete's performance is based on the continous monitoring of the training progresses. As regards the clinical utility, the algorithm is able to eliminate the transitory phases (from pseudo-resting to exercise, and from exercise to recovery) which would affect any clinical heart risk index.
However, the algorithm has been demonstrated to have only one limitation: the exercise phase must not contain peaks over the set range. That is, from the physiological point of

view, if the patient undergoes an unexpected great recovery during the exercise phase, the individuation of the exercise-recovery transition phase by the algorithm is falsified. However, this algorithm has been developed to deal only with middle-running athletes, who undergo a great effort during their performance, with no change of great recoveries. Anyway, the present algorithm lends itself to modifications, depending on the kind of sport practised by the athlete, in future works. Therefore, an apparent point of weakness can be turned into a strength.

The downside of the algorithm is represented by all the clinical informations that can be extracted from the same heart-rate signal. All risk indeces of the heart, such as QT-index or the HRV, must be estimated during stable cardiac conditions. This means that the only tracts of the heart-rate signal which can be taken into consideration are the pseudo-resting phase, the exercise phase and the recovery phase. In other words, the hypothetic preservation of the two transition phases (resting-exercise and exercise-recovery) would completely falsify the estimation of any index. Since the algorithm automatically identifies these two transition phases, it would be enough delete them for a further processing of the new signal, or simply analyze the tachogram in order to have a clear picture of the HRV.

In conclusion, the algorithm already shows its reliability as regards the optimization of the performance, and its extreme utility in the evaluation of the most important risk indeces of the heart. In addition to this, it promises to adapt to all kinds of sports, making of itself a ‘universal tool’ in the world of sport.

Bibliography

[1] F. H. Netter. *Atlas of Human Anatomy*. Elsevier. 2018. 7th edition.

[2] Klabunde R E. *Cardiovascular Physiology Concepts*. Wolters Kluwer – Lippincott Williams & Wilkins. 2011. Second Edition.

[3] Boron W F, Boulpaep E L. *Medical Physiology*. Elsevier Saunders. 2012. Updated Second Edition.

[4] Plowman S A, Smith D L. *Exercise Physiology for Health, Fitness, and Performance*. Wolters Kluwer – Lippincott Williams & Wilkins. 2011. Third Edition.

[5] Romero S A, Minson C T, Halliwill H R. *The Cardiovascular System after Exercise*. Journal of Applied Physiology (2017); 122(4):925-932.

[6] Michael S, Graham K S, Devis OAM G M. *Cardiac Autonomic Responses during Exercise and Post-exercise Recovery Using Heart Rate Variability and Systolic Time Intervals-A Review*. Frontiers in Physiology (2017); 8(301):1-19.

[7] Roy S, Singh N, Gupta R. *Heart rate variability in different intensities of static and dynamic exercises graded using similar heart rate*. Sport Sciences for Health (2020).

[8] Nystoriak M A, Bhatnagar A. *Cardiovascular Effects and Benefits of Exercise.* Frontiers in Cardiovascular Medicine (2018); 5(135):1-11.

[9] Baggish A L, Wood M J. *Athlete's Heart and Cardiovascular Care of the Athlete – Scientific and Clinical Update*. Circulation (2011); 123:2723-2735.

[10] Pelliccia A, Maron BJ, Spataro A, Proschan MA, Spirito P. *The upper limit of physiologic cardiac hypertrophy in highly trained elite junior athletes*. N Engl J Med. 1991; 324:295-301.

[11] Sharma S, Maron BJ, Whyte G, Firoozi S, Elliott PM, McKenna WJ. *Physiologic limits of left ventricular hypertrophy in elite junior athletes: relevance to differential diagnosis of athlete's heart and hypertrophic cardiomyopathy*. J Am Coll Cardiol. 2002; 40:1431-1436.

[12] Morganroth J, Maron BJ, Henry WL, Epstein SE. *Comparative left ventricular dimensions in trained athletes*. Ann Intern Med. 1975; 82:521-524.

[13] Gilbert CA, Nutter DO, Felner JM, Perkins JV, Heymsfield SB, Schlant RC. *Echocardiographic study of cardiac dimensions and function in the endurance-trained athlete*. Am J Cardiol. 1977; 40:528-533.

[14] Baggish AL, Yared K, Weiner RB, Wang F, Demes R, Picard MH, Hagerman F, Wood MJ. *Differences in cardiac parameters among elite rowers and subelite rowers*. Med Sci Sports Exerc. 2010; 42:1215-1220.

[15] Baggish AL, Wang F, Weiner RB, Elinoff JM, Tournoux F, Boland A, Picard MH, Hutter AM Jr, Wood MJ. *Training-specific changes in cardiac structure and fucntion: a prospective and longitudinal assessment of competitive athletes*. J Appl Physiol. 2008; 104:1121-1128.

[16] Hauser AM, Dressendorfer RH, Vos M, Hashimoto T, Gordon S, Timmis GC. *Symmetric cardiac enlargement in highly trained endurance athletes: a two-dimensional echocardiographic study*. Am Heart J. 1985; 109:1038-1044.

[17] Henriksen E, Landelius J, Wesslen L, Arnell H, Nystrom-Rosander C, Kangro T, Jonason T, Rolf C, Lidell C, Hammarstrom E, Ringqvist I, Friman G. *Echocardiographic right and left ventricular measurements in male elite endurance athletes*. Eur Heart J. 1996; 17:1121-1128.
[18] Schartag J, Schneider G, Urhausen A, Rochette V, Kramann B, Kindermann W. *Athlete's heart: right and left ventricular mass and function in male endurance athletes and untrained individuals determined by magnetic resonance imaging*. J Am Coll Cardiol. 2002; 40:1856-1863.
[19] Babaee Bigi MA, Aslani A. *Aortic root size and prevalence of aortic regurgitation in elite strength trained athletes*. Am J Cardiol. 2007; 100:528-530.
[20] D'Andrea A, Cocchia R, Riegler L, Scarafile R, Salerno G, Gravino R, Vriz O, Citro R, Limongelli G, Di Salvo G, Cuomo S, Caso P, Russo MG, Calabro R, Bossone E. *Aortic root dimensions in elite athletes*. Am J Cardiol. 2010; 105:1629-1634.
[21] Pelliccia A, Di Paolo FM, De Blasiis E, Quattrini FM, Pisicchio C, Guerra E, Culasso F, Maron BJ. *Prevalence and clinical significance of aortic root dilation in highly trained competitive athletes*. Circulation. 2010; 122:698-706.
[22] Hoogsten J, Hoogeven A, Schaffers H, Wijn PF, van der Wall EE. *Left atrial and ventricular dimensions in highly trained cyclists*. Int J Cardiovasc Imaging. 2003; 19:211-217.
[23] Pelliccia A, Maron BJ, Di Paolo FM, Biffi A, Quattrini FM, Pisicchio C, Roselli A, Caselli S, Culasso F. *Prevalence and clinical significance of left atrial remodeling in competitive athletes*. J Am Coll Cardiol. 2005; 46:690-696.
[24] D'Andrea A, Riegler L, Cocchia R, Scarafile R, Salerno G, Gravino R, Golia E, Vriz O, Citro R, Limongelli G, Calabro P, Di Salvo G, Caso P, Russo MG, Bossone E, Calabro R. *Left atrial volume index in highly trained athletes*. Am Heart J. 2010; 159:1155-1161.
[25] Basavarajaiah S, Boraita A, Whyte G, Wilson M, Carby L, Shah A, Sharma S. *Ethnic differences in left ventricular remodeling in highly-trained athletes: relevance to differentiating physiologic left ventricular hypertrophy from hypertrophic cardiomyopathy*. J Am Coll Cardiol. 2008; 51:2256-2262.
[26] Majumder S, Mondal T, Jamal Deen M. *Wearable Sensors for Remote Health Monitoring*. Sensors (2017); 17(130):1-45.
[27] Lam Po Tang S. *Textiles for Sportswear*. – *Wearable sensors for sports performance*. Elsevier – The Textile Institute. 2015.
[28] Wu J, Li J, Seely A, Zhu Y, Huang S, Wang X, Zhao L, Wang H, Cristophe H. *Chronotropic Competence Indices Extracted from Wearable Sensors for Cardiovascular Diseases Management*. Sensors (2017); 17(2441):1-11.
[29] Finkelstein J, Jeong I. *Using Heart Rate Variability for Automated Identification of Exercise Exertion Levels*. Driving Quality in Informatics: Fullfilling the Promise - Studies in health technology and informatics (2015); 208:137-141.
[30] Toninelli G, Vigo C, Vaglio M, Porta A, Lucini D, Badilini F, Pagani M. *Dynascope: a Software Tool for the Analysis of Heart Rate Variability During Exercise*. Computing in Cardiology (2012); 39:181-184.
[31] Vaglio M, Porta A, Pizzinelli P, Di Marco S, Lucini D, Badilini F, Pagani M. A Fully Automatic Algorithm for the Analysis of Heart Rate Changes and Cardiac Recovery during Exercise. Computers in Cardiology (2007); 34:309-312.

[32] Badilini F, Pagani M, Porta A. *HeartScope: a Software Tool Addressing Autonomic Nervous System Regulation*. Computers in Cardiology (2005); 32: 259-262.
[33] Sbrollini A, Morettini M, Maranesi E, Marcantoni I, Nasim A, Bevilacqua R, Riccardi G. R, Burattini L. *Sport Database: Cardiorespiratory data acquired through wearable sensors while practising sports*. Data in brief – Elsevier (2019); 27: 1-7.
[34] Agostinelli A, Morettini M, Sbrollini A, Maranesi E, Migliorelli L, Di Nardo F, Fioretti S, Burattini L. *CaRiSMA 1.0: cardiac risk self-monitoring assessment*. Open Sports Sci. J. (2017); 10:179-190.
[35] Conconi F, Ferrari M, Ziglio P. G, Droghetti P, Codeca L. *Determination of the anaerobic threshold by a non-invasive field test in runners.* J. Appl. Physiol. (1982); 52(4):869-873.

Acknowledgements

First of all, I would like to thank Professor Laura Burattini who allowed me, in a very real sense, to graduate. She deserves all my gratitude not only for her excellent work as my advisor, but also for letting me reach a degree which, without her, would never come. It may sounds as only a sentence of circumstance, but it is definitely not; it is just too early to clarify important aspects that would contaminate the joy and the satisfaction of a so desired achievement. “We must be patient and giving time to time”, as my aunt used to say.

I would also like to thank Doctor Agnese Sbrollini, first fellow student and then excellent supervisor, and Doctor Sofia Romagnoli, for the unrivalled patience shown towards me. Without their contribution and valuable advices, I could never have complete this work in such a complete and detailed way. I want to tell them they are the real beating heart of the university.

My deepest thanks go to my parents, who gave me the possibility to study through huge economic sacrifices. They taught me day after day how it is important to never give up because the sacrifice is as strenous as satisfying and rewarding. I wish them to fully enjoy their “second half of their lives” under the banner of health, wellness, happiness and serenity. Despite several misunderstanding, they always fulfilled what is the real duty of the parents, namely to enable their sons to “leave the nest”. I must acknowledge you this fact. I hope this graduation is a source of pride for you.

My girlfriend, or better my “baby” deserves a special mention. She turned out a wonderful leading figure in the dark moments. She was able to stimulate, encourage, support, but above all she had the merit to undestand the difficulties that occurred during my period of study. She made me feel able to measure up. No one better than her, who have suffered so much – unexpectedly too much compared to the good she has done for her family, her friends, many acquaintances, and for me – can show how to move forward in spite of continuous difficulties. There have been moments of tensions, I must say. But I am the one to blame, because I was so blinded by my frustration of feeling inadequate and incompetent that I was not able to better look inside her to find the right way to release her purity of soul. Short supply these days.

Dear grandma, days go by between arguments, debates and smiles. You probably will not be seeing me married, but I know how much you wanted this graduation. One step at a time, you are an iron-grandma!

I would like to conclude with a reference to Dante Alighieri. The Divine Comedy begins:

Midway upon the journey of our life
I found myself within a forest dark,
For the straighforward pathway had been lost.

This first tercet represents my current situation: I am 31 years old and a deep fear of the future. But I very much hope that my path in life is similar to that of Dante through Hell, Purgatory and Paradise, and that it will end as the last canto of Paradise describes:

But my desire and will were moved already
Like a wheel revolving uniformly
By the Love that moves the sun and the other stars.

Love must be considered as a divinity; this means that sometimes if you have faith, it can appear. My family and my girlfiend have appeared on the course of my life; this is the reason why I would dedicate this graduation to them.